

UNCLASSIFIED

---

---

AD **267 010**

---

*Reproduced  
by the*

ARMED SERVICES TECHNICAL INFORMATION AGENCY  
ARLINGTON HALL STATION  
ARLINGTON 12, VIRGINIA



---

---

UNCLASSIFIED

NOTICE: When government or other drawings, specifications or other data are used for any purpose other than in connection with a definitely related government procurement operation, the U. S. Government thereby incurs no responsibility, nor any obligation whatsoever; and the fact that the Government may have formulated, furnished, or in any way supplied the said drawings, specifications, or other data is not to be regarded by implication or otherwise as in any manner licensing the holder or any other person or corporation, or conveying any rights or permission to manufacture, use or sell any patented invention that may in any way be related thereto.

CATALOGED BY ASTIA # 267010  
AS AD NO. \_\_\_\_\_

XEROX  
62-1-3

870 700

First Quarterly Report  
for the  
THERMIONIC EMITTER MATERIALS  
RESEARCH PROGRAM  
(TEE-4015-1)



Submitted by  
Thermo Electron Engineering Corporation  
85 First Avenue  
Waltham 54, Massachusetts

for the period  
1 July 1961 - 30 Sept 1961

Approved by:

  
J.H. Weinstein  
Project Manager

LEGAL NOTICE

This report has been prepared under Contract No. NONR-3563(00), Office of Naval Research. It is funded by ARPA under the cognizance of Dr. J. Huth and technically supervised by Dr. J. J. Connelly, Jr., Material Sciences Division, ONR.

Reproduction in whole or in part is permitted for any purpose of the United States Government.

Distribution List

NONR-3563(00)

| <u>Addressee</u>   | <u>No. Copies</u> |
|--|-------------------|
| Chief of Naval Operations<br>Department of the Navy<br>Washington 25, D. C.<br>Attn: Op-752<br>Op-07G  | 1<br>1            |
| Chief of Naval Research<br>Department of the Navy<br>Washington 25, D. C.<br>Attn: Code 429<br>400X  | 4<br>1            |
| Chief, Bureau of Ships<br>Department of the Navy<br>Washington 25, D. C.<br>Attn: Code 370<br>1500   | 1<br>1            |
| Chief, Bureau of Naval Weapons<br>Department of the Navy<br>Washington 25, D. C.<br>Attn: RRNU-11  | 1                 |
| Director<br>U. S. Naval Research Laboratory<br>Washington 25, D. C.<br>Attn: Mr. A. McClinton (Code 5560)<br>Code 6430<br>Technical Information Office             | 1<br>1<br>1       |
| Advanced Research Projects Agency<br>General Research Office<br>Pentagon: Room 3D-148<br>Washington 25, D. C.<br>Attn: Dr. J. H. Huth                              | 5                 |
| Assistant Director for Advanced Systems<br>Division of Reactor Development<br>U. S. Atomic Energy Commission<br>Washington 25, D. C.<br>Attn: CDR W. A. Schoenfeld | 1                 |

| <u>Addressee</u>  | <u>No. Copies</u> |
|---|-------------------|
| Assistant Director (Army Reactors)<br>Division of Reactor Development<br>U.S. Atomic Energy Commission<br>Washington 25, D. C.<br>Attn: LCDR C. W. Mallory, USN<br>(Mail Station F-311) | 1                 |
| Westinghouse Electrical Corporation<br>Astronuclear Laboratory<br>250 Mt. Lebanon Blvd.<br>Pittsburgh 34, Pennsylvania<br>Attn: Dr. R. C. Cunningham                                    | 1                 |
| Commanding Officer<br>Office of Naval Research Branch Office<br>Box 39, Navy No. 100<br>Fleet Post Office<br>New York, New York   | 3                 |
| Office of Naval Research<br>495 Summer Street<br>Boston 10, Mass.<br>Attn: Dr. F. Gardner   | 1                 |
| Inspector of Naval Material<br>495 Summer Street<br>Boston 10, Mass.<br>Attn: Mr. A. Doddis   | 1                 |
| National Aeronautics & Space Administration<br>Lewis Research Center<br>21000 Brookpark Road<br>Cleveland 35, Ohio<br>Attn: Frank Ron   | 1                 |
| Roland Breitwieser  | 1                 |
| Bernard Lubarsky  | 1                 |
| North American Aviation Incorporated<br>Atomics International<br>P.O. Box 309<br>Canoga Park, California<br>Attn: Dr. N. R. Rasor   | 1                 |

| <u>Addressee</u>  | <u>No. Copies</u> |
|---|-------------------|
| National Aeronautics & Space Administration<br>1512 H Street N. W.<br>Washington 25, D. C.<br>Attn: James J. Lynch  | 1                 |
| Oak Ridge Operations Office<br>U. S. Atomic Energy Commission<br>Oak Ridge, Tennessee<br>Attn: Dr. D. F. Cope, Director<br>Reactor Development              | 1                 |
| Texas Instruments Incorporated<br>P. O. Box 1079<br>Dallas, Texas<br>Attn: Dr. Richard A. Chapman   | 1                 |
| Office of Technical Services<br>Department of Commerce<br>Washington 25, D. C.  | 1                 |
| Commanding Officer<br>Office of Naval Research Branch Office<br>10th Floor, The John Crerar Library Bldg.<br>86 East Randolph Street<br>Chicago 1, Illinois | 1                 |
| Armed Services Technical Information Agency<br>Arlington Hall Station<br>Arlington 12, Virginia   | 10                |
| Power Information Center (SP-01)<br>University of Pennsylvania<br>Moore School Building<br>200 South 33rd Street<br>Philadelphia 4, Pennsylvania            | 1                 |
| Director of Special Projects (SP-001)<br>Department of the Navy<br>Washington 25, D. C.<br>Attn: Dr. J. Craven  | 1                 |
| Commanding Officer<br>U. S. Army Signal R&D Lab.<br>USASRDA-XE<br>Fort Monmouth, New Jersey<br>Attn: G. K. Gaule  | 2                 |

## TABLE OF CONTENTS

| <u>Section</u>    | <u>Title</u>                    | <u>Page</u> |
|-------------------|---------------------------------|-------------|
| 1.0               | INTRODUCTION                    | 1-1         |
| 2.0               | SUMMARY                         | 2-1         |
| 3.0               | EXPERIMENTAL RESULTS            | 3-1         |
| 3.1               | Electrical Characteristics      | 3-1         |
| 3.1.1             | General                         | 3-1         |
| 3.1.2             | I-V Characteristics             | 3-1         |
| 3.1.3             | Work Function                   | 3-2         |
| 3.1.4             | Ion Currents                    | 3-7         |
| 3.1.5             | Ignition                        | 3-8         |
| 3.2               | Thermal Characteristics         | 3-11        |
| 3.2.1             | Cesium Conduction               | 3-11        |
| 3.2.2             | Electron Cooling                | 3-12        |
| 3.2.3             | Radiation                       | 3-12        |
| 3.3               | Power and Efficiency            | 3-12        |
| 3.4               | Spacing                         | 3-17        |
| 4.0               | PLANS FOR THE SECOND QUARTER    | 4-1         |
| 5.0               | REFERENCES                      | 5-1         |
| <u>APPENDICES</u> |                                 |             |
| A                 | THE TEST VEHICLE                | A-1         |
| B                 | TEST SET-UP AND INSTRUMENTATION | B-1         |
| C                 | TEST PROCEDURES                 | C-1         |
| C.1               | I-V Curves                      | C-1         |
| C.2               | Ignition                        | C-2         |
| C.3               | Ion Currents                    | C-2         |
| C.4               | Back Emission                   | C-2         |
| C.5               | Electron Cooling                | C-3         |

| <u>Section</u> | <u>Title</u>   | <u>Page</u> |
|----------------|--|-------------|
| C.6            | Cesium Gas Conduction  | C-4         |
| C.7            | Radiation  | C-5         |
| D              | CESIUM CORROSION STUDY   | D-1         |
| E              | THERMODYNAMIC DERIVATION OF THE DEPENDENCE<br>OF CESIUM ARRIVAL RATE UPON EMITTER SURFACE<br>TEMPERATURE | E-1         |
| F              | SELECTED DATA  | F-1         |

## 1.0 INTRODUCTION

The original objectives of this contract called for a study of six or more refractory metals as emitter materials for thermionic converters. The properties to be studied included:

(1) The coverage characteristics of the metals over a range of cesium pressures and emitter temperatures to improve our understanding of the work function of cesium-covered refractory metals.

(2) The evaporation and corrosion characteristics of the same materials at various pressures and current densities.

(3) The compatibility of these materials with uranium carbide, of the type used in nuclear reactors.

The experimental work had barely been initiated when it became apparent that evaluation of emitter materials was inseparable from an understanding of the basic phenomena that control the performance of a cesium diode. Past experimental practice often called for collecting sufficient data to plot several I-V curves and from these data to approximate an optimum performance point. Such superficial examinations have often been used as a basis for classifying the performance of various materials. Conclusions based upon such work can be misleading since they fail to examine the physical reasons for the observed performance, and any attempt to generalize from such limited information is inherently unsound.

In preparation for this investigation, therefore, the following objectives were fixed.

(1) To gather data on each parameter that seemed at that time to affect performance significantly and, as the investigation progressed, on any other parameters that were brought to light as being particularly significant.

(2) To plan our experiments so that the data gathered on each parameter would be sufficient to give a clear understanding of that parameter's effect on performance.

Such comprehensive information should enable us (by the end of the program) to construct an analytical model with sufficient foundation in experiment to describe

accurately the processes occurring in a thermionic converter. In addition, the use of different emitter materials should enable us to determine how specific material properties affect operation. The combination of an analytical model and the knowledge of the manner in which the material properties interact within this framework will describe the performance of the particular material tested, and will also provide a valuable basis for predicting the behavior of other materials under similar conditions.

## 2.0 SUMMARY

During the first quarterly period, two diodes were tested. One converter used a tantalum emitter and a molybdenum collector, and the other used a molybdenum emitter and a molybdenum collector. For each tube, the experimental investigation was begun by determining current-voltage (I-V) characteristics.

One of the most unique features of this work was that, under certain conditions, the I-V curves exhibited two branches, as shown in Fig. 3-2. The following discussion is an attempt to examine some of the paths revealed by these data.

Each branch of the I-V curve approaches a constant current value as output voltage is reduced. This behavior leads to the association of an apparent work function with each constant current value. However, without additional information, it cannot be determined whether either of these apparent work functions corresponds to the true work function of a cesium-covered surface.

The analytical work of Saha and Langmuir has related the ion production rate to the surface temperature, gas pressure, and surface work function. The relationship enables the calculation of the surface work function if the ion current can be measured. Therefore, a technique was developed for measuring the ion current in the experimental diode.

Still another method of investigating the magnitude of emitter work function is by determination of "electron cooling." Electron cooling is the average energy, measured in volts, carried from the emitter to the collector by the electrons. For an electron to travel from the emitter to the collector, it must have sufficient energy to overcome the highest potential barrier in its path. This may be either the emitter work function, a point in the interelectrode space, or the sum of the collector work function and the output voltage. In any case, the emitter work function

cannot be higher than the value of electron cooling. Thus, if electron cooling can be measured, an upper limit to the emitter work function is determined. The realization of the value of being able to measure electron cooling led to the development of a technique for accurate determination of this quantity.

In addition to its relationship to emitter work function, electron cooling measurements make it possible to evaluate one of the most important heat losses in diode operation. A portion of the energy transported by the electrons from the emitter is converted to useful power at the terminals, while the remainder is irreversibly converted to heat when the electrons arrive at the collector. The magnitude of this loss accounts for one-third to one-half of the total heat lost by the diode during operation.

Until this method of measuring electron cooling was developed, diode design calculations required that an assumption be made of electron cooling loss. These measurements now reveal that the assumptions that were used regularly were often in error by 20 to 30%. Thus, the designer has been supplied with a tool for improving the accuracy of his calculations.

Another heat loss that affects diode performance is conduction of heat by the cesium vapor. Under this program, a technique has been developed for accurate measurement of this quantity. To the best of our knowledge, this technique supplies the most detailed and accurate measurements to date of cesium conduction under operating conditions. A comparison of the data with the Knudson analytical equation and the kinetic theory conduction value in the appropriate regions shows good agreement.

An additional area of investigation introduced by examination of the I-V curves is the mechanism of the transition from the lower branch or "extinguished" mode of operation to the upper or "ignited" mode. Experiment shows that if the output voltage of a diode operating in the extinguished mode is reduced sufficiently, a

point is reached at which the observed current increases abruptly, usually by an order of magnitude, while the voltage remains constant. This higher value of current corresponds to a point on the ignited mode curve. The voltage at which the phenomenon occurs is termed the ignition point. This ignition point has been found to vary as a function of other diode parameters.

It is felt that a thorough study of the ignition phenomenon will greatly facilitate understanding of the ignited mode, which has great value for high-performance operation. Therefore, a study was initiated to correlate the relationship of the ignition point to such variables as ion currents and the ratio of cesium mean-free path to interelectrode spacing. At this point, a substantial volume of data has been accumulated. Although only a portion of the data has been processed, initial attempts at correlation have begun, and some important relationships have already been indicated.

Finally, the variable spacing feature of the test diode allows investigation that could otherwise be performed only with a prohibitive number of individual test vehicles. Such a program would require time and money far in excess of the current program. One very significant result of the variable spacing tests has been the discovery of an apparent optimum spacing for a range of emitter temperatures, which is greater than the minimum obtainable spacing.

It is now obvious that this program is of great importance to the entire area of thermionic development. Never before has a program in this field attempted to amass the type of data which is now being produced. The lack of such data has left an important gap in the development of a fundamental understanding of vapor converters. It appears certain that continued and expanded work in the areas described above will significantly improve the basic understanding of diode operation and will lead to a useful analytical model of the thermionic system.

## 3.0 EXPERIMENTAL RESULTS

### 3.1 Electrical Characteristics

#### 3.1.1 General

Extensive data have been taken on two test diodes. One has a tantalum emitter and a molybdenum collector, and the other uses molybdenum for both emitter and collector. The measured characteristics include current-voltage (I-V) relationships, ion currents, electron cooling, ignition potential, and back emission. The data were obtained over a broad range of emitter and collector temperatures, cesium pressure, and interelectrode spacing. The experimental procedures and descriptions of the test vehicle, test facility, and instrumentation are given in Appendices A, B, and C. Appendix E contains a representative group of curves plotted from the test data.

#### 3.1.2 I-V Characteristics

For the purpose of illustrating the following discussion, three representative current-voltage characteristics of the Mo-Mo diode and one of the Ta-Mo curves have been selected. These curves are shown in Figs. 3-1 through 3-4.

Selecting Fig. 3-2, let us examine the characteristic shape of the curve. Assume that the tube is at open-circuit condition ( $I = 0$ ,  $V = 1.75$  volts), and let a voltage be applied across the output terminals. For the purpose of this analysis, consider that the unit remains at equilibrium with the emitter and collector temperatures and cesium gas pressure equal to the values tabulated on Fig. 3-2. The output voltage is gradually decreased and the lower branch is traced from O. C. through points A and B. When the voltage reaches  $-180$  mv (point B), the value of current abruptly increases from  $0.76$  to  $20.0$  amp, while the voltage remains constant. This brings us to point C, which is a point on the upper branch of the curve. If the applied voltage is either increased or decreased from this point, the upper branch will be traced. By increasing the voltage of  $+700$  mv, we arrive

again at point A, which is the intersection of the two branches of the characteristic. Further variation in the voltage in either direction will result in tracing the lower branch again.

It can now be seen that two distinct modes of converter operation exist when the voltage lies between points A and B. We shall designate the upper branch as the ignited mode due to the abrupt change which brings us from point B to point C. The lower branch is then termed the extinguished mode. Point B is called the ignition point, and point A is called the extinguishing point. The values of current and power obtained by operating in the useful region of the ignited mode are an order of magnitude greater than the values obtained at the corresponding voltage in the extinguished mode.

### 3.1.3 Work Function

The two modes of the I-V curves have similar shapes. The extinguished mode tends toward a constant current as the diode voltage is reduced with respect to the open-circuit voltage. Consequently, for the asymptotic current value, a work function can be calculated with the aid of the Richardson equation. For the ignited mode curve, a pseudo saturation current can be estimated and a work function calculated from it:

$$I_s = AT_E^2 \exp\left(-\frac{\phi}{kT_E}\right), \quad (3-1)$$

where  $I_s$  is the saturation current in amperes per square centimeter,  $A = 120 \text{ amp cm}^{-2} \text{ } ^\circ\text{K}^{-2}$ ,  $T_E$  is the emitter temperature in degrees Kelvin,  $\phi$  is the work function in electron volts, and  $k$  is Boltzmann's constant (11,600 eV/ $^\circ\text{K}$ ). The resulting values of work function for several cases are tabulated in Table 3-1.

Additional information relating to the ignited mode "work function" may be obtained when the value of "electron cooling" is known. Electron cooling (which was accurately measured for the first time under this program), is the average energy, measured in volts, carried from the emitter to the collector by the electrons. The magnitude of this energy is indicative of the highest potential barrier that must be

overcome for an electron originating in the interior of the emitter to arrive at and be absorbed by the collector. This highest potential barrier may be either the emitter work function, a point in the potential field which exists in the interelectrode space, or the sum of the collector work function and the output voltage. No matter which of the three potentials is the highest, the emitter work function cannot be greater than the measured value of electron cooling.

It is valuable to compare the "work function" information computed from the I-V curves and the electron cooling data to a previous measurement of the work function of a cesium-covered surface.

Measurements of the work function of molybdenum were recently reported by J. M. Houston [1].\* Houston presents S-curves that allow the determination of the work function  $\phi$  for any value of emitter temperature at two values of cesium pressure. These cesium pressures are considerably lower than those used in our diodes; therefore, it is necessary to extrapolate the data to a higher range. A similar extrapolation was employed by Langmuir and Taylor [2] with good results for the case of cesium on tungsten.

Figure 3-5 shows the results of the extrapolation of Houston's data. The technique used to construct this figure, following the example of Langmuir and Taylor, depends upon the following relationship, which exists between atoms evaporated from the emitter, and the emitter surface temperature:

$$\nu_a = CT_E^2 \exp\left(-\frac{B}{T_E}\right), \quad (3-2)$$

where  $\nu_a$  is the number of cesium atoms evaporated per square centimeter per second, C is a constant depending upon the emitter surface properties related to the number of atoms available for a specific cesium coverage, B is another constant depending upon the energy necessary to remove a cesium atom from the surface of a specific emitter material at a specific cesium coverage, and  $T_E$  is the temperature of the emitter surface in degrees Kelvin. This equation, which can be derived from

---

\*References are given in Section 5.0.

fundamental thermodynamic considerations (see Appendix E), is analagous to the Richardson equation. While the Richardson equation specifies an electron current density as a function of emitter surface properties, Eq. (3-2) specifies an atom current as a function of similar properties. A basic assumption of the equation is that the constants C and B are functions of cesium coverage on a particular emitter material and are independent of surface temperature.

Each of the curves of constant work function in Fig. 3-5 represents a plot of Eq. (3-2) for particular values of B and C. These values of B and C were determined from Houston's data, as described below.

Figure 3-6 is a schematic representation of Houston's S-curves. Choosing a value of  $\phi = 3$ , observe the intersection of the line  $\phi = 3$  with each of the S-curves for molybdenum at points M and N. The following information is now known:

$$\text{At point M: } (T_E)_1, (T_{Cs})_1, \phi_1 = 3.$$

$$\text{At point N: } (T_E)_2, (T_{Cs})_2, \phi_2 = 3.$$

Since  $\phi_1 = \phi_2$ , the cesium coverage must be the same for each point.

In addition,  $T_{Cs}$  can be related to the arrival rate of cesium atoms at the emitter surface ( $\mu_a$ ) from a relationship developed by Nottingham [3]:

$$\mu_a = 7.48 \times 10^{29} \times T_{Cs}^{-1} \exp\left(-\frac{8910}{T_{Cs}}\right), \quad (3-3)$$

where  $\mu_a$  is the atom arrival rate measured in atoms per square centimeter per second.

In turn, the atom arrival rate can be related to the atom evaporation rate since, for steady-state conditions,

$$\mu_a = \nu_a + \nu_p, \quad (3-4)$$

where  $\nu_a$  is the number of atoms evaporating from each square centimeter of the surface per second and  $\nu_p$  is the ion production rate of the surface in ions per square centimeter per second.

In the region of interest, however,  $\nu_p \ll \nu_a$ ; therefore,

$$\nu_a = \mu_a.$$

The following items are now determined:

At point M:  $(T_E)_1$ ,  $(T_{Cs})_1$ ,  $\phi_1 = 3$ , and  $(\nu_a)_1$ .

At point N:  $(T_E)_2$ ,  $(T_{Cs})_2$ ,  $\phi_2 = 3$ , and  $(\nu_a)_2$ .

We repeat Eq. (3-2):

$$\nu_a = CT_E^2 \exp\left(-\frac{B}{T_E}\right). \quad (3-2)$$

Since B and C depend only on cesium coverage and since the equality of  $\phi_1$  and  $\phi_2$  indicates identical coverage for conditions M and N, the values of  $T_E$  and  $\nu_a$  for points M and N may now be substituted in Eq. (3-2), and the values of B and C are determined.

Having determined the constants, Eq. (3-2) can be used to plot the curve for  $\phi = 3$  in Fig. 3-5. This calculation is then repeated, and the values of B and C are determined for other work functions. Thus, Fig. 3-5, which interpolates and extends the range of cesium reservoir temperatures, may be plotted from Houston's data.

With the use of the methods described above, the work functions for the emitter surface under the conditions given in Figs. 3-1 through 3-3 were computed and are listed in Table 3-I. Also listed in Table 3-I are the work function values derived from the "saturation" current condition of each figure for both the ignited and the extinguished modes. Note that in each of the three cases the value computed by extrapolating the Saha-Langmuir data falls between the values computed for extinguished and ignited modes from the respective "saturation" currents. The range of electron cooling values for the barrier (measured in the ignited mode)

is in good agreement with the ignited mode work function.

From these data and the above analysis, some preliminary qualitative conclusions can be drawn with regard to the mechanism of diode operation. Although no evidence has been found to contradict the hypothesis that follows, considerably more experimental evidence is needed to confirm it.

Figure 3-7 shows motive diagrams representing the extinguished and the ignited modes. The true emitter work function is represented by  $\phi_E$ . The collector is at a potential equal to  $\phi_C$  plus  $V_0$ . Following the extinguished mode diagram, the highest potential point is equal to  $\phi_E$  plus  $\delta$ , where  $\delta$  represents a negative space-charge barrier. The value of  $\delta$  is small (a few tenths of a volt) and the sum of  $\phi_E$  and  $\delta$  remains relatively unaffected by reducing  $V_0$ . This leads to a relatively constant value of current at low  $V_0$  and the value of the potential barrier associated with this current (column 2, Table 3-1) is higher than the true work function (column 3) by the space charge barrier  $\delta$ .

As  $V_0$  is reduced, the conditions existing in the ion trap (the most negative region in the interelectrode space) become unstable and the motive diagram assumes the ignited mode configuration. Thus, a plasma is established between two ion sheaths. The creation of the plasma-sheath configuration is accompanied by an apparent reduction of the emitter work function ( $\Delta\phi$  in Fig. 3-5). This phenomenon can be caused by one or more of the following mechanisms:

- (1) The high concentration of ions in the emitter sheath region effectively increases the arrival rate of cesium at the emitter, and thus lowers the emitter work function.

- (2) The steep potential gradient of the sheath causes field emission of electrons from the emitter.

- (3) Secondary emission of electrons is caused by ion bombardment of the emitter.

The ignited mode work function, then, must be lower than the value extrapolated from the Houston data, which is a true surface work function. An examination of

Table 3-I shows that this is indeed the case.

#### 3.1.4 Ion Currents

In a thermionic diode operating at a given emitter temperature and cesium pressure, a certain number of ions are generated at the emitter surface. The resulting flow of ions from the surface is called the ion current. Under this program, ion currents have been closely investigated for the first time.

The function of ions in a vapor diode is the neutralization of the electron space charge. This enables higher electron currents to pass from emitter to collector, and a higher output is obtained. Therefore, a knowledge of the ion current is important in the understanding of vapor diode operation. In addition, the emitter work function can be computed from the value of the ion current as follows.

$$I_i = I_a \left( \frac{kT_g}{2\pi M} \right)^{1/2} \left[ 2 \exp \left( - \frac{\phi_E - V_i}{\bar{V}} \right) \right] + 1, \quad (3-5)$$

where  $V_i$  is the ionization potential of cesium in volts,  $I_i$  is the ion current in amperes per square centimeter,  $I_a$  is the atom arrival rate expressed as a current (in amperes per square centimeter),  $k$  is Boltzmann's constant in volts per degree Kelvin,  $T_g$  is the temperature of the cesium gas in degrees Kelvin,  $M$  is the mass per atom in kilograms, and  $\bar{V}$  is the voltage equivalent of temperature.

During the reporting period, a technique was devised for taking ion current measurements. The object of this technique is to measure the ions produced by surface ionization at the emitter face. This is accomplished by making the collector negative with respect to the emitter and measuring the current passing between the electrodes. This measurement includes ion current plus any electron back emission from the collector, since electrons emitted by the collector are accelerated toward the emitter by the same potential field that causes the positive ions to flow in the opposite direction. To eliminate the effect of the back emission,

it is subsequently measured by lowering the emitter temperature (so that no ions are generated) and maintaining the collector temperature, cesium pressure, and applied electric field at the same values. The current produced under this condition is the back emission. This value is then subtracted from the first reading and yields an accurate measurement of the ion current, which should be independent of collector temperature if Eq. (3-5) is valid.

The initial results sharply contradicted this prediction. The values of ion current measured by this method show a strong variation with collector temperature. Figure 3-8 is a plot of the ion current against collector temperature, with constant emitter and cesium bath temperatures. This curve shows that a change of 100°K in collector temperature (from 460 to 560°K) results in a tenfold increase in ion current (10 to 100 ma). One possible cause of this behavior is secondary emission of electrons from the collector produced by cesium ion bombardment as a result of the strong electric fields applied in the experiment.

An effort is now under way to devise more refined experimental procedures to take such phenomena into account and make it possible to isolate and measure the true ion current generated at the emitter.

#### 3.1.5 Ignition

The discontinuity observed in Fig. 3-2, when the output current value jumps from point B to point C, is called "ignition." This is the phenomenon that shifts the operating point from the extinguished mode to the more desirable and physically more complex ignited mode. It is expected that a better understanding of the ignition phenomenon will make it possible to formulate the mechanism of ignited mode operation.

An experimental program was started late in the reporting period to gather data on ignition. This program is still in its initial stages, but some tentative conclusions may be drawn from the available data.

Figure 3-9(a) shows the variation of ignition potential with cesium pressure for a fixed emitter temperature (1653°K). Three curves are plotted, each corresponding to a different collector temperature. On the ordinate of this graph are plotted the values of the potential of the emitter with respect to the collector that permit ignition. The values below zero indicate that the emitter is positive with respect to the collector. This is the polarity of the unit for power generation. Values above zero indicate that the emitter is negative with respect to the collector and that power is consumed by the unit from an external voltage source. The greater the negative potential required for ignition, the more energy must be supplied from the external source.

For the purpose of this discussion, let us select curve 2 and follow its course from low to high values of cesium pressure. It may be observed that, at low cesium pressure, ignition requires extremely high negative potentials, but as the pressure is increased above 0.1 mm Hg, the required negative potential rapidly decreases until it becomes positive at about 0.4 mm Hg. A further increase in pressure results in a reversal of the curve, which then climbs back into the negative region and reaches a peak at 0.5 mm Hg. As cesium pressure continues to rise, another drop in potential is observed, followed by a region of relatively constant ignition potential from about 1 to 10 mm Hg. Finally, as the pressure is raised above 10 mm Hg, the ignition potential exhibits a slow rise.

Referring to Fig. 3-7, we have postulated that ignition occurs when the extinguished mode potential distribution (shown by the upper line in the figure) becomes unstable. This instability arises through an overabundance of ions trapped in the region labelled "ion trap." The density of ions trapped in this region depends on the ion production rate and the number of collisions. The dependency upon ion production rate is obvious. The generated ions experience a force from the electric field which tends to return them to the emitter. The number of collisions is a measure of the resistance that the ions encounter while returning to the emitter.

Therefore, the greater the number of collisions, the longer the ions reside in the ion trap; hence, the higher the density of ions. The ion production rate (expressed as an ion current) and a measure of the number of collisions (ratio of interelectrode spacing to mean-free path) are plotted in Fig. 3-9(b) on the same cesium pressure scale used for the ignition potential curve. Although no quantitative relationship among these three variables has yet been formulated, a qualitative explanation may be attempted.

At cesium pressures below 0.3 mm Hg, we observe high values of ion current, which rapidly decline as cesium pressure rises. On the other hand, the number of collisions in the interelectrode space is extremely small, as indicated by the value of  $w/\lambda$ . This means that a large number of ions are generated, but they are not effective in increasing the ion density. As the cesium pressure is increased, the ion current decreases. However, the increase in  $w/\lambda$  and, therefore, the number of collisions, more than offsets the ion current decrease, and the ion density increases. Thus, the ignition potential becomes less negative. This relationship continues until a pressure of about 0.35 mm Hg is reached. At this point, virtually all the ions are being retarded by collision and are trapped, and the continued increase of  $w/\lambda$  no longer increases the ion density. Thus, a reversal occurs in the ignition potential curve since the ion current is still decreasing at a substantial rate. When a pressure of about 1 mm Hg is reached, the rate of decrease of ion current is greatly reduced, and the change of ignition potential with cesium pressure becomes negligible.

The above analysis cannot be considered as an exact description of the relationships among the parameters in question, but it will serve as a guide for further experimentation. It should be noted, however, that for the first time a framework is available for developing a sound theory of cesium diode operation in more than one mode.

## 3.2 Thermal Characteristics

### 3.2.1 Cesium Conduction

One of the mechanisms through which heat is lost from the emitter is that of conduction through the cesium vapor. Practically, all of this heat is conducted to the collector since the space between emitter and collector is at least an order of magnitude smaller than that between the emitter and any other part of the diode. A knowledge of this quantity is of great value in efficiency calculations and is an important tool for diode design.

Figure 3-10 is a summation of the experimental data obtained on cesium conduction during the reporting period. It is a plot of cesium gas conductivity against cesium pressure. For pressures below 0.5 mm Hg, the conductivity is negligible. In the pressure range of 0.5 to 20 mm Hg, the conductivity increases as pressure increases. In this region, the cesium may be considered as a rarefied gas; therefore, the conductivity should vary with pressure. When cesium pressure is about 20 mm Hg, the ratio of spacing to mean-free path is quite large, and for higher cesium pressures the conductivity remains constant.

For comparison, Fig. 3-10 includes plots of the variation in cesium conductivity with pressure as calculated by the Knudson free-molecule conductivity equation [4] and the kinetic theory of gases [5] in the regions where each is applicable.

Computations using the Knudson equation assumed an accommodation coefficient of 1.0. In reality, however, this coefficient is less than unity, and the resulting curve is an upper limit of conductivity values. Thus, the position of our experimental results below the Knudson plot is in accord with the analytical prediction.

To compute gas conductivity by kinetic theory, a value must be chosen for the collision cross section of the cesium atoms. The values for this cross section reported in the literature are not consistent and, depending on the one chosen, the

resulting thermal conductivity value may vary by  $\pm 30\%$ . Therefore, it may be concluded that our experimental results are in good agreement with the kinetic theory.

### 3.2.2 Electron Cooling

Electron cooling has been defined, and its significance as an electrical characteristic has been discussed previously (Section 3.1.3). However, it is also important to examine electron cooling as a thermal property since it represents an irreversible process in which a portion of higher-order energy is converted to heat. The electrons leave the emitter with an energy equal to the electron cooling value. Upon arrival at the collector, a portion of the energy of the electrons is recovered as useful output, and the remainder is converted to heat which then is rejected at the collector temperature to the thermodynamic heat sink.

In terms of diode design, especially in heat balance and efficiency calculations, knowledge of electron cooling values is extremely important. The data obtained under this program have, for the first time, supplied accurate electron cooling information, and now permit significantly improved design predictions.

### 3.2.3 Radiation

Radiation heat transfer between emitter and collector is another important heat loss mechanism which requires investigation. The test vehicle used in these experiments (see Appendix A) permits accurate measurement of this quantity. Appendix C describes the method used to measure the radiation.

During the first quarter, no experiments were performed to determine radiation values. This work will be initiated during the second quarter.

## 3.3 Power and Efficiency

Power and efficiency are the two prime indicators of performance in an operating unit, and the ultimate aim of all thermionic research and development

is the achievement of high power densities and, consequently, high efficiencies. It has been the basic philosophy of this program to approach these goals by developing a thorough understanding of thermionic generator operation, rather than by trial and error, as has often been the case in the past. Therefore, the test vehicle, which is the tool for achieving this goal, has been designed to yield a maximum amount of information over the entire range of parameter variation. Consequently, this diode test vehicle has not been designed for maximum efficiency.

In view of these considerations, the efficiency of this test vehicle is of little significance. However, the data collected at any given operating condition permit the prediction of efficiencies for a generator that would be optimized for that particular condition. This is accomplished through the use of the experimental values of output power and thermal losses which have been made available through carefully controlled experimentation with the test vehicle.

Figure 3-11 shows the maximum power density obtained at each emitter temperature by optimizing all other variables for this condition. A plot is shown for each of the experimental diodes tested during this quarter. The diode that uses molybdenum for both the emitter and the collector exhibits approximately double the power density of the diode that has a tantalum emitter and a molybdenum collector when the two tubes are operated at the same emitter temperature. From another point of view, it may be said that the Mo-Mo tube gives the same performance as the Ta-Mo tube, but at emitter temperatures 100 to 150° lower. Since lower-temperature operation means lower heat losses, a substantial improvement in efficiency results.

A typical computation to predict efficiency from the type of data which has been collected on this program is presented below. An emitter temperature of 1600°K has been chosen for this sample computation, since this is the point at which the most complete set of data is available for both experimental tubes.

(1) Tabulated values.

| <u>Item</u>                             | <u>Ta-Mo</u>          | <u>Mo-Mo</u>          |
|---|-----------------------|-----------------------|
| Emitter temperature $T_E$               | 1600°K                | 1600°K                |
| Collector temperature $T_C$             | 925°K                 | 925°K                 |
| Cesium bath temperature $T_{Cs}$        | 553°K                 | 553°K                 |
| Cesium pressure                         | 1 mm Hg               | 1 mm Hg               |
| Output power density                    | 0.5 w/cm <sup>2</sup> | 2.7 w/cm <sup>2</sup> |
| Output current density                  | 1 amp/cm <sup>2</sup> | 9 amp/cm <sup>2</sup> |
| Output voltage                          | 0.5 v                 | 0.3 v                 |
| Electron cooling ( $V = w/\text{amp}$ ) | 2.7 v                 | 2.5 v                 |
| Radiation emissivity factor             | 0.22                  | 0.19                  |

(2) Heat losses.

a. Radiation.

$$Q_R = \mathcal{F} (Q_{bbE} - Q_{bbC}),$$

where

$$Q_{bbE} = \text{blackbody radiation at emitter temperature} \\ = 37 \text{ w/cm}^2 [6],$$

$$Q_{bbC} = \text{blackbody radiation at collector temperature} \\ = 4 \text{ w/cm}^2 [6],$$

$$\mathcal{F} = (\epsilon_E^{-1} + \epsilon_C^{-1} - 1)^{-1}.$$

$$\begin{aligned} \text{Ta-Mo} \\ Q_R &= 0.22 \times (37 - 4) \\ &= 7.3 \end{aligned}$$

$$\begin{aligned} \text{Mo-Mo} \\ Q_R &= 0.19 \times (37 - 4) \\ &= 6.3 \end{aligned}$$

b. Cesium conduction

$$Q_R = \Lambda (T_E - T_C);$$

$\Lambda$  = conduction heat loss ( $w \text{ cm}^{-2} \text{ }^\circ\text{C}^{-1}$ ).

Since both diodes operate at the same cesium pressure (1 mm Hg) and at the same emitter and collector temperatures, they will have the same value of  $Q_{Cs}$ .

$\Lambda$  at 1 mm Hg is found from Fig. 3-10 to be  $0.001 w \text{ cm}^{-2} \text{ }^\circ\text{C}^{-1}$ .

Then

$$Q_{Cs} = 0.001 (1600 - 925) = 0.775 w/\text{cm}^2.$$

c. Emitter lead conduction.

$Q_c$  = conduction losses through the emitter lead (emitter support sleeve).

For the design of a lead optimized to give minimum (electrical and thermal) losses under particular operating conditions, the following equation is used:

$$Q_c = I \left( \frac{1 - \eta}{\eta} \right) \left( \frac{2\eta}{2 - \eta} \right)^{1/2} (\rho k \Delta T)^{1/2},$$

$\eta$  = diode efficiency,

$\rho$  = electrical resistivity of lead material (ohms-cm),

$k$  = thermal conductivity of lead material ( $w \text{ }^\circ\text{C}^{-1} \text{ cm}^{-1}$ ),

$\Delta T = T_E - T_C$  ( $^\circ\text{C}$ ).

The use of a tantalum lead is most probable. Therefore,

$$\rho_{Ta} = 55 \times 10^{-6} \text{ ohm-cm},$$

$$k_{Ta} = 0.585 w \text{ }^\circ\text{C}^{-1} \text{ cm}^{-1},$$

$$\Delta T = 1600 - 925 = 775^\circ\text{C}.$$

The solution of this equation is an iterative process since an efficiency must be assumed in order to find  $Q_c$ .

$$Q_c = \frac{\text{Ta-Mo}}{0.52 w/\text{cm}^2}$$

$$Q_c = \frac{\text{Mo-Mo}}{3.6 w/\text{cm}^2}$$

d. Electron cooling.

$$Q_{ec} = E_c \times I;$$

$Q_{ec}$  = electron cooling (includes heat loss and power output),

$E_c$  = measured electron cooling (volts),

$I$  = output current (amp).

$$\begin{aligned} \frac{\text{Ta-Mo}}{Q_{ec}} &= 2.7 \times 1 \\ &= 2.7 \end{aligned}$$

$$\begin{aligned} \frac{\text{Mo-Mo}}{Q_{ec}} &= 2.5 \times 9 \\ &= 22.5 \end{aligned}$$

(3) Efficiency.

$$\eta = \frac{P_o}{Q_R + Q_{Cs} + Q_c + Q_{ec}}$$

( $Q_{ec}$  includes the value of  $P_o$ ).

$$\begin{aligned} \frac{\text{Ta-Mo}}{\eta} &= \frac{0.5}{7.3 + 0.775 + 0.52 + 0.27} \\ &= \frac{0.5}{11.3} = 4.43\% \end{aligned}$$

$$\begin{aligned} \frac{\text{Mo-Mo}}{\eta} &= \frac{2.7}{6.3 + 0.775 + 3.6 + 2.25} \\ &= \frac{2.7}{33.2} = 8.14\% \end{aligned}$$

These values of efficiency are for diode operation at the point of maximum power output for a given emitter temperature. They do not represent the maximum achievable efficiency for the same emitter temperature. To determine the maximum efficiency for a given emitter temperature, it is necessary to perform a number of similar computations at other points on the same I-V curve, and then to perform a similar series of calculations for other I-V curves, obtained at the same emitter temperature but various collector temperatures and cesium pressures.

This type of calculation would at first glance seem to require an immense volume of data and machine computation. However, our experiments have shown that the only quantity that seriously affects the optimization of efficiency at a given emitter temperature is electron cooling. Therefore, a limited series of experiments can be planned to determine the variation in electron cooling with output power and allow calculation of optimized efficiency with a reasonable effort. Once a relationship has been established between electron cooling and the experimental variables ( $T_E$ ,  $T_C$ , and  $T_{Cs}$ ), the determination of optimum efficiency will be considerably simpler and more direct. Such a relationship is one of the long-term objectives of the work initiated under this program.

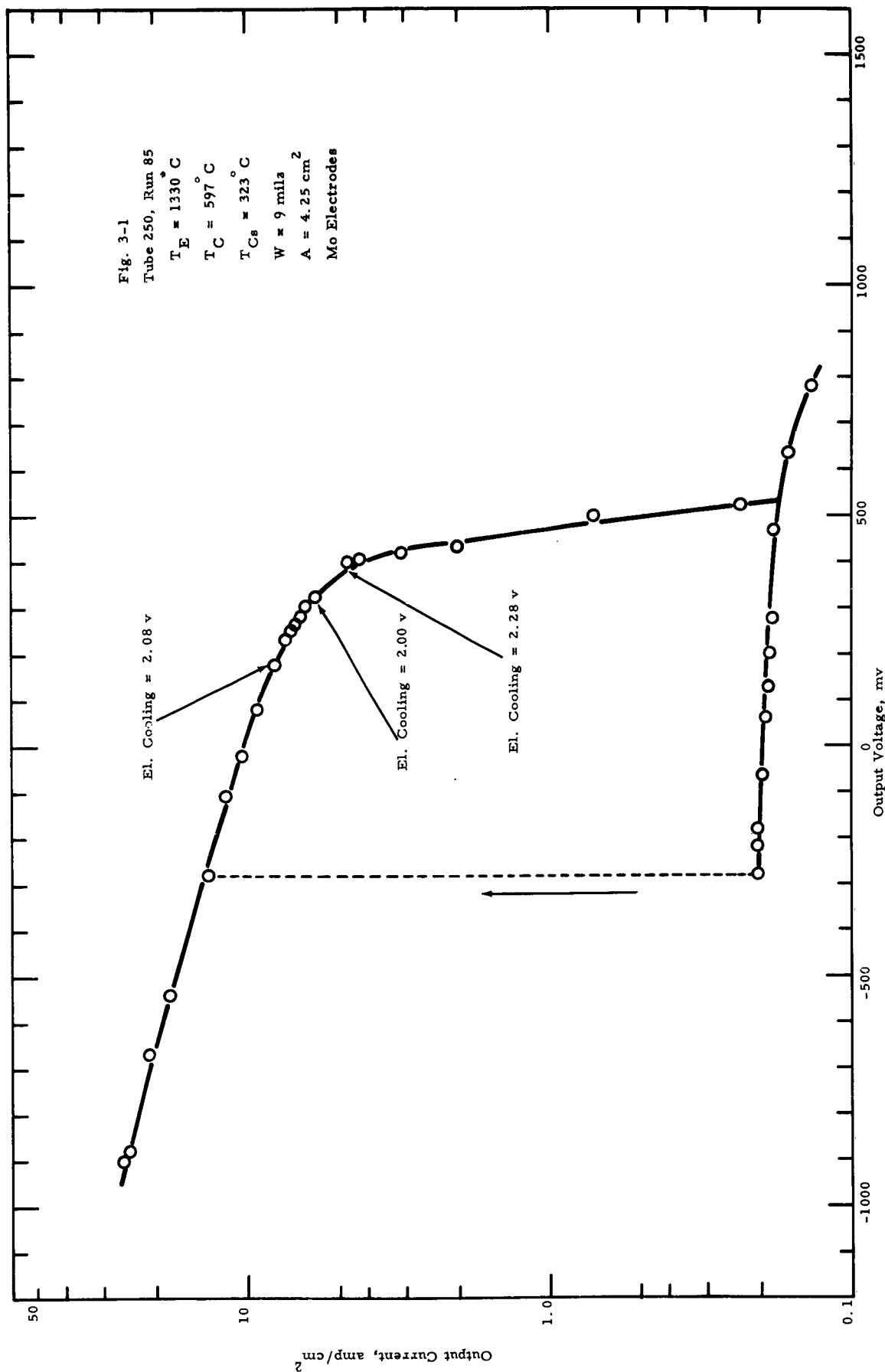
### 3.4 Spacing

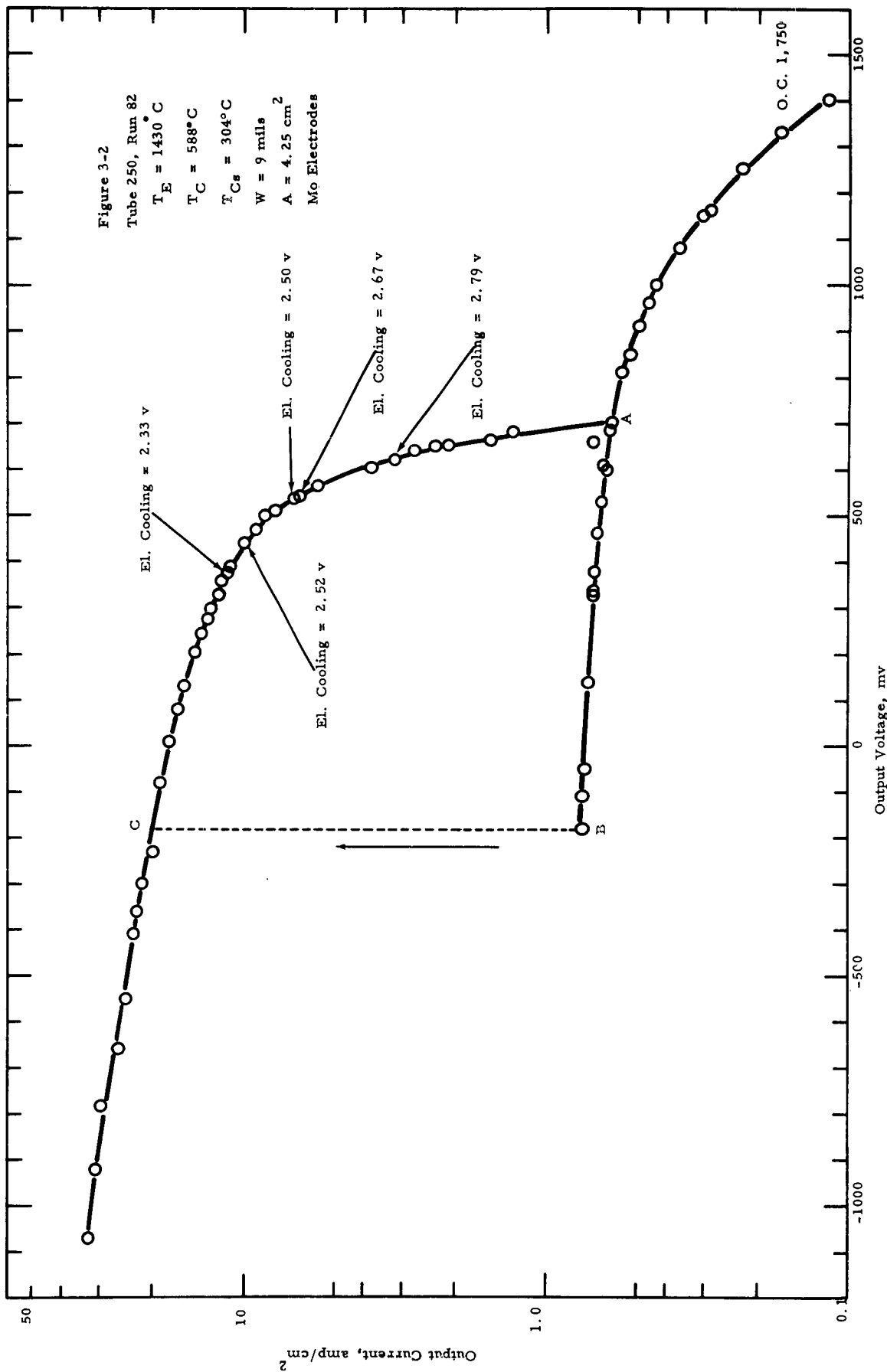
The design of the test vehicle allows for variation of the interelectrode spacing of each of the test diodes. The method of setting the spacing (see Appendix A) enables accurate adjustment of the spacing to a known value.

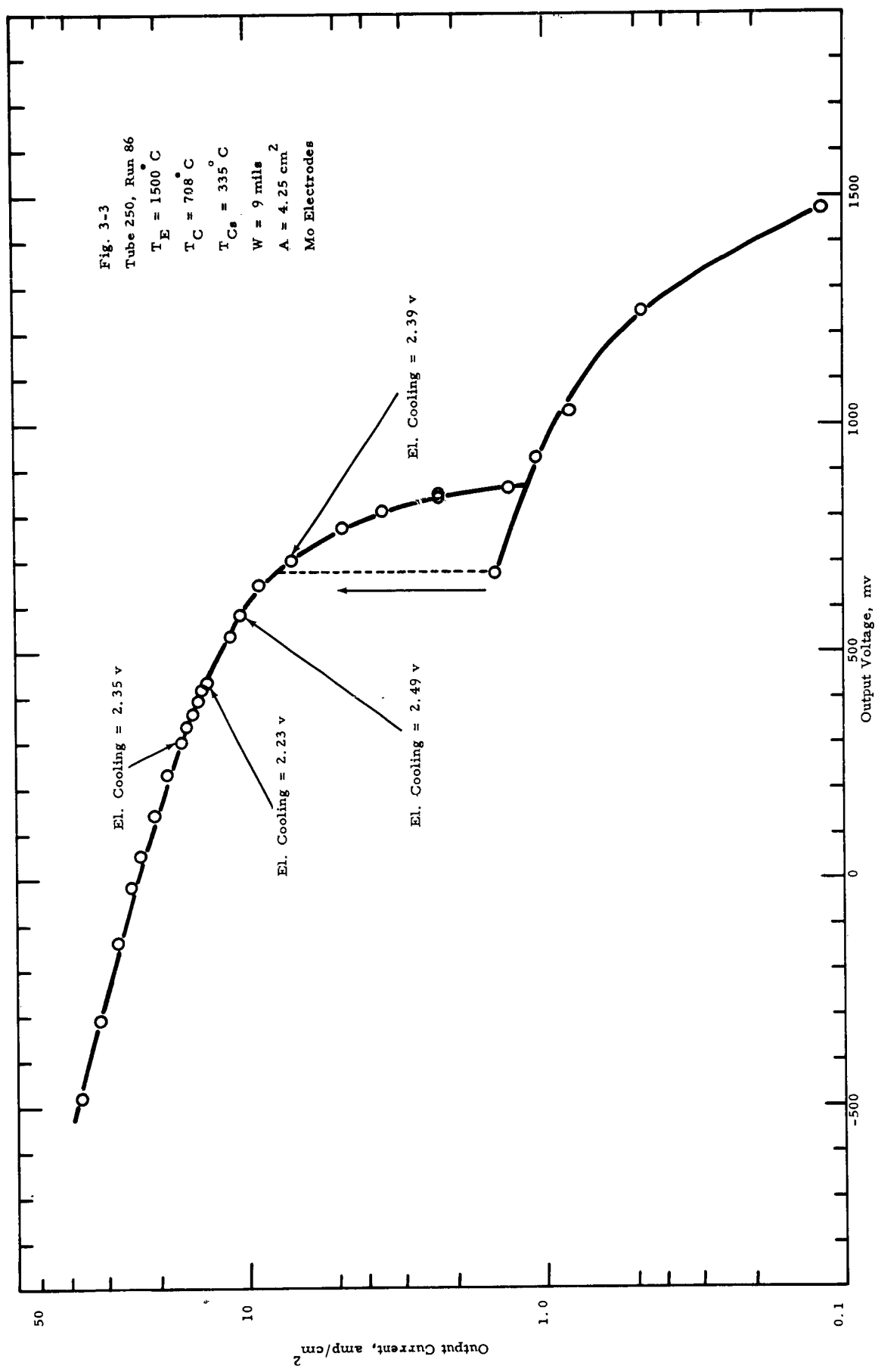
Considerable experimental data were collected by running the Mo-Mo tube at spacings varying from 2 to 12 mils. For the temperature range between 1300 and 1500°C, the data indicate that maximum output power shows a peak at spacings between 8 and 10 mils. Similar experimentation was initiated later in the quarter with the Ta-Mo tube, but sufficient data are not yet available to allow any conclusions to be drawn.

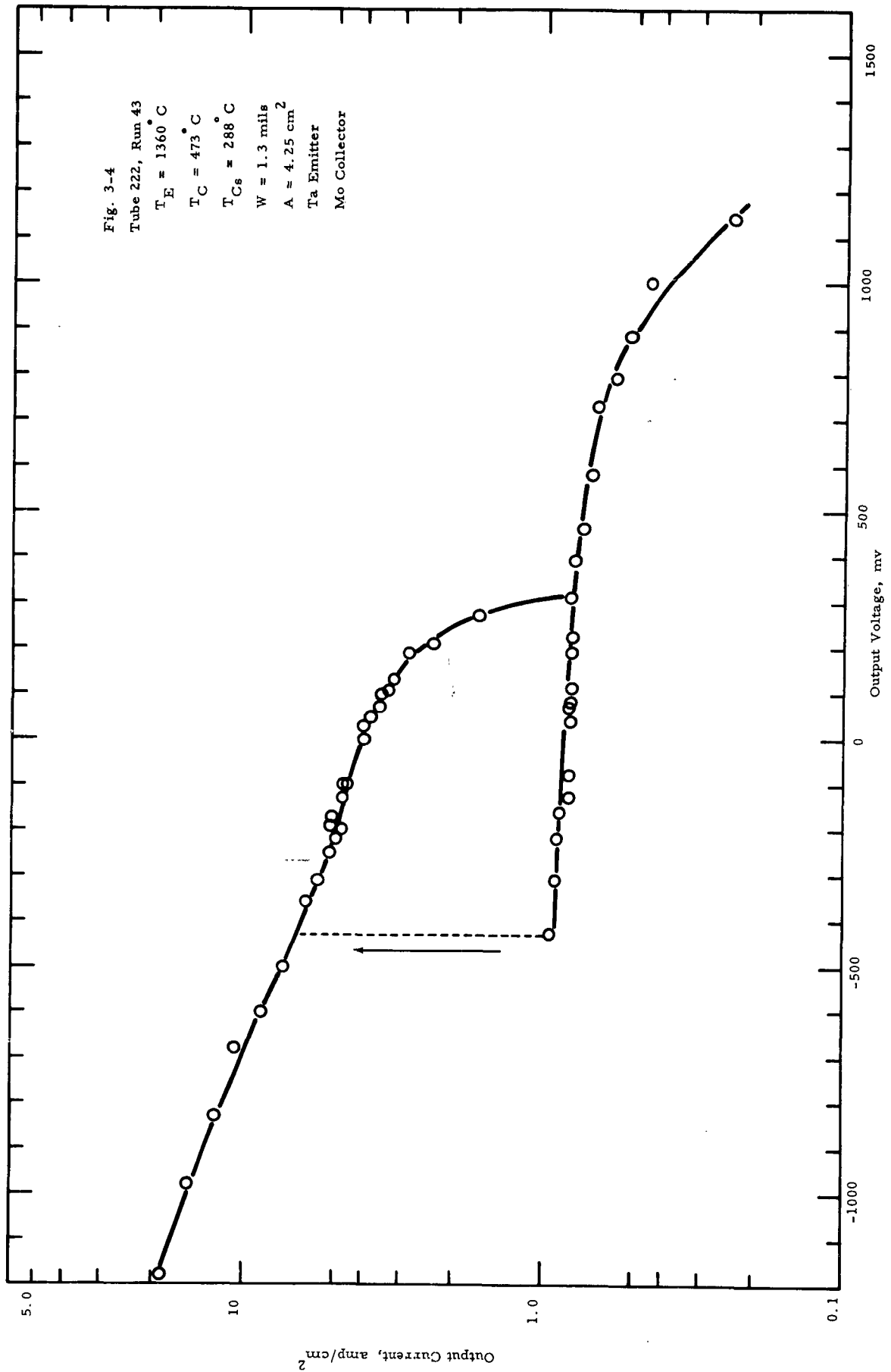
The peak in output power of the Mo-Mo tube at a fairly large spacing had not been predicted by previous studies. The cause of this peak has not yet been explained. It is expected that a theoretical concept can be developed only after further experimentation.

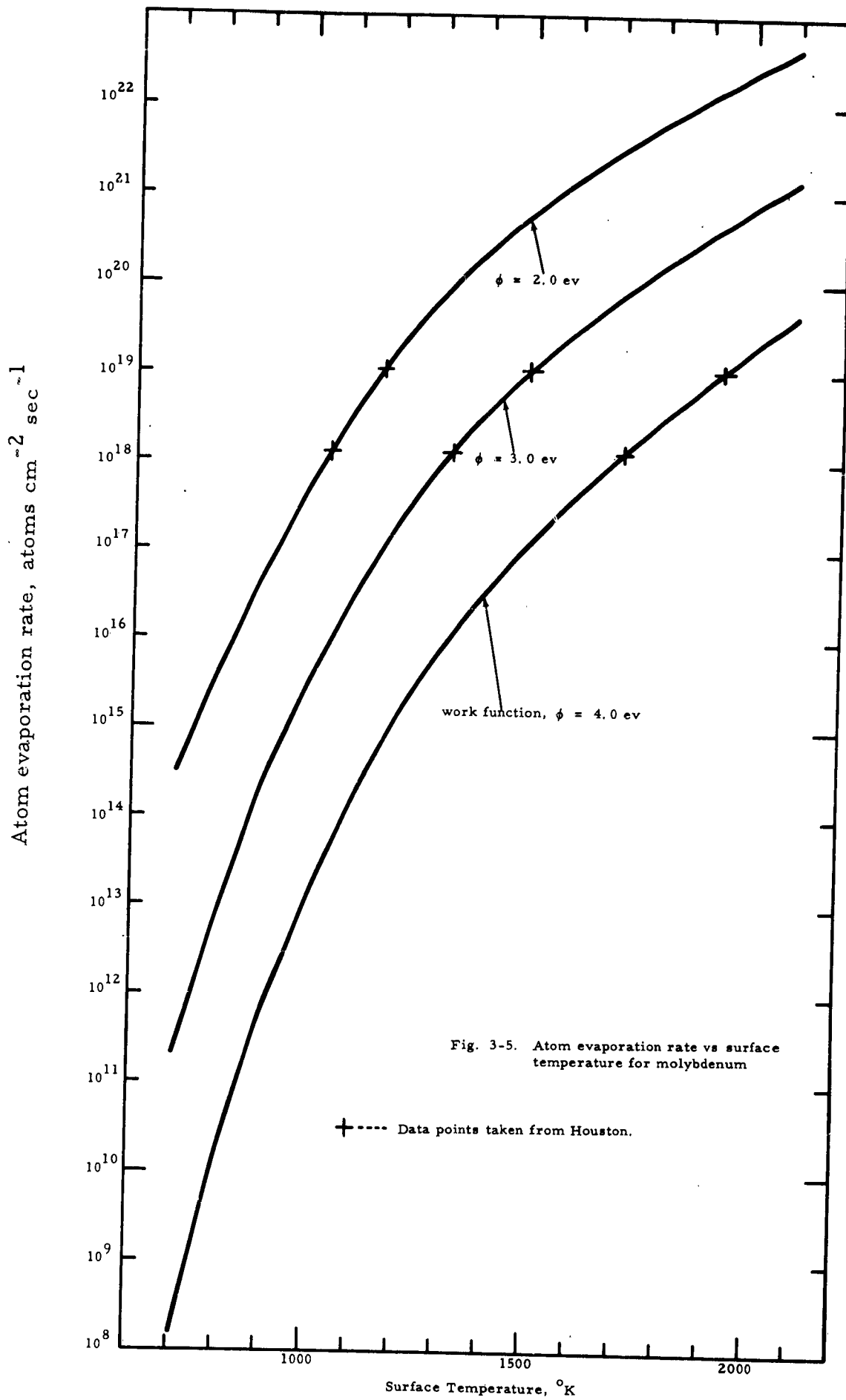
It is fortunate, from the hardware design standpoint, that the optimum spacing, at least at these emitter temperatures, is greater than the minimum attainable.











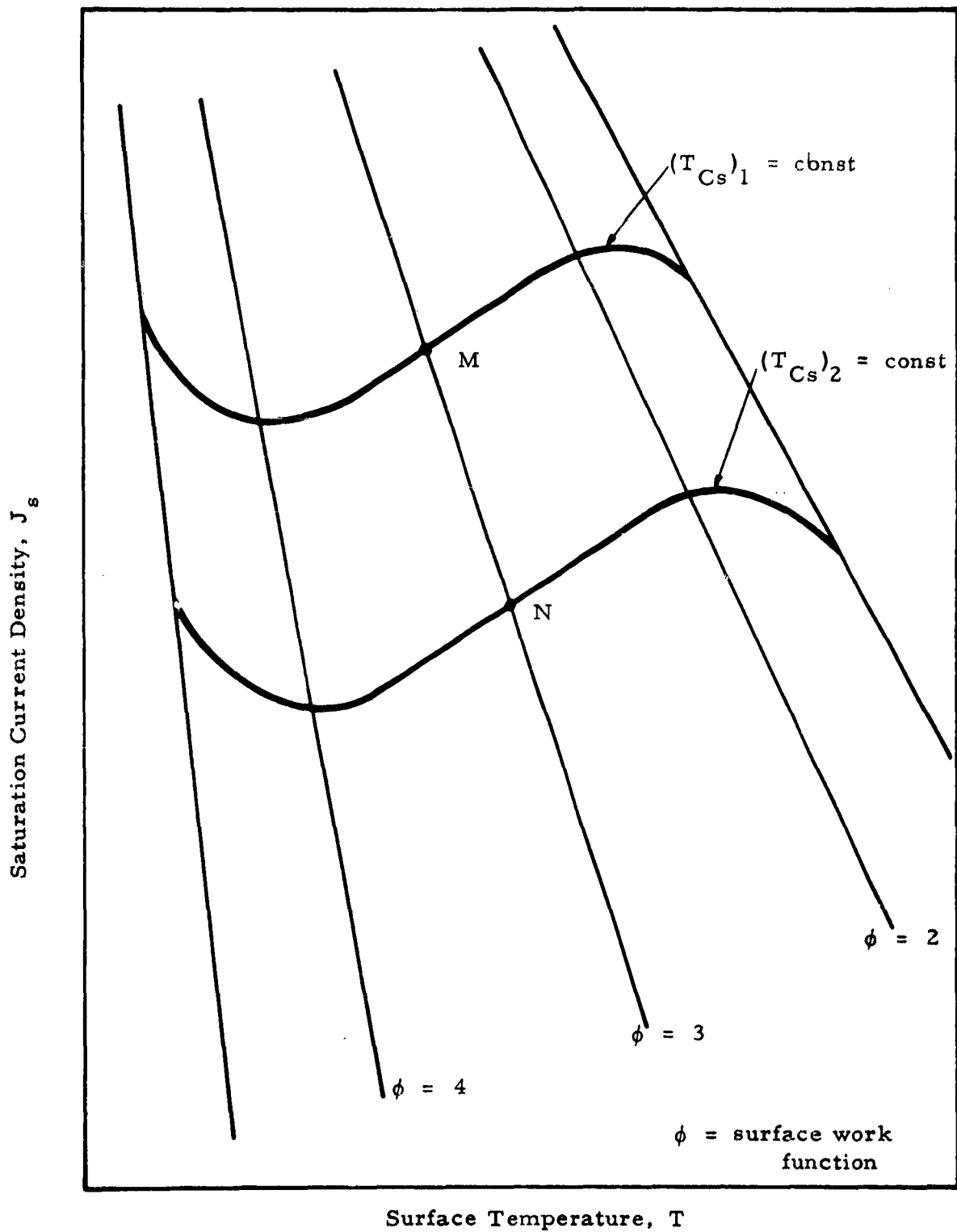


Fig. 3-6. Schematic representation of "S" curves

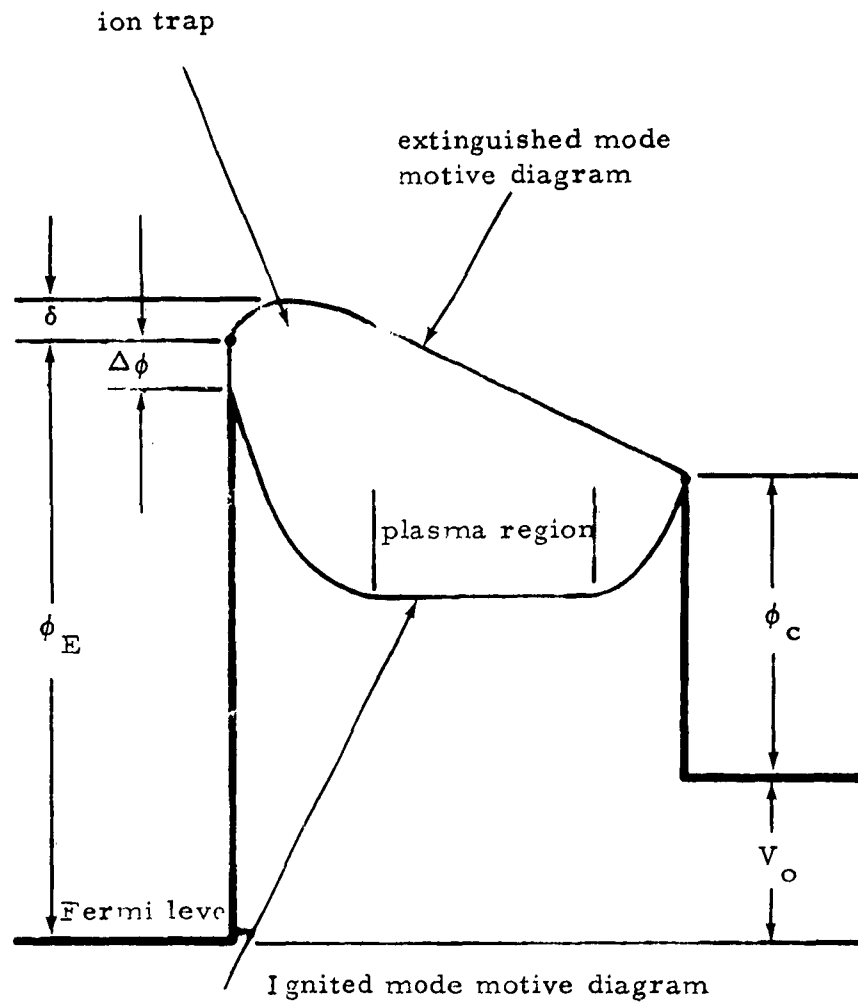


Fig. 3-7. Motive diagram

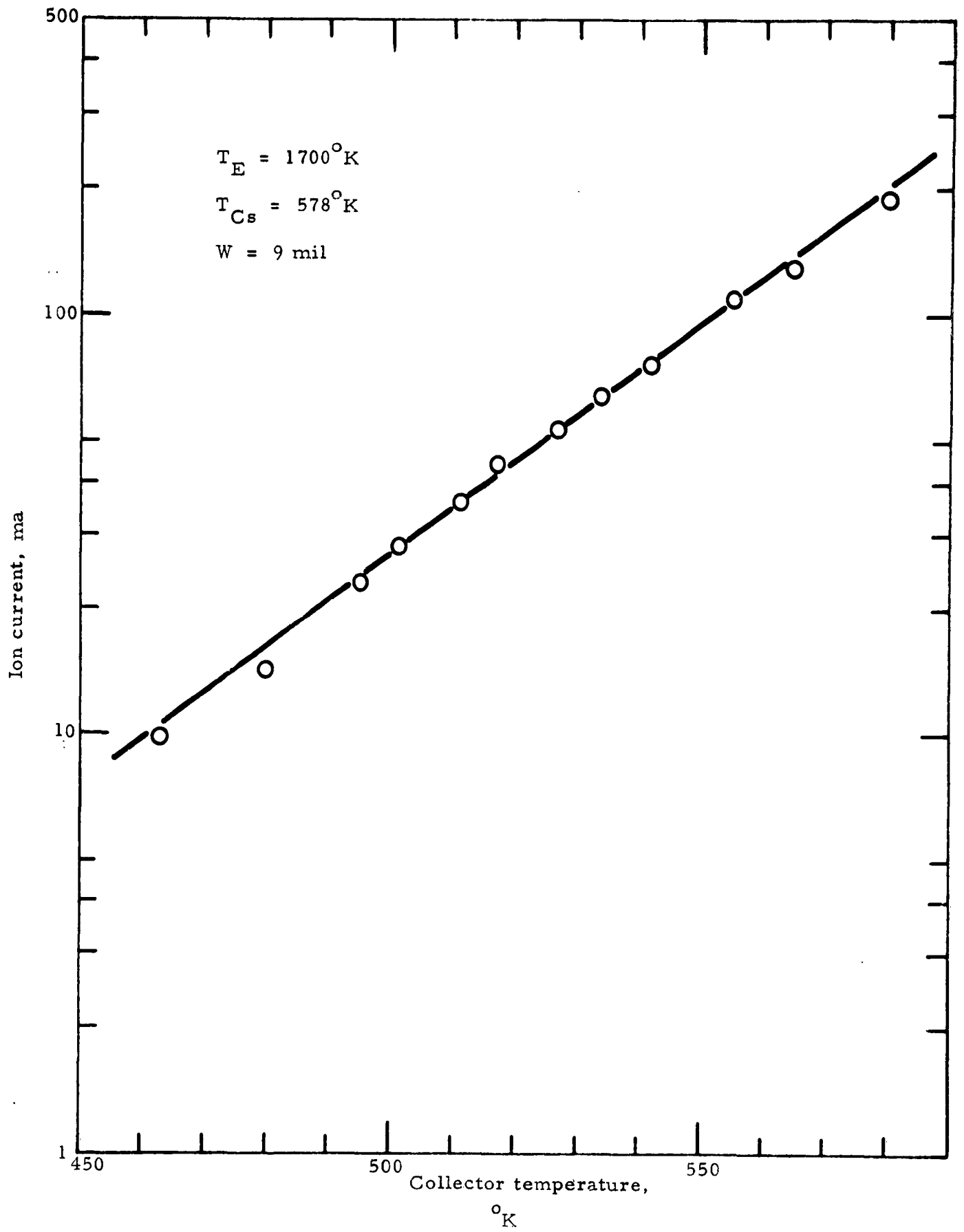


Fig. 3-8. Ion current vs collector temperature

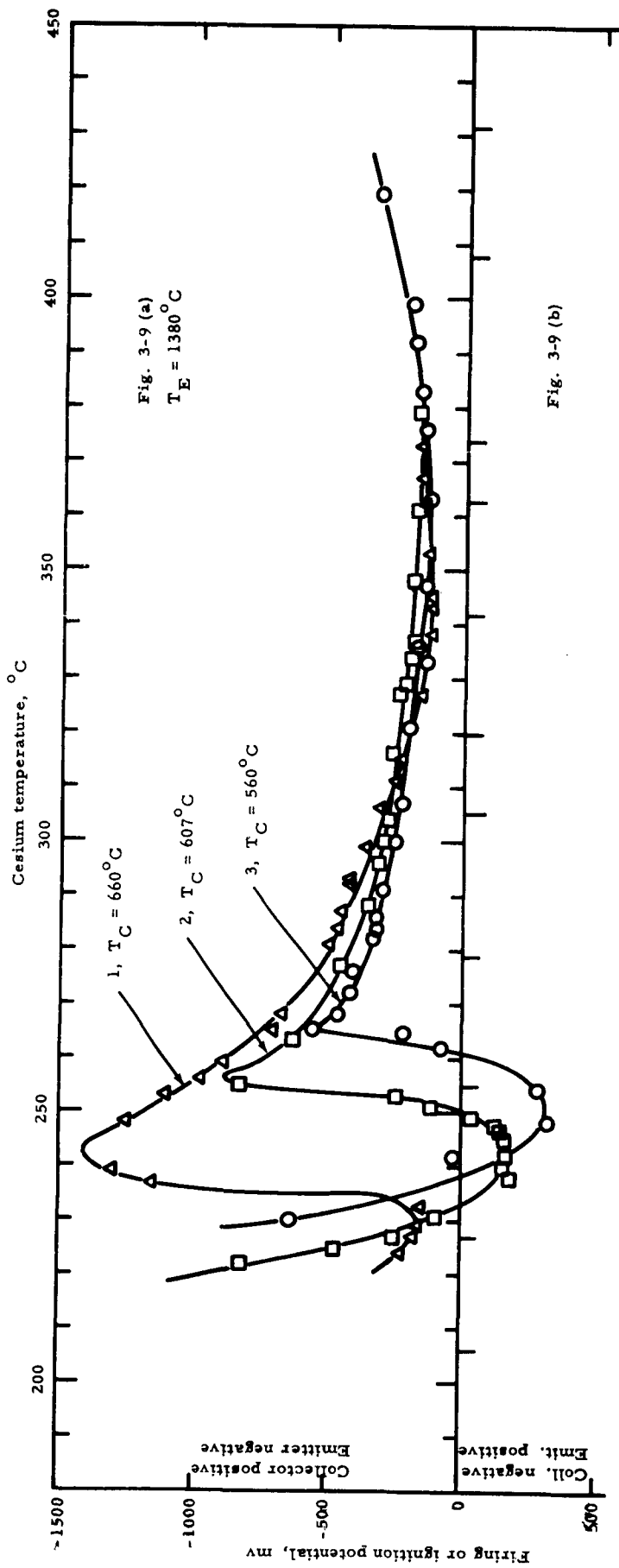
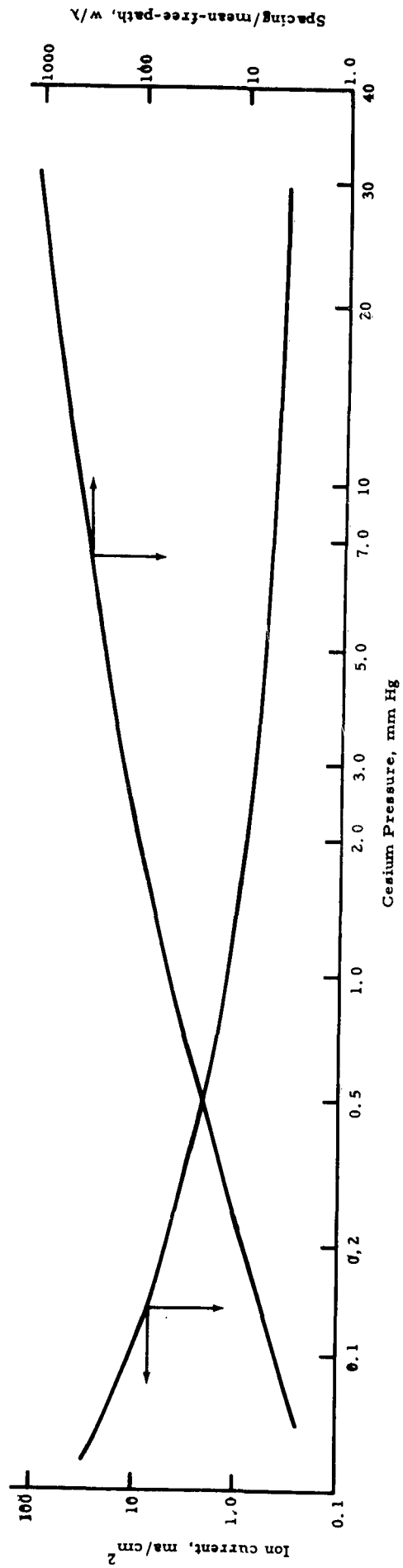
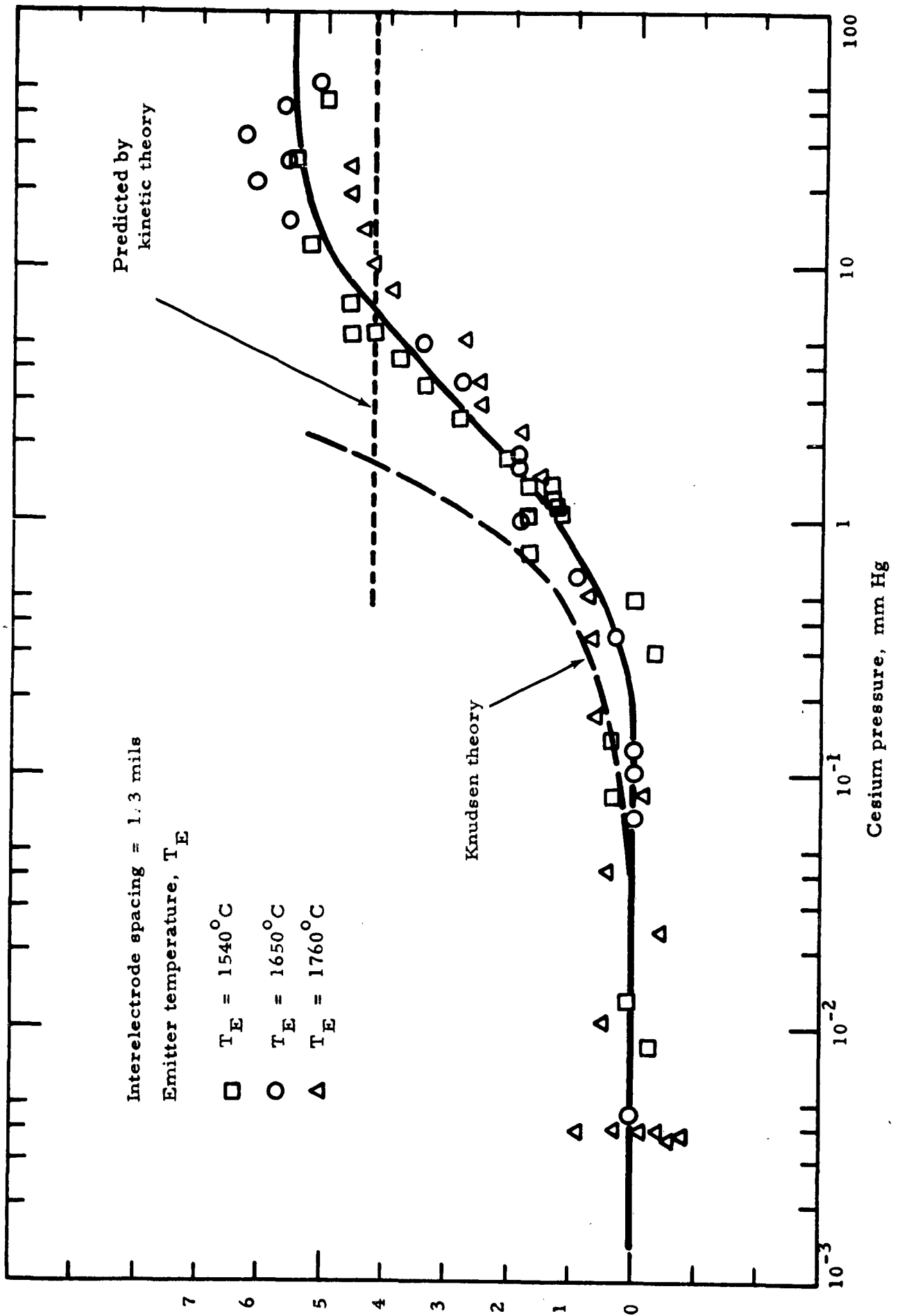


Fig. 3-9 (b)



Spacing/mean-free-path,  $w/\lambda$

Fig. 3-10. Cesium conduction vs cesium pressure



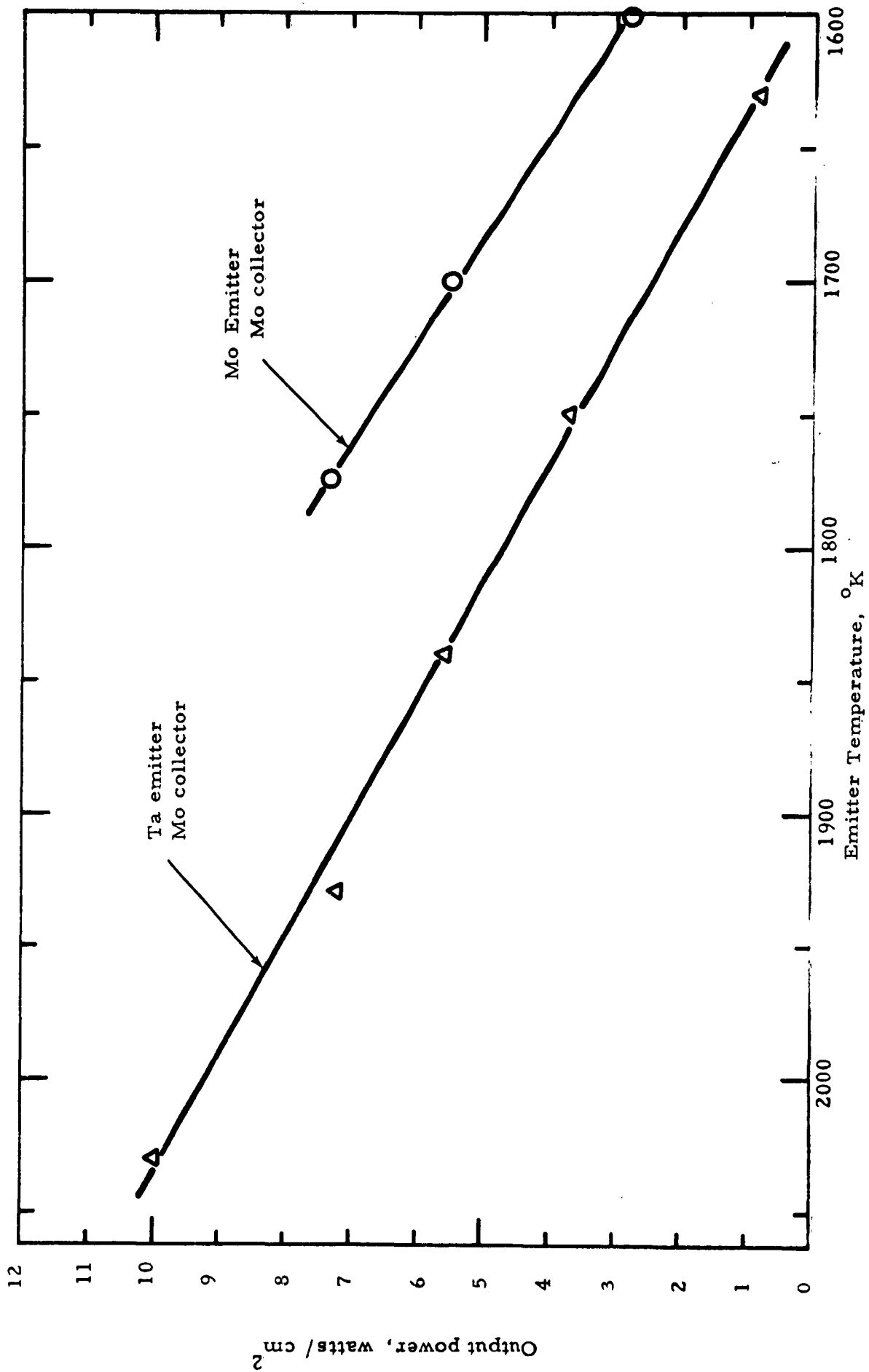


Fig. 3-11. Maximum power output vs emitter temperature

TABLE 3-I

WORK FUNCTIONS OF A CESIUM-COVERED MOLYBDENUM EMITTER  
AS OBTAINED BY VARIOUS METHODS

| Figure | Work function, ev |                   |  |  |
|--------|-------------------|-------------------|--|--|
|        | Ignited mode      | Extinguished mode | Langmuir type extrapolation of saturation data | Electron cooling barrier in ignited mode |
| 3-1    | 2.2               | 2.88              | 2.40   | 2.0 to 2.3                               |
| 3-2    | 2.4               | 2.92              | 2.70   | 2.5 to 2.8                               |
| 3-3    | 2.4               | 2.93              | 2.65   | 2.3 to 2.5                               |

#### 4.0 PLANS FOR THE SECOND QUARTER

During the second quarter, the experimental work will continue with the tantalum-molybdenum and molybdenum-molybdenum diodes. Special attention will be given to improvement of the techniques for accurate measurement of ion currents since the present measurements are not satisfactory. More extensive data will be taken on the Ta-Mo tube at a greater variety of spacings and temperatures to determine whether the optimized spacing is other than the minimum achievable. Radiation loss measurements will be made. On the Mo-Mo tube, operation with an emitter temperature of 1300 °C (or less) will be attempted. By the end of the quarter, the data collected on the Mo-Mo tube should be sufficient to permit accurate correlations to be prepared. At that time theoretical work will be intensified.

The rhenium-molybdenum and tungsten-molybdenum test vehicles will be completed, and experimental work with them will be initiated.

To facilitate the collection and reduction of the massive amount of data required, improvements will be made in the current test set-up and a second test set-up will be completed. The automatic recording and plotting devices that are being integrated into the test set-ups will greatly improve the speed and efficiency of both the experimental work and the data reduction.

Correlation and theoretical analysis will continue and be increased as more test results become available.

If time permits, a diode will be fabricated of a fifth emitter material, to be chosen after careful examination of the significant properties of several materials now under consideration.

Tests to examine the compatibility of various emitter materials with uranium carbide will be examined.

The schedule for the remainder of the contract year is shown in Table 4-I.

TABLE 4-I

CONSOLIDATED WORK SCHEDULE\*

| Task  | Jul | Aug | Sep | Oct | Nov | Dec | Jan | Feb | Mar | Apr | May | Jun |
|---|-----|-----|-----|-----|-----|-----|-----|-----|-----|-----|-----|-----|
| A. Test vehicle construction                |     |     |     |     |     |     |     |     |     |     |     |     |
| B. Test vehicle testing                     |     |     |     |     |     |     |     |     |     |     |     |     |
| C. UC compatibility tests                   |     |     |     |     |     |     |     |     |     |     |     |     |
| D. Test equipment construction and purchase |     |     |     |     |     |     |     |     |     |     |     |     |
| E. Data reduction and analysis              |     |     |     |     |     |     |     |     |     |     |     |     |
| F. Report writing                           |     |     |     |     |     |     |     |     |     |     |     |     |

\*Contract No. 4015 ARPA; NONR-3563(00).

## 5.0 REFERENCES

1. Houston, John M., "Thermionic Emission of Refractory Metals in Cesium Vapor," Appendix F-1, Proc. of the Round Table Discussion on Cathode Emission Investigations and Exptl. Techniques for Fabrication and Operating Thermionic Cells, June 1, 1961, Power Info. Ctr., Univ. of Penn., Philadelphia.
2. Taylor and Langmuir, "The Evaporation of Atoms, Ions and Electrons from Cesium on Tungsten," Phys. Rev. vol. 44, no. 6 (Sept. 15, 1933).
3. Nottingham, W. B., General Theory of the Plasma Diode Energy Converter, report TEE-7002-5, Thermo Electron Engineering Corp., Waltham 54, Mass. (undated).
4. Dushman, Scientific Foundations of Vacuum Technology, p. 52. New York: John Wiley & Sons, Inc., 1949.
5. Sears, An Introduction to Thermodynamics, The Kinetic Theory of Gases, and Statistical Mechanics, 2nd ed. Reading, Mass.: Addison-Wesley Pub. Co., Inc., 1953.
6. American Institute of Physics Handbook. New York: McGraw Hill Book Publishing Co., Inc., 1957.

## APPENDIX A. THE TEST VEHICLE

To fulfill the basic objectives of the program, extensive and reliable data are required. Therefore, a versatile and reliable test vehicle is extremely important.

The test vehicle was carefully designed to produce reliable, reproducible data. To achieve these results, all construction and braze materials that exhibited any sign of corrosion in the previously conducted cesium corrosion study were excluded from the diode. (Appendix D summarizes the cesium corrosion study.) The exclusion of all corrodible materials not only helps to eliminate the possibility of leaks and other braze failures, but also minimizes the possibility of contamination of the cesium vapor, which would alter diode performance with time.

To further guard against contamination, a long and exacting outgassing procedure is employed. After construction, the test vehicle is attached to a VacIon pump for evacuation and all components are brought to temperatures higher than those attained at any time during testing. These conditions are maintained until the pressure stabilizes at a low value; then the unit is cooled and, if no appreciable change in pressure is observed, it is sealed off. A large tantalum piece (part 3, Fig. A-3) is incorporated in the unit. At operating temperature, this piece acts as a getter for gases. Thus, any small amounts of gas that may be released later will be gettered.

As a result of this meticulous design, fabrication, and treatment, the Ta-Mo and Mo-Mo test vehicles have shown completely reproducible results. The reproducibility is checked at the beginning of each test period by reproducing an I-V curve taken previously.

To arrive at a truly versatile vehicle, provisions are made to vary the important parameters independently. These are the emitter temperature, the collector temperature, the interelectrode spacing, and the cesium pressure. The variation in spacing required the development of a special flexible ceramic seal. The collector temperature is controlled by providing a resistance heater and a wide heat path to

a water-cooling coil. Thus a combination of heating and cooling allows very accurate control. The cesium reservoir temperature (and consequently the cesium pressure) is controlled in the same manner as the collector temperature. The instrumentation provides an accurate means of determining each of the variable parameters under any operating condition.

Figure A-1 is a photograph of the instrumented test diode. Figure A-2 is a cut-away view of the diode and its electron-bombardment heater, and Fig. A-3 is a detailed drawing of the emitter-collector assembly.

The accurate adjustment of interelectrode spacing will be described with reference to Fig. A-3. The emitter (1) and the collector (10) are shown. A ceramic disc (7), just large enough to fill the gap between the emitter and collector supports, is inserted when the emitter and collector are touching. Metallic shims (6), equal to the desired spacing, are then used to set the spacing accurately.

The emitter and collector structures are designed so that the spacing is independent of emitter or collector temperature over the operating range of the vehicle. On the collector structure, this is achieved by fabricating the entire heat path, from the collector face to the spacer shim, of the same material and making the inner and outer legs of the structure of sufficient thickness to minimize the temperature drop between them. Thus, the thermal expansion of the inner and outer legs is the same, and the collector face remains fixed with respect to the ceramic shim. On the emitter side, the heat path is up through a length  $l$  of the emitter at high temperature, down through a length  $2l$  of the emitter lead (and support), which is at an average of the high and low temperatures, and up through a length  $l$  at low temperature. Since the material is tantalum throughout, the net displacement of the emitter face relative to the spacer shim is zero, except for second-order effects (variation in thermal expansion coefficient with temperature and nonlinearity of the temperature distribution in the emitter lead).

The emitter temperature is measured by optical-pyrometer observation of the hole (26) on the side of the emitter. The collector temperature is measured by

a Pt|Pt-10% Rh thermocouple (11a), with a suitable correction added. The collector is supported on a copper section (12), which also serves to measure the heat rejected from the collector. The heat flux measuring section is an accurately machined section with two thermocouples (11a and 11b). The temperature difference between (11a) and (11b) is a measure of the heat rejected by the collector. From this heat flux quantity, a temperature drop through the collector is calculated and is added to the (11a) reading to obtain the actual collector face temperature.

The heat flux measuring section is supported on the lower housing (part 13, Fig. A-2), which incorporates a resistance heater and rests on three legs joined to a water-cooled coil. The collector temperature is adjusted by varying the heat supplied by the resistance heater. The balance between the heat transferred to the water-cooling coil and the heat supplied by the resistance heater determines the collector temperature.

Two copper tubes are attached to the lower housing. One tube (15) serves for evacuation and is crimped off. The other tube leads to the cesium reservoir (16). The temperature of the cesium reservoir is again controlled by balancing the heat lost through the cooling strap (21) against the heat put in by the resistance heater, which is wrapped around the cesium reservoir.

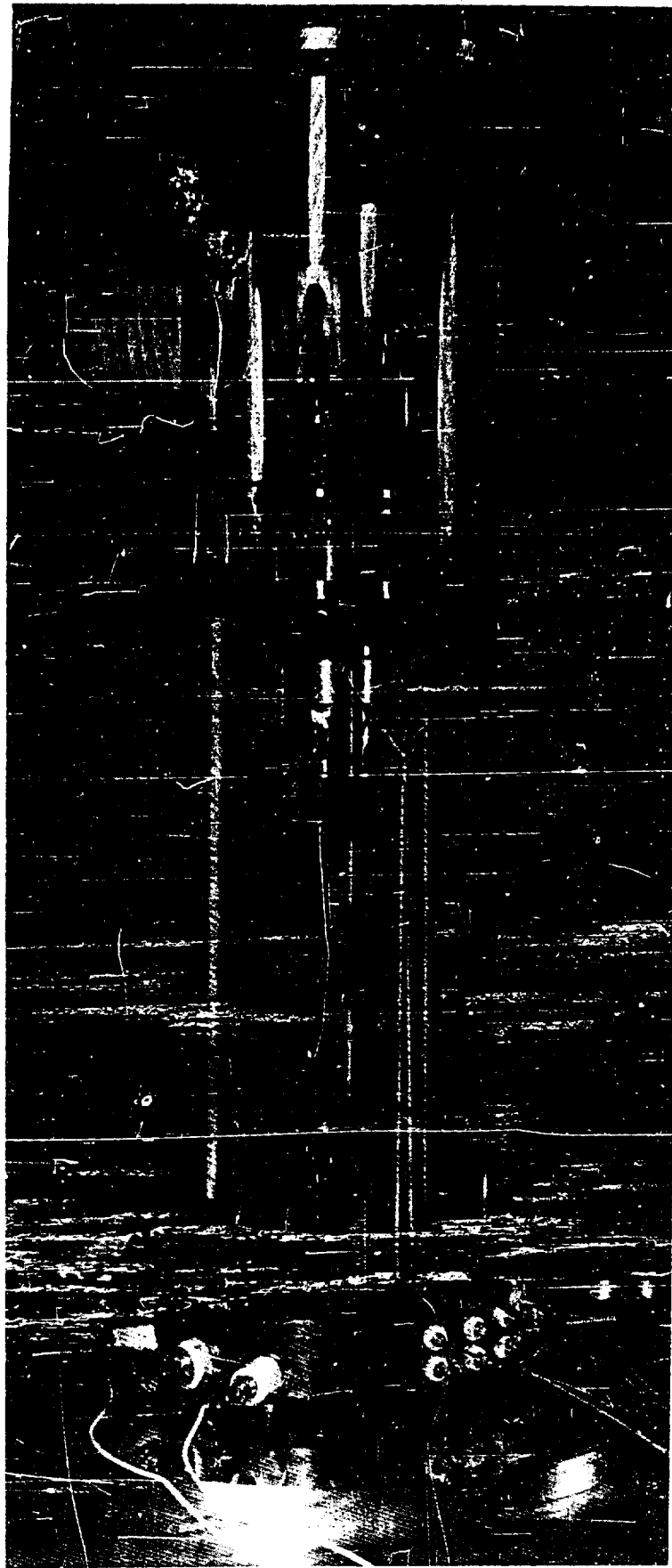


Fig A-1 Cesium diode test vehicle

NOMENCLATURE FOR FIGS. A-2 and A-3

1. Emitter
2. Emitter heat barrier and lead
3. Emitter structure support
4. Electron-bombardment filament radiation shield
5. Electron-bombardment filament
6. Metallic spacing shim
7. Ceramic insert at zero spacing
8. Flexible seal
9. Insulator assembly
10. Collector and collector lease structure
- 11a. Thermocouples
- 11b. Thermocouples
12. Collector cooling cylinder (heat flux measuring section)
13. Electrically heated temperature-control structure
14. Water-cooled temperature-control structure
15. Evacuation tube
16. Cesium reservoir
17. Base plate leadthrough
18. Base plate
19. Tension spring adjuster
20. Tension spring
21. Cesium reservoir cooling strap
22. Cesium tube
23. Emitter structure radiator
24. Collector cooling cylinder radiation shield
25. Conductive post
26. Emitter temperature measurement hole (blackbody for optical pyro

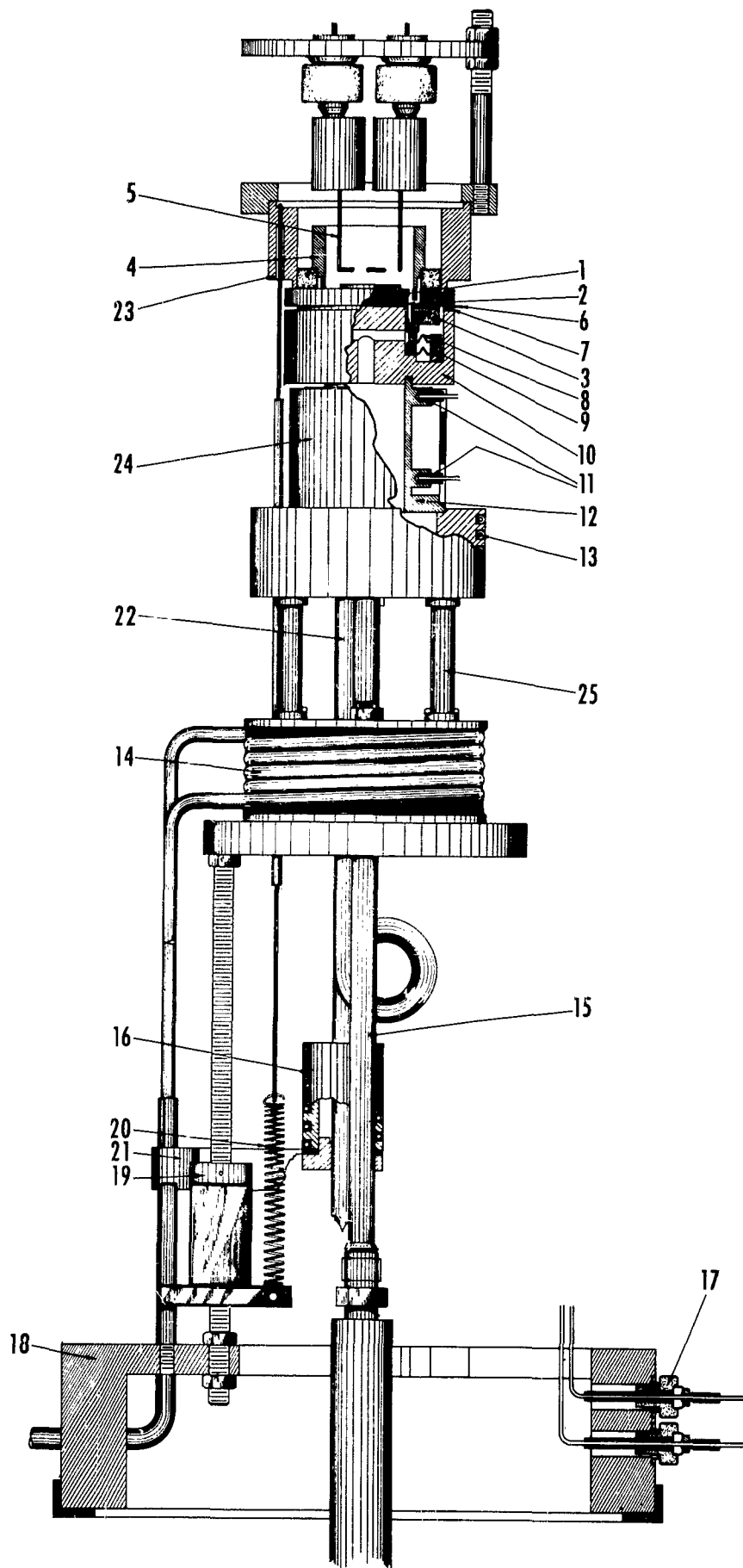


Fig. A-2. Cut-away of test vehicle.

61-10-33a

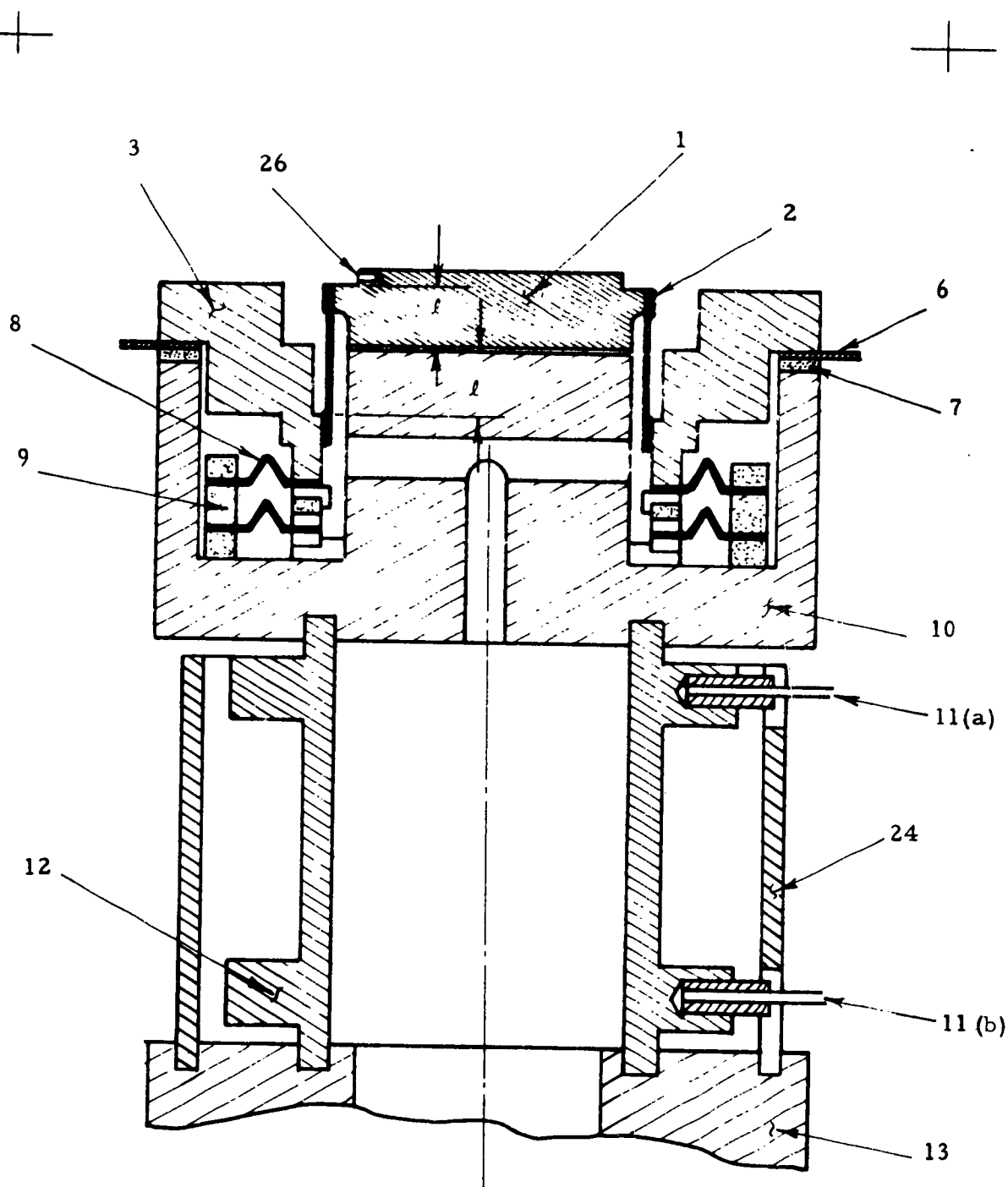


Fig. A-3. Cross-section through test diode

## APPENDIX B. TEST SET-UP AND INSTRUMENTATION

To operate, a thermionic converter requires a heat source to supply the emitter, a cold sink to which heat is rejected, and a load across the two electrodes. The test set-up used with the present converters is essentially that. The cold sink is a water-cooled coil and has been described in Appendix A.

The heat source for the emitter is a stream of electrons accelerated by a high voltage. Figure B-1 is the electrical circuit diagram of the test set-up. The bombardment filament is brought to a high temperature with power supplied by the 50-volt ac supply. A high potential, usually about 1000 volts, is then applied between the bombardment filament and the emitter of the test vehicle. The high potential accelerates the electrons emitted by the hot filament toward the emitter.

The 0-to-50 volt ac supply is stabilized so that once the desired value of bombardment current is set, it does not drift with time. This feature is very important since the emitter temperature must remain constant during a series of measurements.

The output of the test unit is connected to the center posts of double-pole double-throw switch  $S_1$ . When  $S_1$  is thrown to the right, variable-load resistor  $L_1$  is connected across the unit and the output current and voltage are read on meters  $A_3$  and  $V_3$ . When  $S_1$  is thrown to the left, a variable voltage source is connected across the test unit. The variable voltage source consists of a resistor, a battery, and a reversing switch. The voltages applied to the unit can be of a polarity either similar to or the reverse of the output voltage of the unit. Load  $L_1$  is a reference load in the sense that it is connected across the test unit and equilibrium is established under given emitter, collector, and cesium bath temperatures. Load  $L_2$  is an instantaneous load; it is connected momentarily across the unit and the voltage and current are measured. It is then disconnected and  $L_1$  is again connected. When  $S_1$  is thrown to the left, and after contact has been established, push-button  $S_3$  is automatically depressed by switch  $S_1$ .  $S_3$  connects capacitor  $C_1$  across the unit, and  $C_1$  is charged to output voltage.  $S_3$  is then automatically opened before contact with load  $L_2$  is broken; thus,  $C_1$  remains

charged to the output voltage corresponding to load  $L_2$ . This voltage is indicated by electronic voltmeter  $V_4$ . The purpose of this procedure is to minimize the time that  $L_2$  must remain connected to the test unit so that conditions do not drift from equilibrium. The experimenter must read only meter  $A_3$  while  $L_2$  is connected;  $V_4$  can be read after switch  $S_1$  is connected to load  $L_1$ .

This test set-up has been very useful. Current-voltage characteristics and other curves can be taken by first stabilizing the test unit at a fixed combination of emitter, collector, and cesium temperatures under one particular load condition, and then momentarily going to other load conditions without having to wait for equilibrium to be re-established.

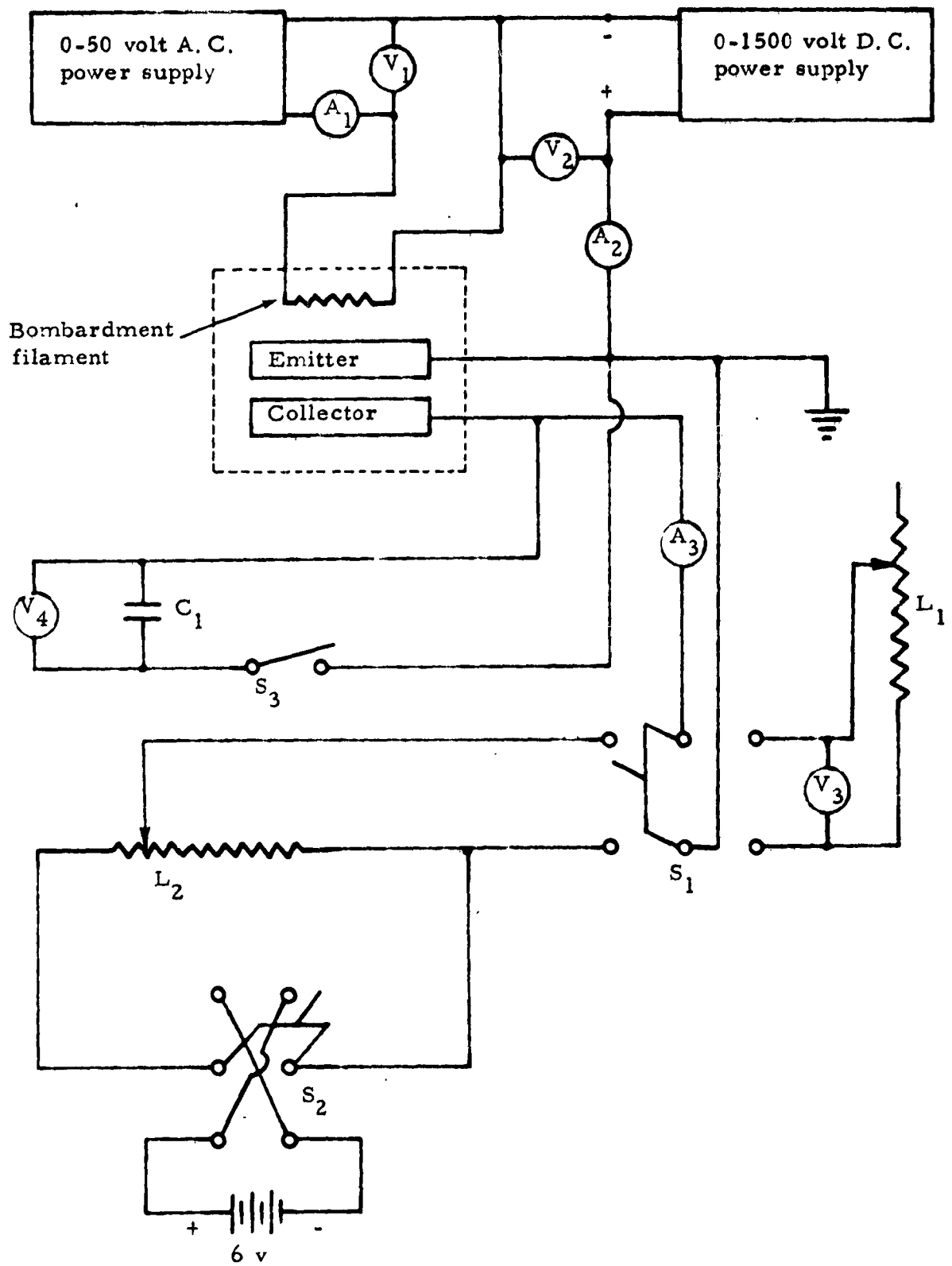


Fig. B-1. Schematic diagram of test set-up.

## APPENDIX C. TEST PROCEDURES

The procedures described below were carefully developed to assure accurate and reliable data.

### C.1. I-V Curves

The I-V curves usually consist of two parts: the upper mode and the lower mode (see Fig. 3-2). Initially, the tube is brought to equilibrium in the upper mode, so that the emitter, collector, and cesium temperatures have the desired values. In practice, this point of equilibrium is chosen near the maximum power point as determined from previous experience. From this point, the tube is switched momentarily by means of the switching circuit described in Appendix B to other points of the upper mode. A sufficient number of points are taken to allow an accurate curve to be drawn through them, which represents the entire upper mode. It is sometimes necessary to allow the tube to return to equilibrium after a point is taken, since more or less current than the equilibrium current cools or heats the emitter. A few seconds is usually sufficient to return the tube to equilibrium, which is indicated by the return of the current and voltage to the original values.

Next, the equilibrium point is set at open circuit; i. e., the load is removed from the diode. This corresponds to point O. C. From this point, the diode is switched to points on the lower mode, and the point of ignition (point B) is determined. Enough data have now been collected to determine the complete I-V curve as shown in Fig. 3-2.

The I-V curve corresponding to maximum power output for a particular emitter temperature and diode spacing is of particular interest. To find the maximum power output, the diode is operated in the upper mode at an output voltage near that which experience has shown to be close to the maximum power point. Since the collector temperature has a smaller influence on power output than the cesium reservoir temperature, the collector temperature is fixed while the cesium reservoir temperature is varied until the maximum output is obtained. An I-V curve is taken at this point. Then, two more curves at different cesium reservoir temperatures, at least one higher and at least one lower than the first

value, are taken. In this manner, the maximum power point is either determined or bracketed by the three curves for the specific collector temperature. The collector temperature is then changed, and the process is repeated until sufficient information is obtained to identify and plot the maximum power curve.

### C. 2 Ignition

Special precautions are taken to determine the ignition point accurately. The unit is operated at the open-circuit condition, and progressively lower voltages are applied momentarily until the ignition voltage is exceeded. The ignition voltage has now been bracketed by the last two applications of voltage. Further momentary applications of voltage are made in this region until the exact value of ignition voltage is identified. This value is then recorded.

### C. 3 Ion Currents

The determination of the ion current is actually an extension of the I-V curve in which one applies higher than open-circuit voltages across the diode and observes the value of the current. However, two steps are necessary. The diode is first brought to equilibrium under open-circuit conditions with the particular emitter, collector, and cesium reservoir temperature of interest. From this point, the voltage is switched to values higher than open-circuit voltage, so that the collector becomes even more negative with respect to the emitter, thus attracting the ions generated at the emitter. Electrons coming from the emitter cannot reach the collector because of its highly negative potential. A curve similar to curve A (Fig. C-1) is obtained in this manner. However, this curve does not represent the ion current since electrons emitted by the collector flow to the emitter at the same time the ions are flowing to the collector. This electron flow, termed the back emission, must be measured separately and subtracted from the above curve.

### C. 4 Back Emission

The back emission is measured by lowering the emitter temperature until the ion current produced at the emitter face is negligible, while maintaining the same collector temperature and cesium pressure as noted in Section C. 3. Points are taken for voltages at which the collector is again highly negative, so that all

the electrons emitted by the collector go to the emitter. The data taken in this manner result in a curve similar to curve B (Fig. C-1). The ion current is then given by (curve C) = (curve A) - (curve B). Each of these curves reaches an asymptotic limit. This limit is actually the meaningful part of the data since, before the asymptote is reached, not all the ions or electrons are collected on the appropriate diode element.

### C. 5 Electron Cooling

This quantity is defined as the average energy in electron volts carried away from the emitter by one electron. The units of electron cooling enable an easy comparison between the electron cooling and the work function of emitter materials.

Since the electron cooling appears as a heat flow from the emitter, it also represents a major factor in the efficiency of operation of the diode. In this connection, it is more convenient to speak of electron cooling in terms of watts per ampere; i. e., each ampere that flows from the emitter to the collector cools the emitter by a certain number of watts.

The magnitude of the electron cooling may be observed graphically with the aid of Fig. 3-7. To escape from the emitter, the electrons must surmount a barrier, given by

$$V_{\text{barrier}} = \phi_E + \delta. \quad (\text{C-1})$$

In addition, the electrons that escape have an average thermal energy equal to  $2kT_E$ . Thus the total energy carried away from the emitter by each electron is

$$V_{\text{electron}} = V_{\text{barrier}} + 2kT_E = \phi_E + \delta + 2kT_E. \quad (\text{C-2})$$

Each electron that carries heat away from the emitter supplies heat to the collector. This "electron heating" is the average thermal energy in electron volts that each electron delivers to the collector. This value is given by

$$V_{\text{electron heating}} = V_{\text{electron cooling}} - V_o. \quad (\text{C-3})$$

Thus, a portion of the energy carried from the emitter by the electron appears

as power output, and the remainder is converted to heat, which is dissipated through the collector.

The test vehicle is capable of measuring both electron heating and electron cooling, directly and simultaneously. First, the diode is brought to equilibrium under open-circuit conditions, and the heat input to the emitter is measured. Then, a load is placed across the diode, and the tube is again brought to equilibrium so that the temperature of emitter, collector, and cesium reservoir are the same as in the open-circuit case. Now, a higher input to the emitter is necessary. The difference represents the electron cooling at the particular operating point in question, all other heat losses being the same in the two cases.

The electron heating of the collector is measured simultaneously with the electron cooling. In the open-circuit condition, the heat flux from the collector is determined by means of the two thermocouples in the heat flux measuring section (see Appendix A). This heat flux is measured again with a load across the tube. As in the case of the emitter, the difference in the two heat flux values represents the electron heating. The measurements of electron heating and electron cooling may be checked against each other by recording power output and using Eq. (C-3).

#### C.6 Cesium Gas Conduction

In a manner similar to that used for the measurement of electron heating and cooling, the cesium gas conduction can be measured.

With the diode operating under open-circuit conditions and with a cold cesium reservoir (so that the cesium pressure is very low), the heat flux from the collector is measured by the heat flux measuring section.

Then measurements of the heat flux are made with successively higher cesium temperatures, which correspond to higher cesium pressures. The difference in heat flux between that obtained with a cold cesium reservoir and that obtained with a hotter reservoir represents cesium conduction at a specific

pressure. After many such measurements are taken, a curve (Fig. 3-10) may be drawn. The heat flux measuring section, rather than the emitter input power, is employed for these measurements because the former is more sensitive to small changes in heat flow.

#### C. 7 Radiation

The amount of heat flux from the collector at zero cesium pressure represents the total heat loss to the collector from the emitter by radiation. A slight correction, stemming from the geometry of the tube, is required, however. Consider Fig. C-2. Most of the radiation comes to the collector from the emitter face. This is the quantity one wishes to measure. The collector also receives heat from the space between the emitter and the thin metal spacer. This space acts like a cavity, with an emissivity that approaches that of a blackbody. This approximation is used to calculate the heat radiated from the space. It is estimated that half the heat from this space flows to the collector and the other half to the thin spacer wall next to the collector. Therefore, half the heat from this space is subtracted from the heat flux down the collector to obtain a value for the radiation from emitter to collector. This correction is usually about 5%.

No other corrections are necessary since the thin metal spacer drops the high emitter temperature to a value close to the collector temperature. Therefore, little heat flows across the  $\text{Al}_2\text{O}_3$  spacer, and little heat exchange by radiation takes place between the collector and the lower part of the emitter structure.

Note that the heat input to the emitter is not a good measurement of the radiation to the collector because of the heat loss from the emitter back-side by radiation and the radiation from the emitter radiator. The input to the emitter is good only for difference measurements, where the unknown back radiation loss cancels out.

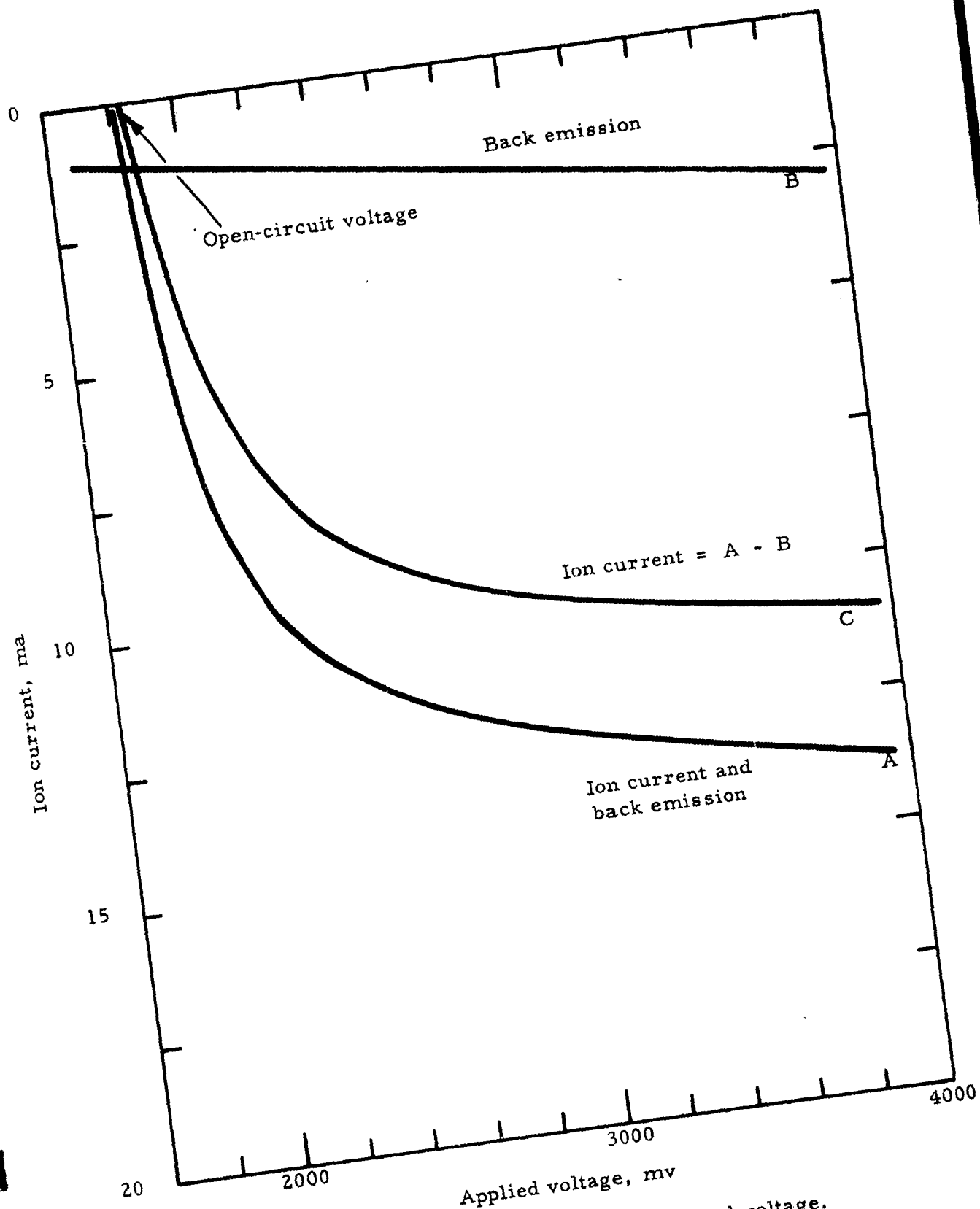


Fig. C-1. Ion current vs applied voltage.

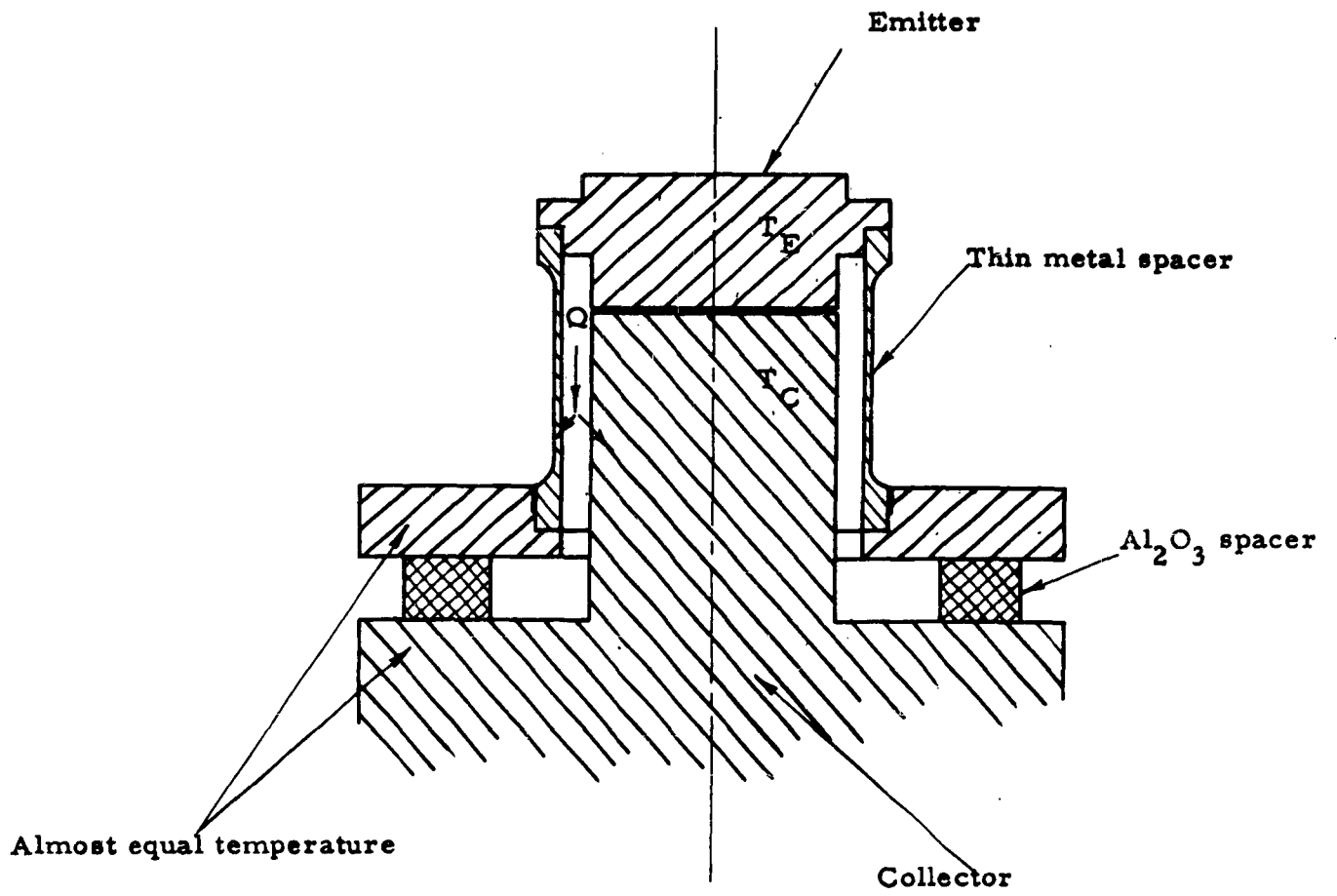


Fig. C-2. Radiation heat transfer schematic

#### APPENDIX D. CESIUM CORROSION STUDY

Several months before the initiation of NONR 3563(00), Thermo Electron had conducted a thorough investigation of the cesium-corrosion resistance of the structural and brazing materials that were considered most promising for use in thermionic converters.

One or more samples of each of the materials listed in Table D-I were placed in an evacuated copper tube with one gram of liquid cesium. The copper tube was heated in a hydrogen furnace for 24 hours at 650°C. The tube was then removed from the furnace and cut open while immersed in oil, and the sample was removed. After being washed with water, the sample was compared under a microscope with a control sample taken from the same stock. Any alteration in the appearance of the surface (i. e. , discoloration, etching, or disintegration) was recorded.

Materials that exhibited no visible alteration whatever were classified in the "no corrosion" category shown in Table D-I. Materials that exhibited some alteration but no etching or pitting of the surface were classified under the "slight corrosion" category. Finally, materials that exhibited any removal of material from the surface of the sample (pitting, etching, solution by the cesium) were placed in the "high corrosion" category. A very important result of this study was that the noble metals, which are prime constituents of many available brazing alloys, were identified as being highly susceptible to cesium corrosion. This has led to the development of diode fabrication techniques that circumvent the use of noble-metal brazes. Some of these techniques are unique developments of Thermo Electron and have enabled the development of the experimental test vehicle, which is the basic tool of the current program.

TABLE D-I  
 SUSCEPTIBILITY OF SEVERAL METALS  
 TO CESIUM CORROSION

| Sample | No corrosion | Slight corrosion | High corrosion |
|--------|--------------|------------------|----------------|
| Ta     | X            |                  |                |
| Mo     | X            |                  |                |
| Ni     | X            |                  |                |
| Cu     | X            |                  |                |
| Ti     | X            |                  |                |
| Zr     | X            |                  |                |
| V      |              | X                |                |
| Au     |              |                  | X              |
| Ag     |              |                  | X              |
| Fe     | X            |                  |                |
| Ni-Au  |              |                  | X              |
| Cu-Ni  | X            |                  |                |
| Ag-Cu  |              |                  | X              |
| Ni-Fe  | X            |                  |                |
| Ni-Ti  | X            |                  |                |

APPENDIX E. THERMODYNAMIC DERIVATION OF THE DEPENDENCE OF  
CESIUM ARRIVAL RATE UPON EMITTER SURFACE TEMPER-  
ATURE

This appendix presents the derivation of Eq. (3-2), which describes the relationship between the number of cesium atoms evaporated from a metal surface and the temperature of the surface. That is,

$$v_a = CT^2 e^{-B/T}. \quad (E-1)$$

This relationship may be derived by considering that there exists at the surface of the emitter a layer of cesium atoms that has a temperature equal to the metal surface temperature. These atoms see a potential barrier due to an attraction between them and the metal. The atoms in this layer are assumed to act like a perfect gas.

The Gibb's function for this gas of atoms can be written as

$$g = h - Ts, \quad (E-2)$$

where  $g$  is the Gibb's function,  $h$  is the enthalpy of the gas,  $T$  is the temperature of the metal surface, and  $s$  is the entropy of the gas. Langmuir has suggested [2] that it is reasonable to assume that the Gibb's free energy is primarily a function of coverage and a very weak function of temperature. Therefore, we will consider  $g$  to be constant for a specific cesium coverage.

From fundamental thermodynamics, we may write the following property relationship for any pure substance:

$$dh = T ds + v dp. \quad (E-3)$$

This may be rearranged as follows:

$$ds = \frac{1}{T} dh - \frac{v}{T} dp. \quad (E-4)$$

For a perfect gas,

$$dh = c_p dT, \quad (E-5)$$

where  $c_p$  is the specific heat at constant pressure and  $pv = kT$ . For a perfect gas, Eq. (E-4) becomes

$$ds = c_p \frac{dT}{T} - k \frac{dp}{p}, \quad (\text{E-6})$$

which can be integrated to yield

$$s = c_p \ln T - k \ln p + s_o, \quad (\text{E-7})$$

where  $s_o$  is a constant of integration. The Gibbs function may now be written as

$$g = c_p T - c_p T \ln T + kT \ln p + s_o T. \quad (\text{E-8})$$

If the cesium coverage is fixed, then  $g$  is assumed to be fixed and Eq. (E-8) represents a relationship between pressure and temperature of the gas at the metal surface.

Rewriting Eq. (E-8) and making use of the perfect gas relationship

$$c_p = \frac{5}{2} k, \quad (\text{E-9})$$

we have that

$$\ln p = \frac{g}{T} + \frac{5}{2} \ln T + \frac{c_p - s_o}{k} \quad (\text{E-10})$$

or

$$p = \frac{c_p - s_o}{k} T^{5/2} e^{g/kT}. \quad (\text{E-11})$$

For a perfect gas, the collision frequency of the gas on a surface is [4]

$$\nu = p (2\pi MkT)^{1/2} \quad (\text{E-12})$$

where  $M$  is the mass of a cesium atom.

Finally, combining Eqs. (E-11) and (E-12), we have that

$$\nu = \frac{c_p - s_o}{k} (2\pi Mk)^{1/2} T^2 e^{g/kT}. \quad (\text{E-13})$$

We can now rewrite Eq. (E-13) in the form of Eq. (E-1):

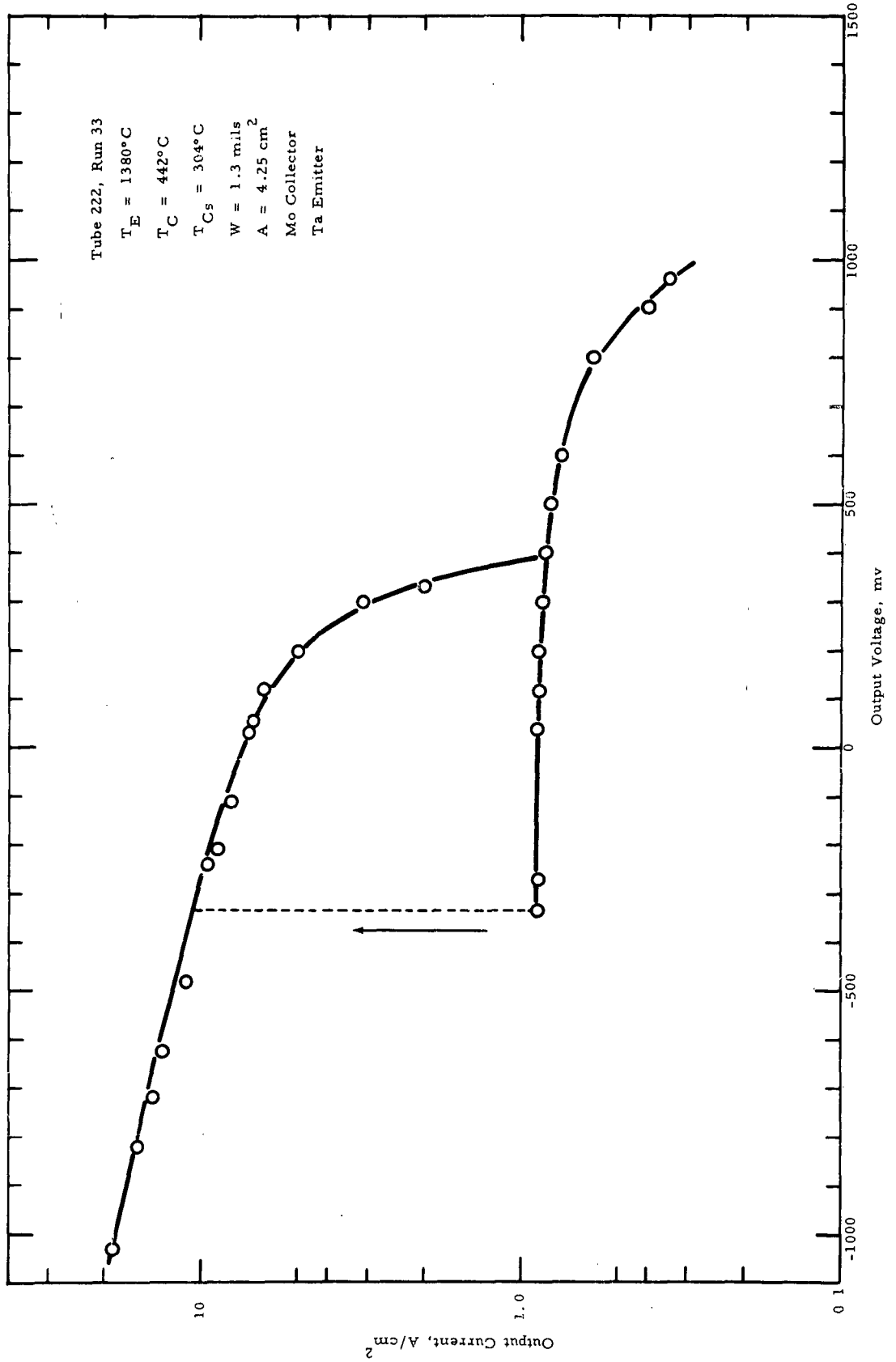
$$\nu = CT^2 e^{-B/T}, \quad (\text{E-14})$$

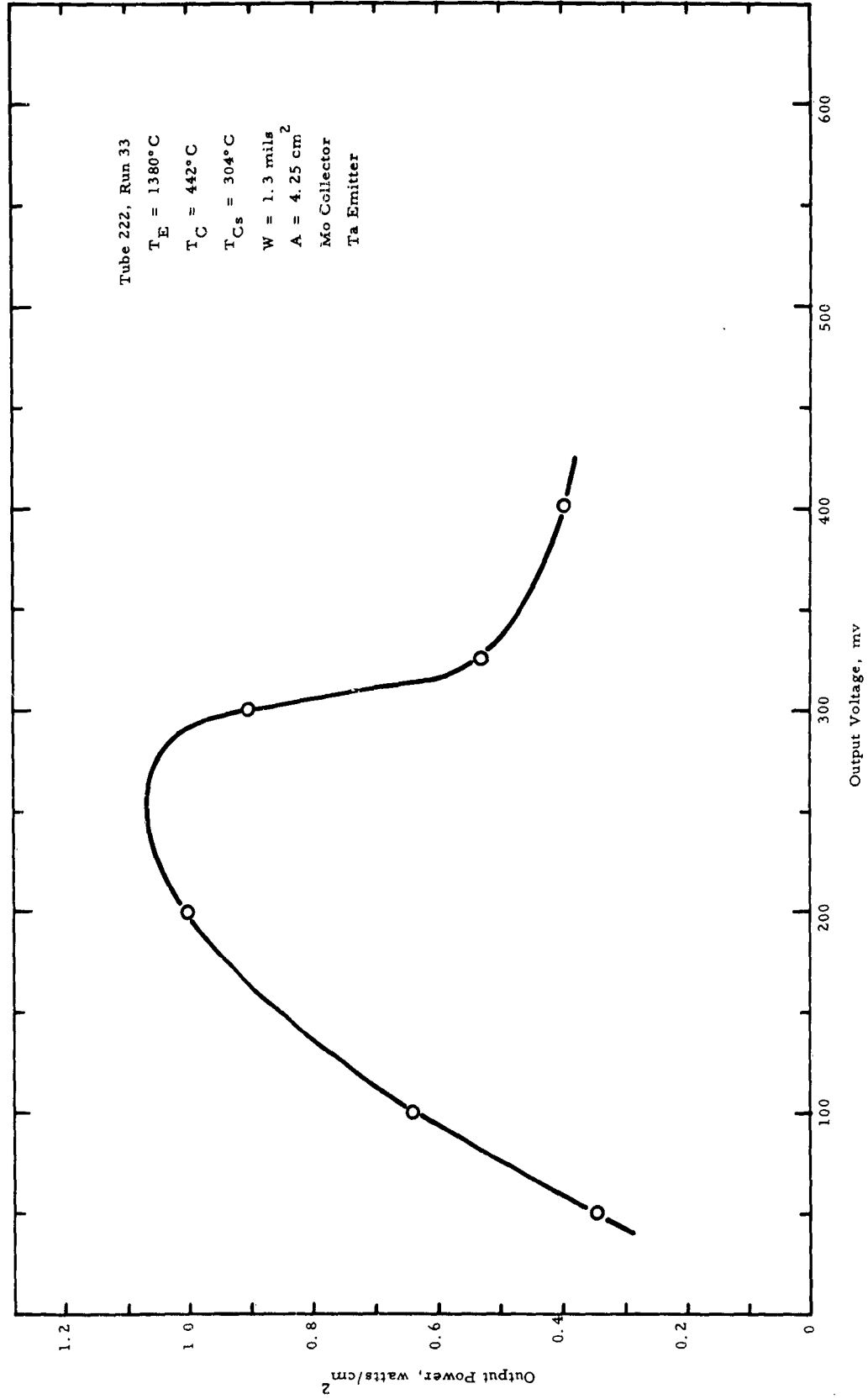
where

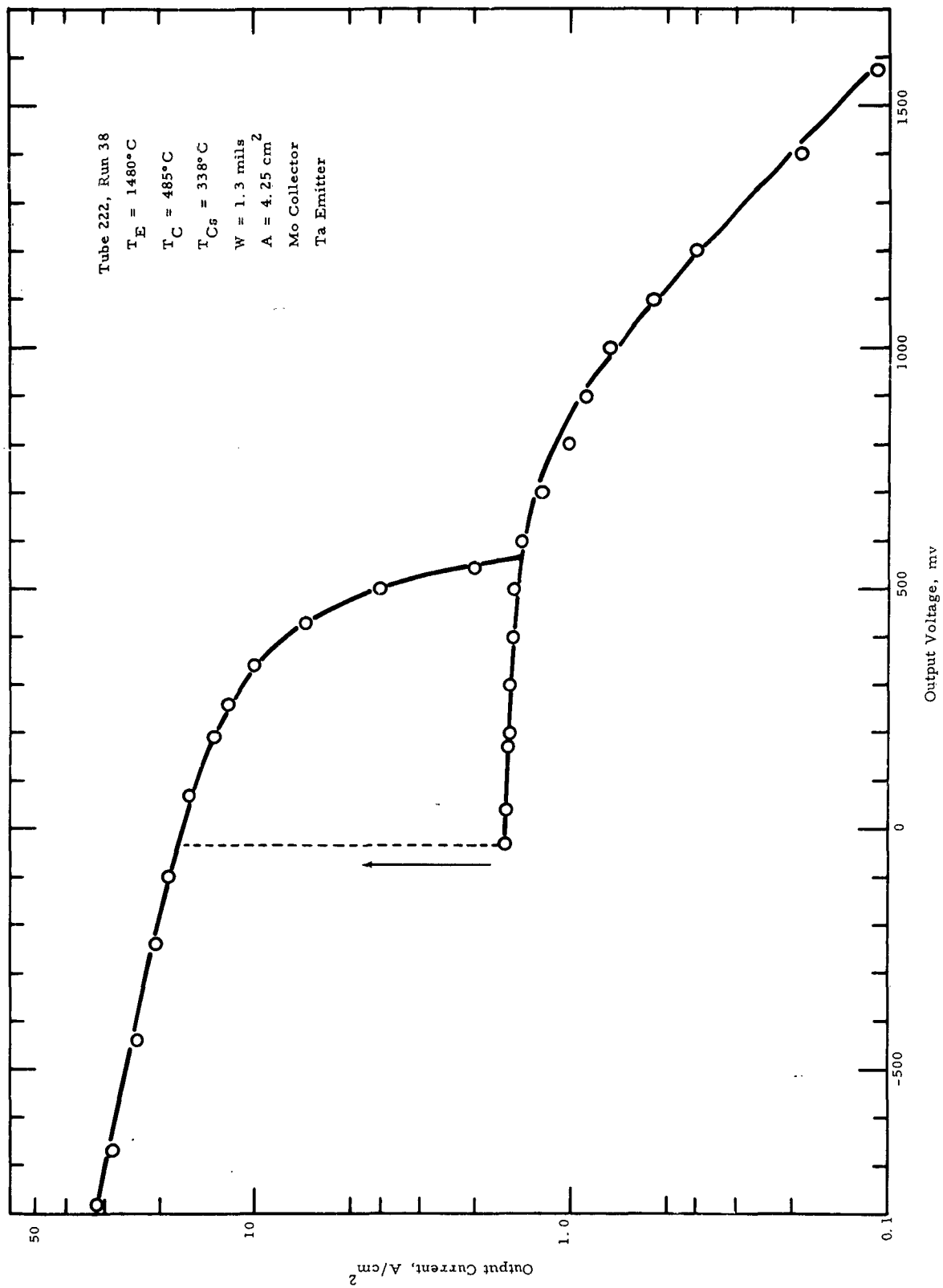
$$C = \frac{c_p - s_o}{k} (2\pi Mk)^{-1/2}. \quad (\text{E-15})$$

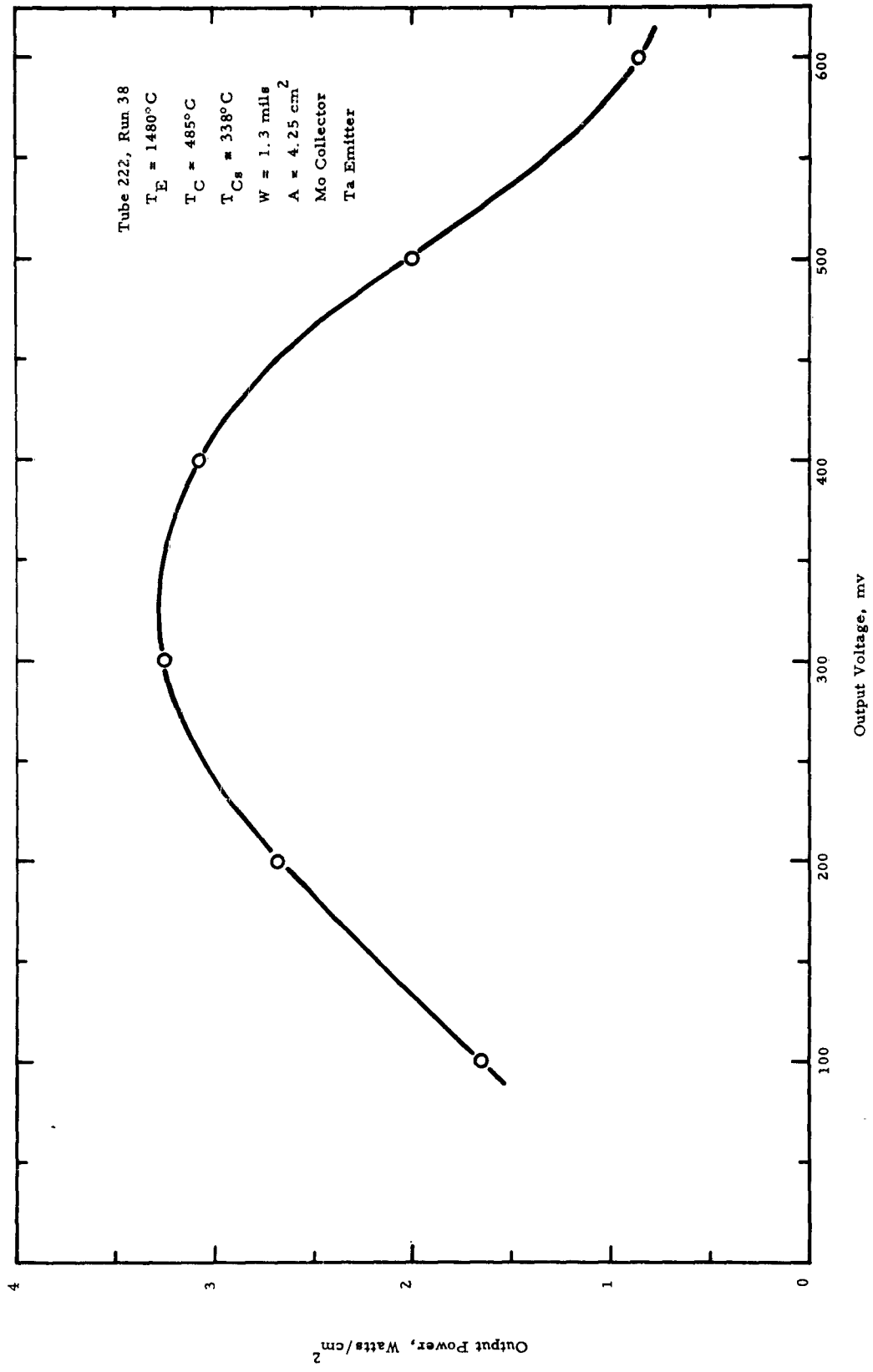
APPENDIX F. SELECTED DATA

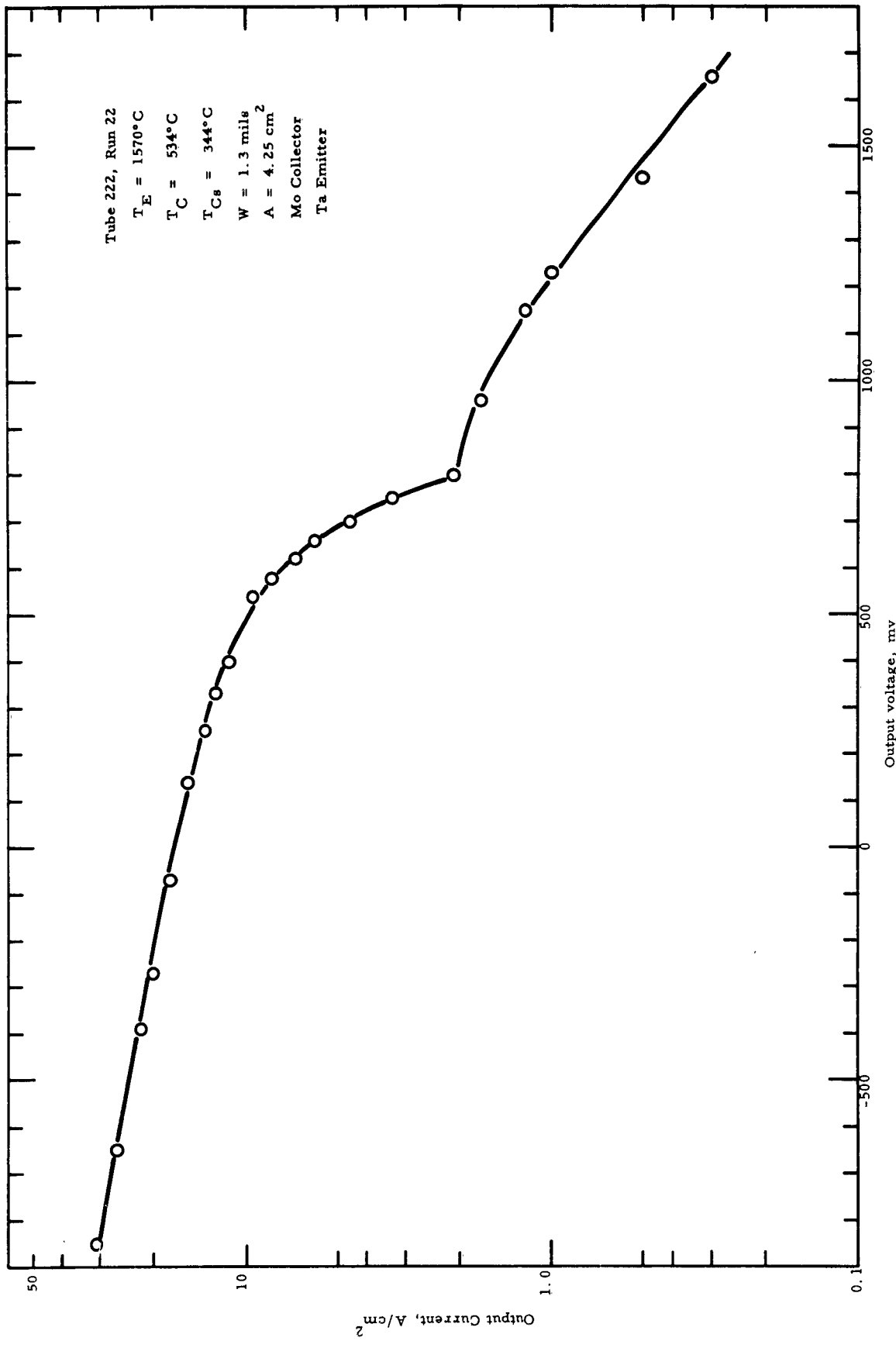
The curves presented in this appendix are I-V and output power curves taken at various combinations of emitter temperature, collector temperature, cesium pressure, and interelectrode spacing. The first 10 curves were taken from the Ta-Mo tube, and the remaining 40 were taken from the Mo-Mo tube.

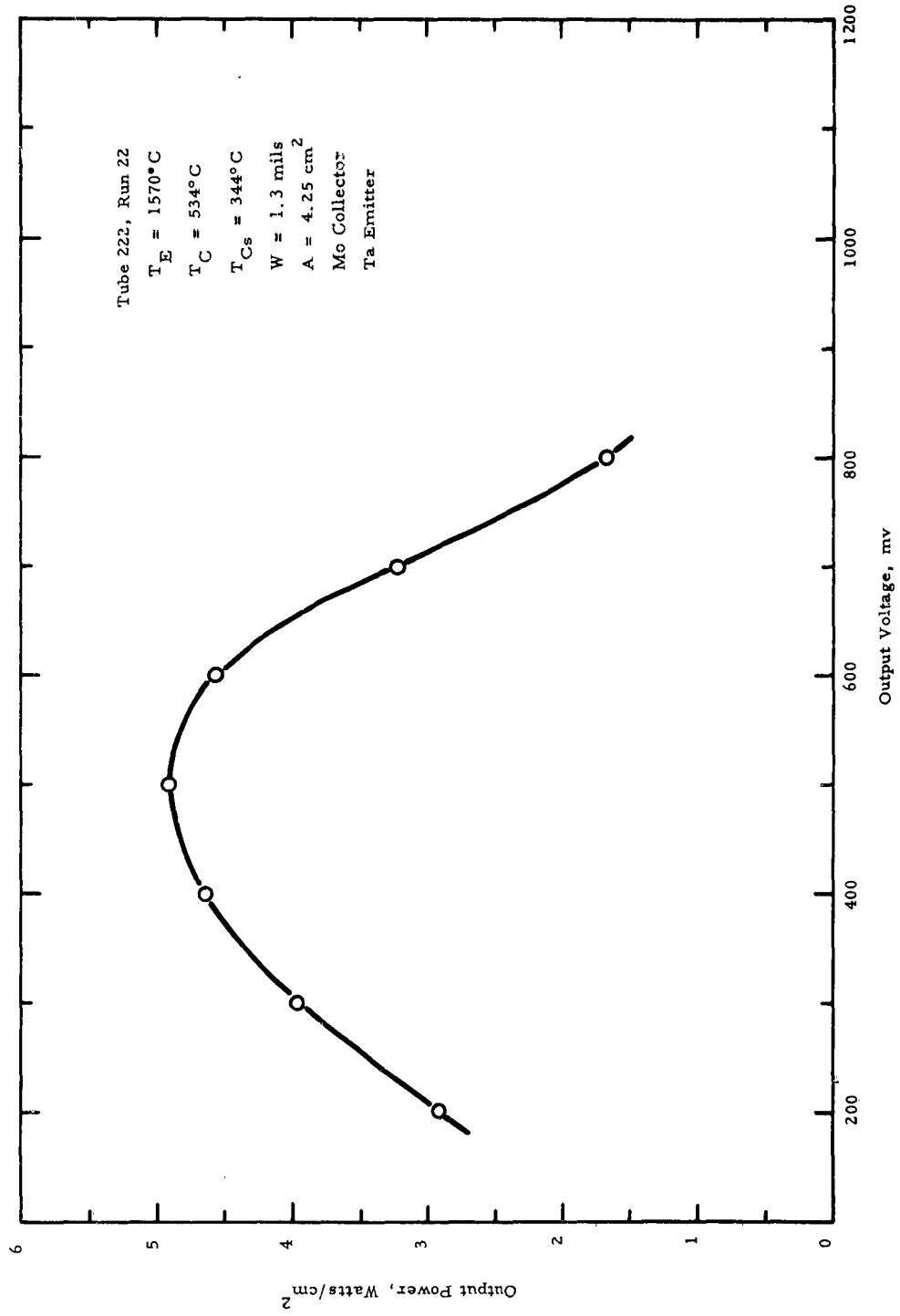


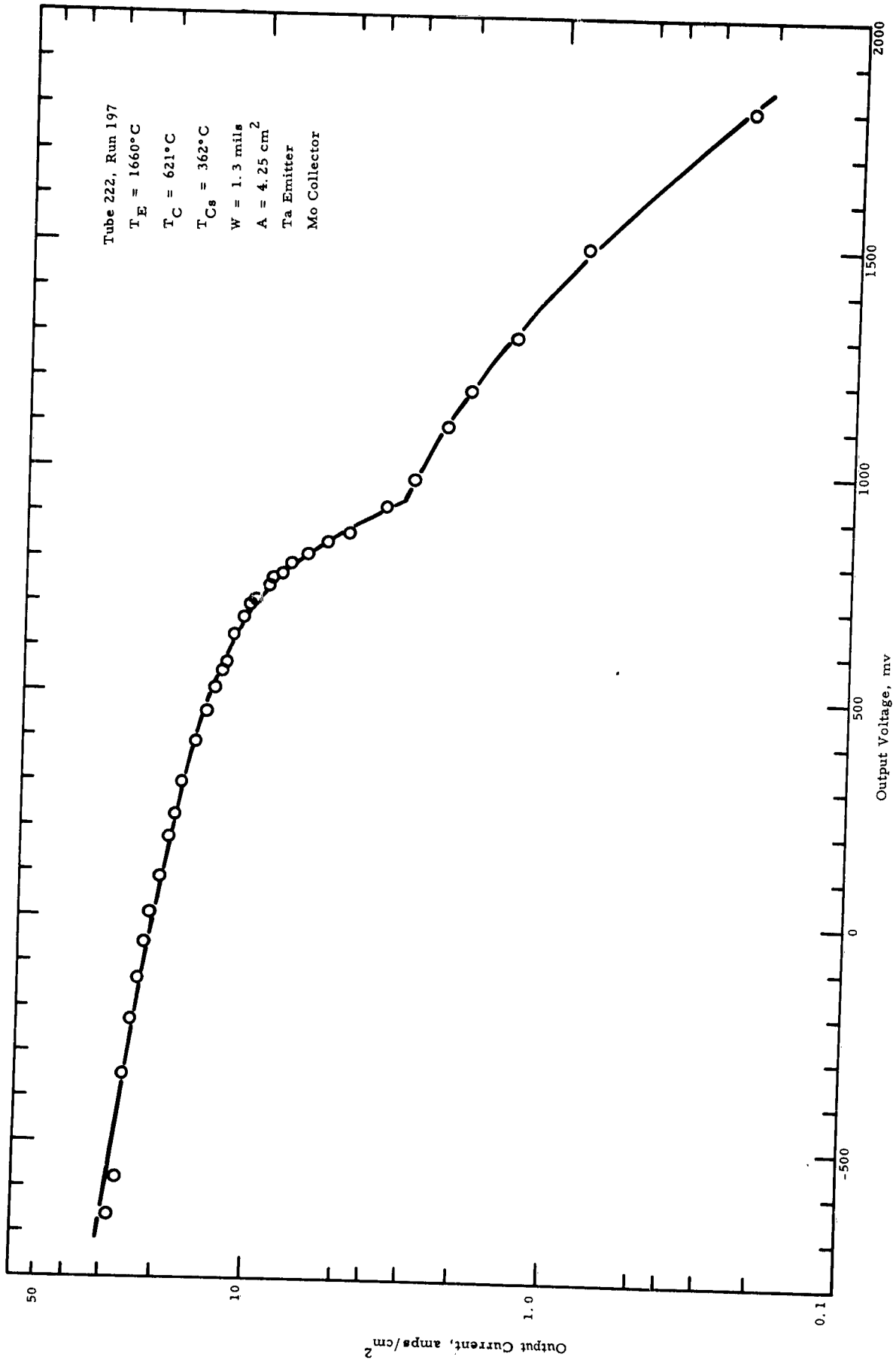


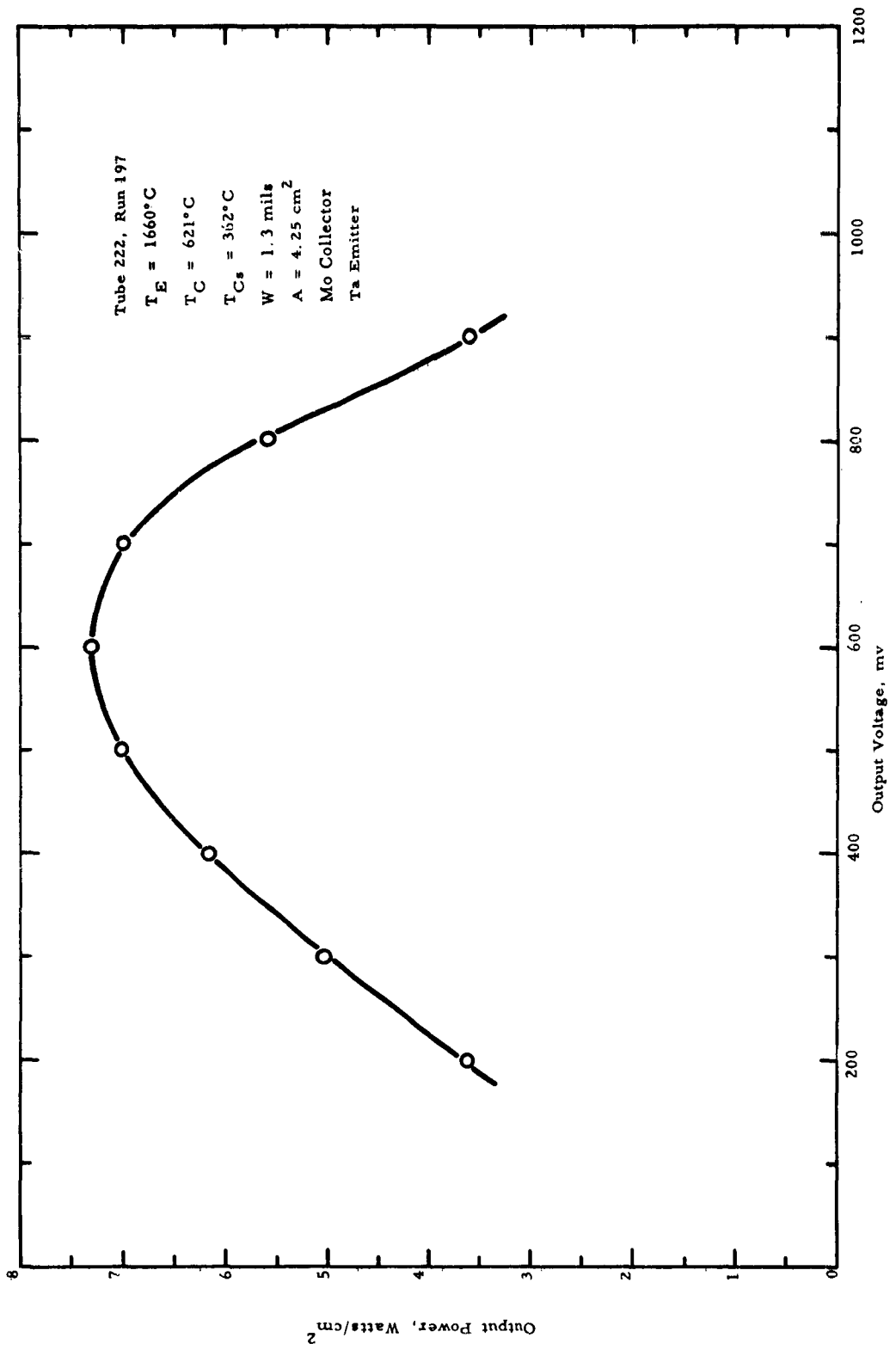












Tube 222, Run 11

$T_E = 1760^\circ\text{C}$

$T_C = 503^\circ\text{C}$

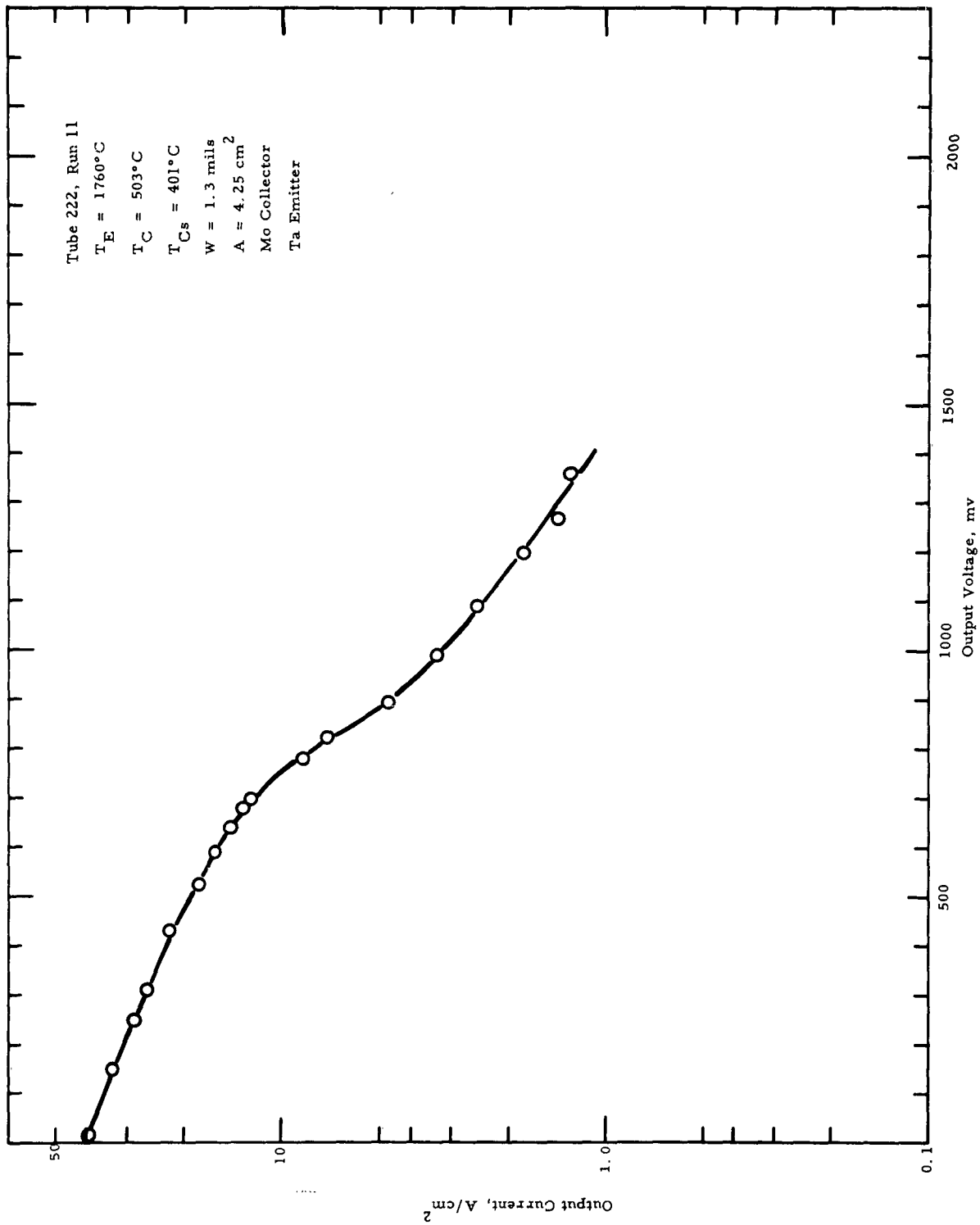
$T_{Cs} = 401^\circ\text{C}$

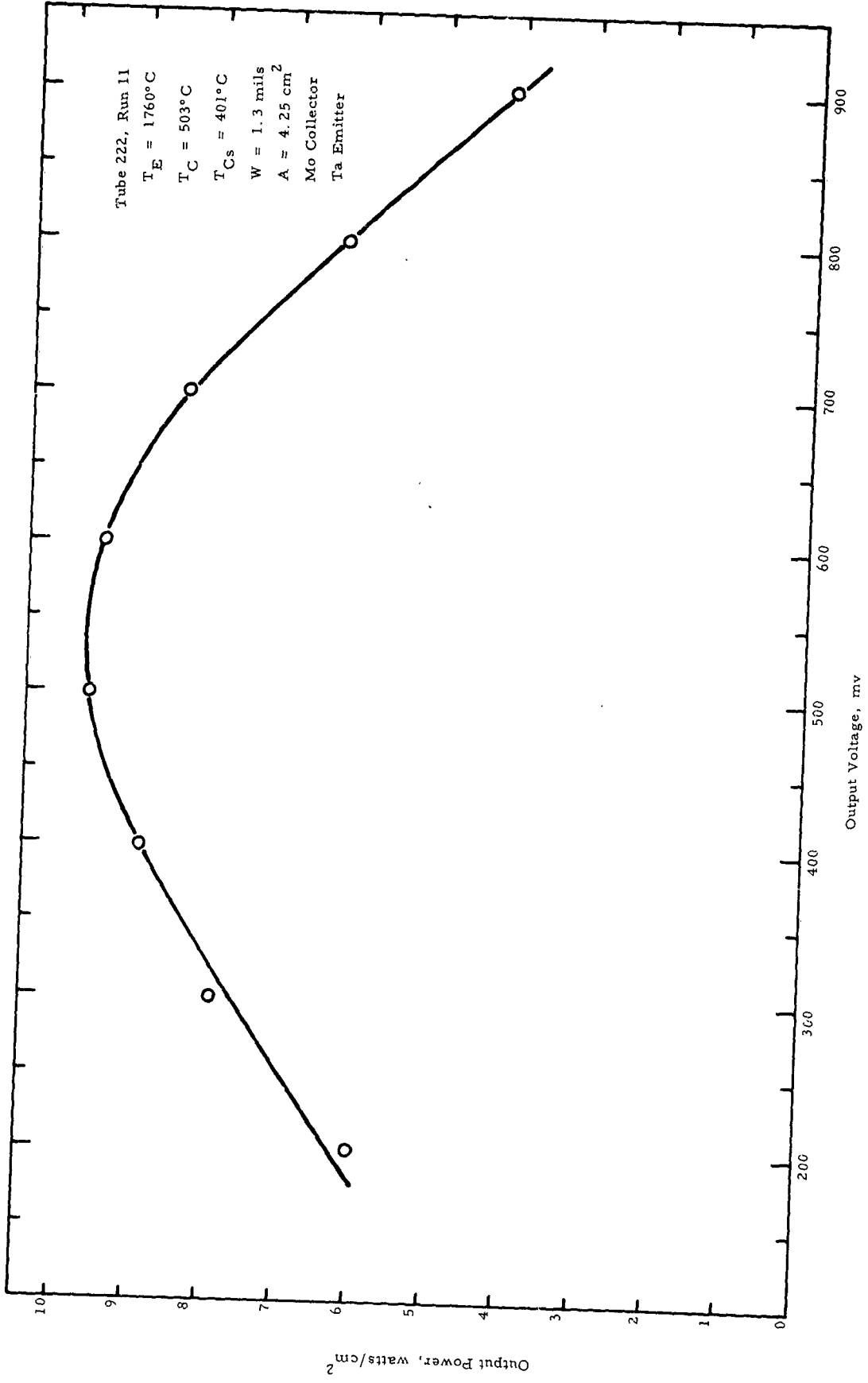
$W = 1.3 \text{ mils}$

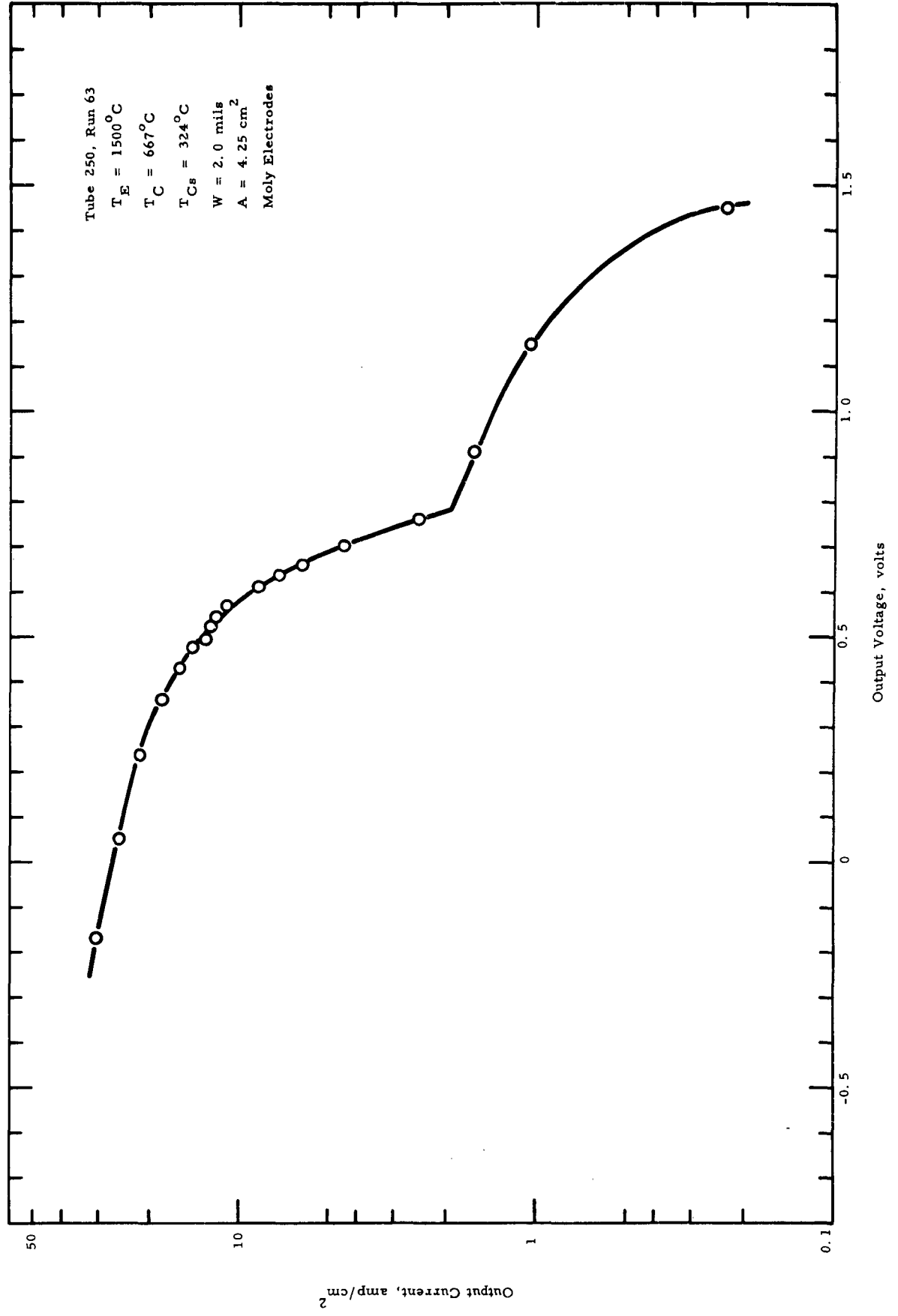
$A = 4.25 \text{ cm}^2$

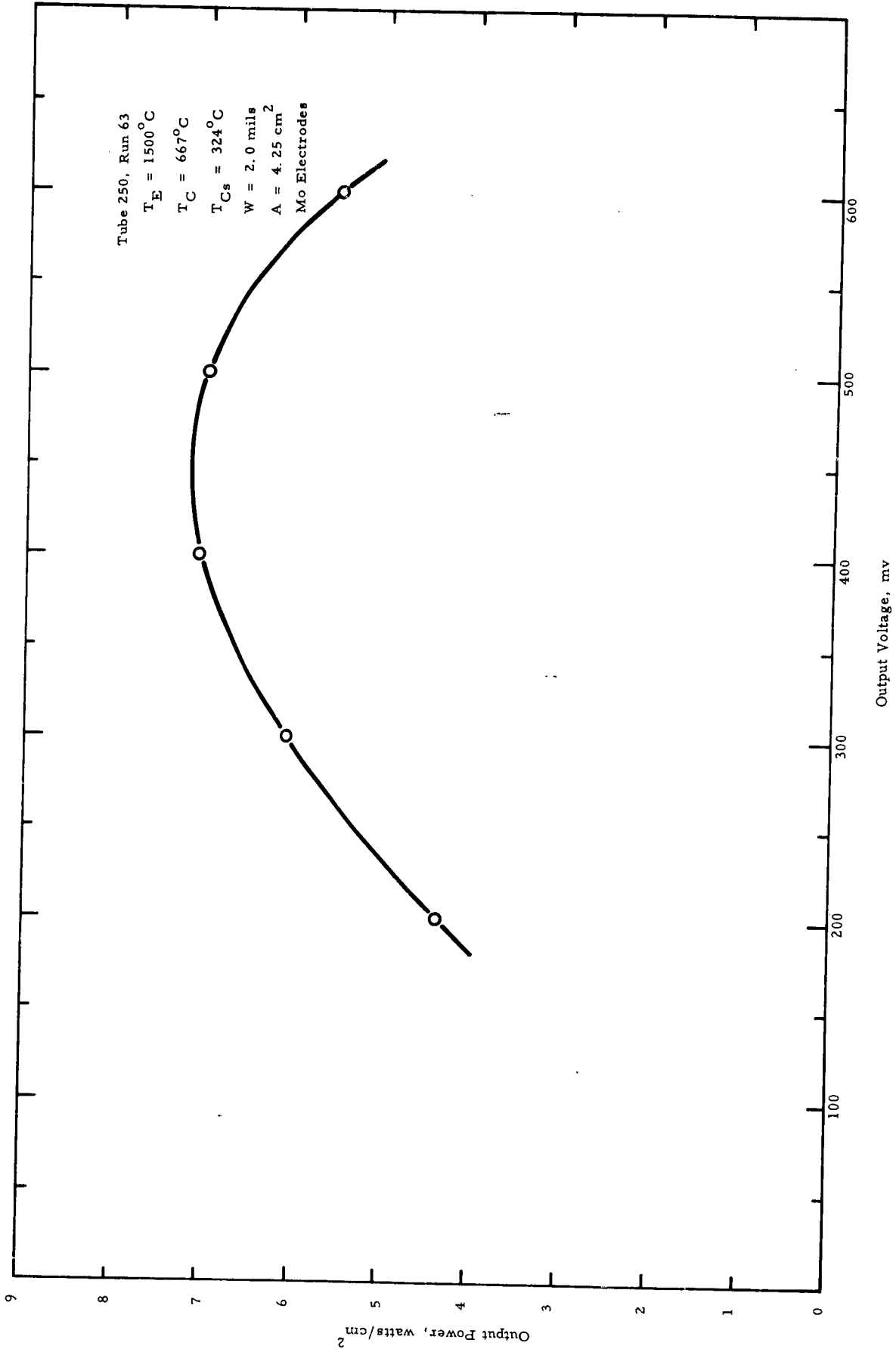
Mo Collector

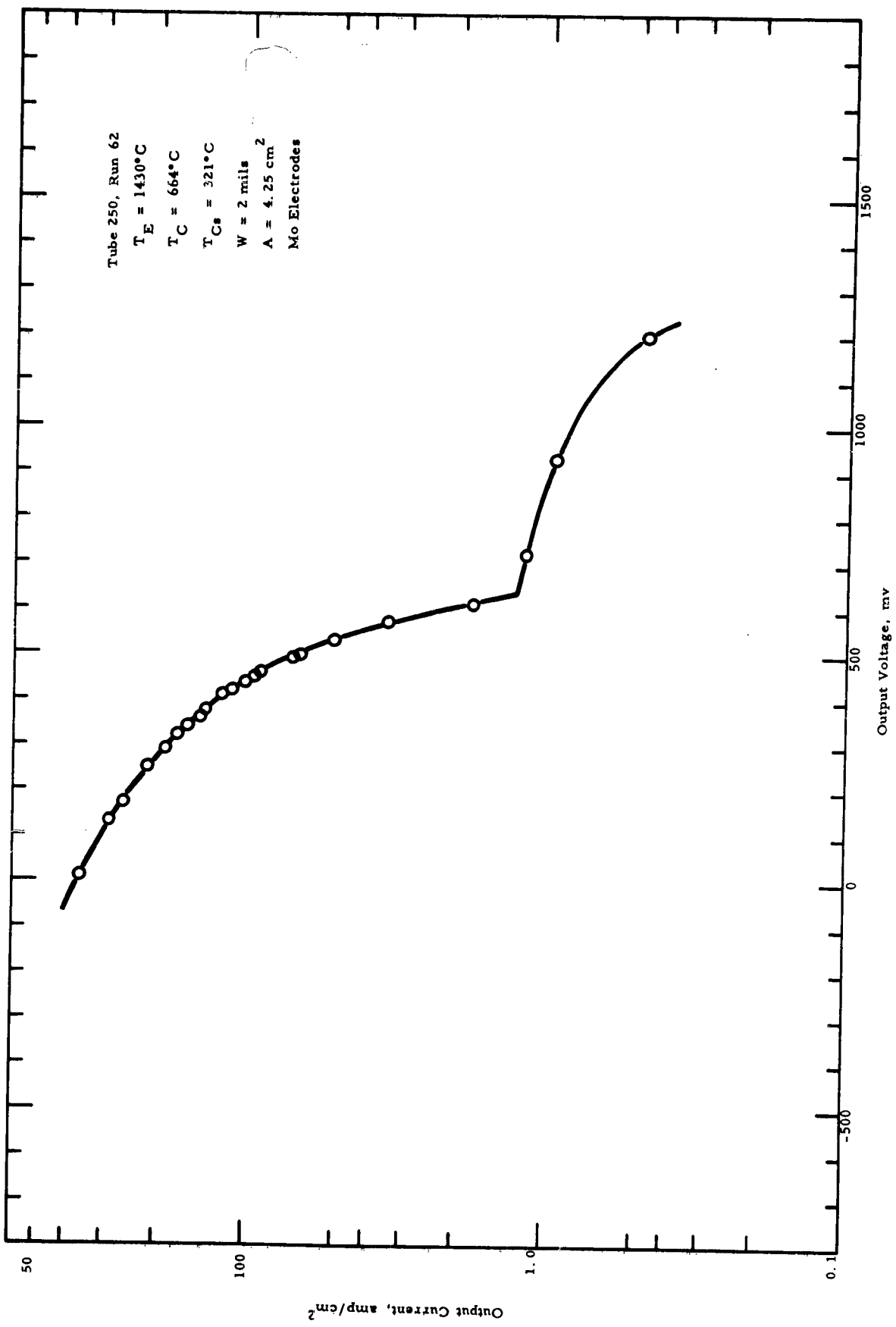
Ta Emitter

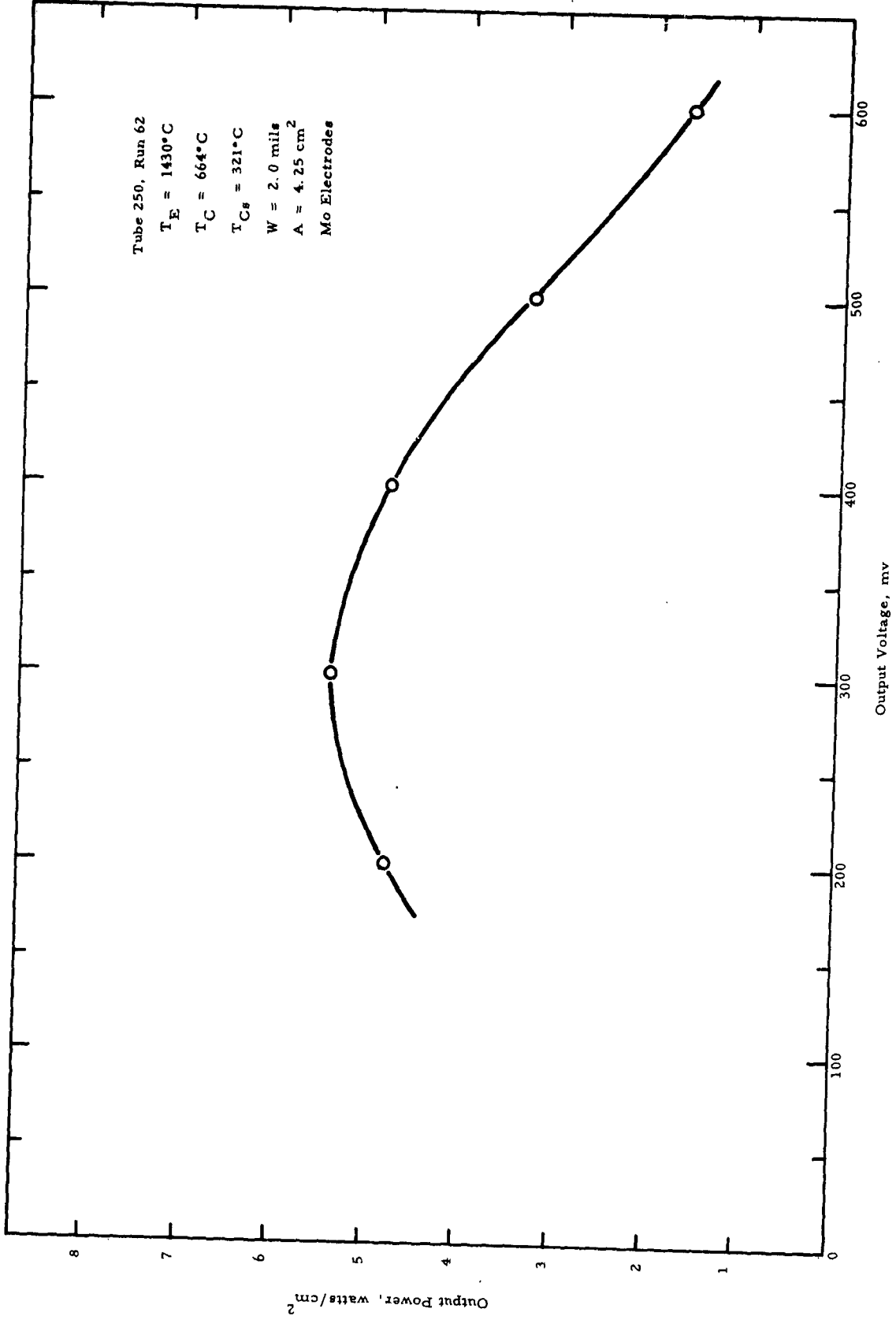


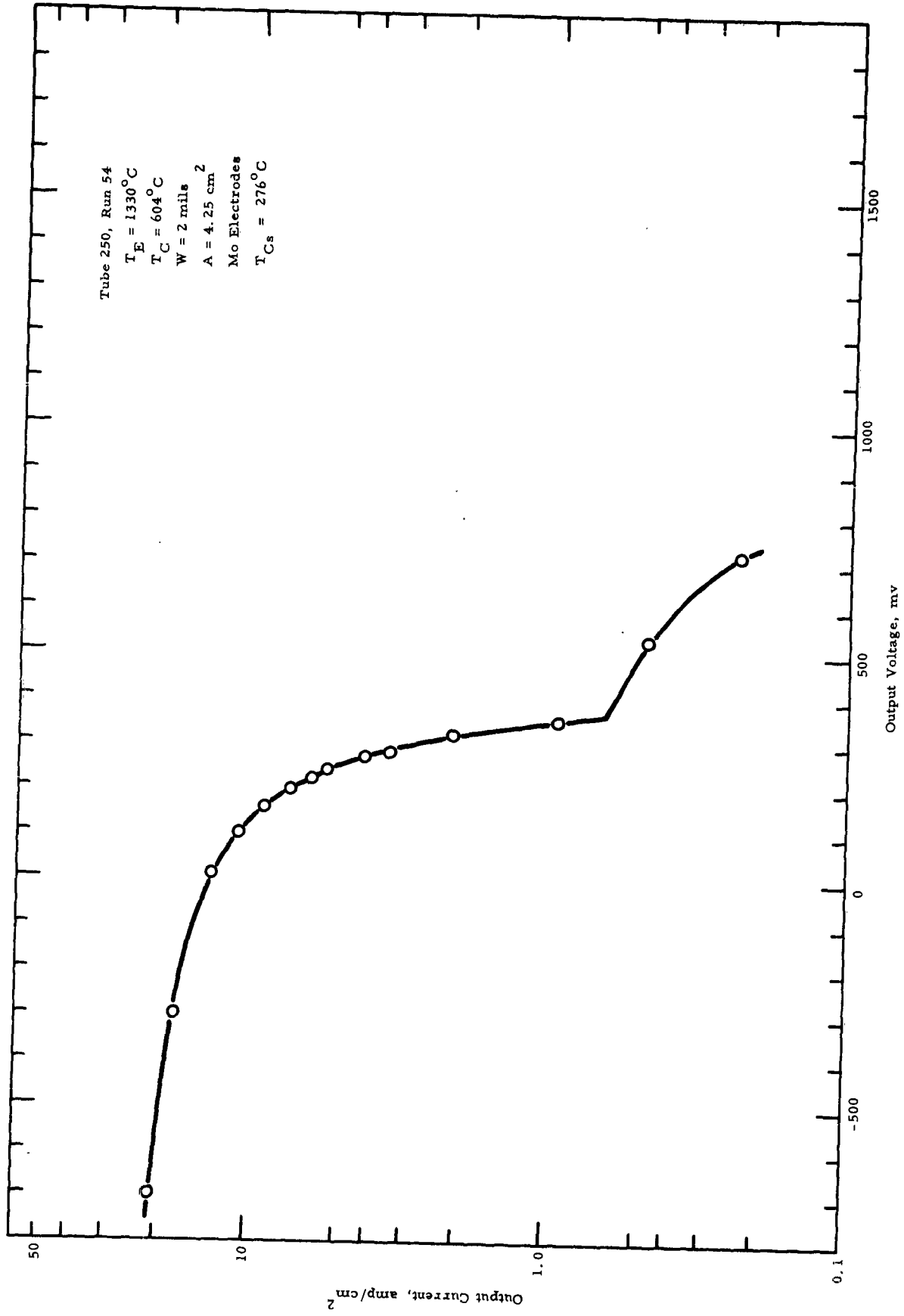


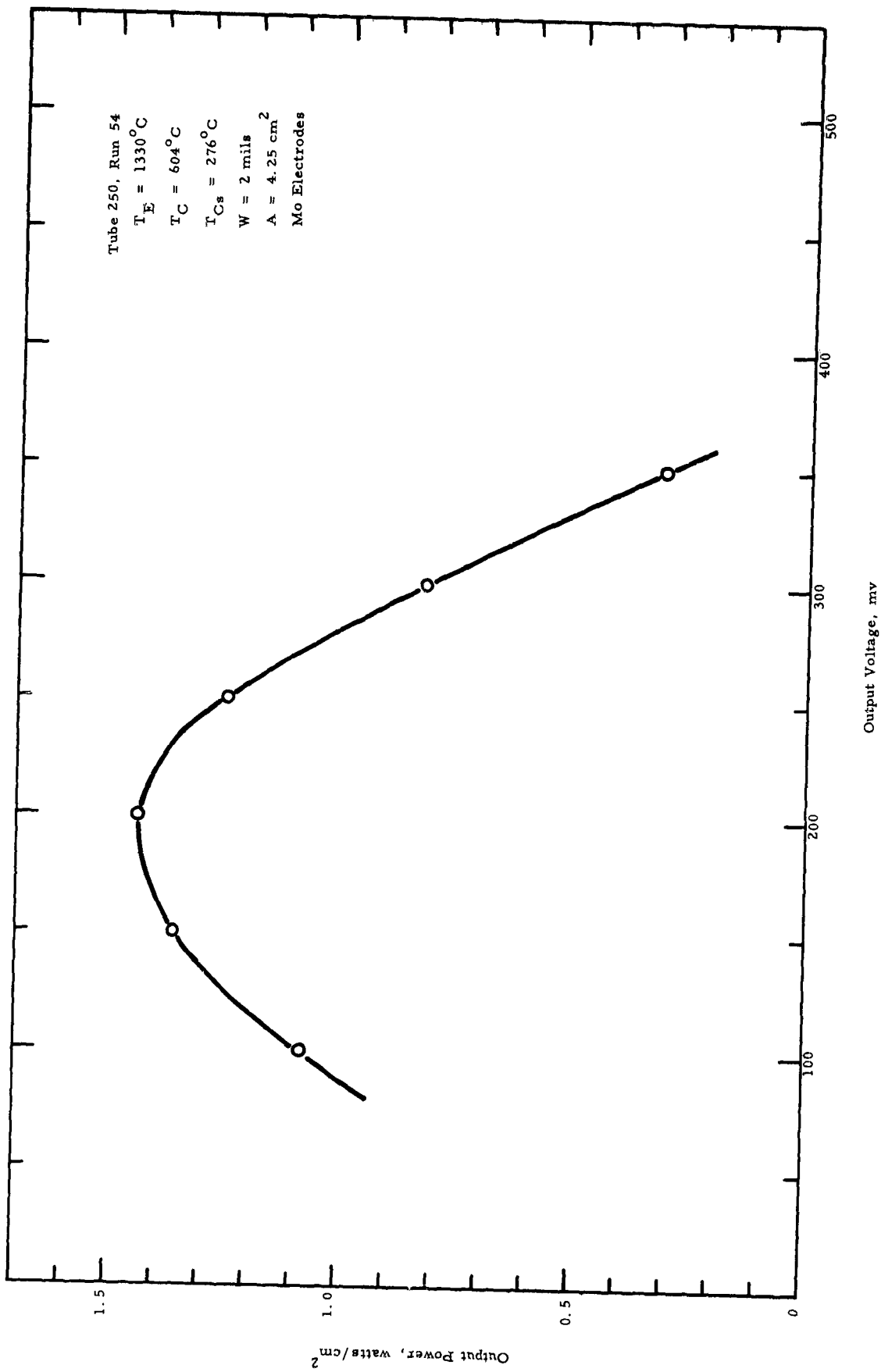


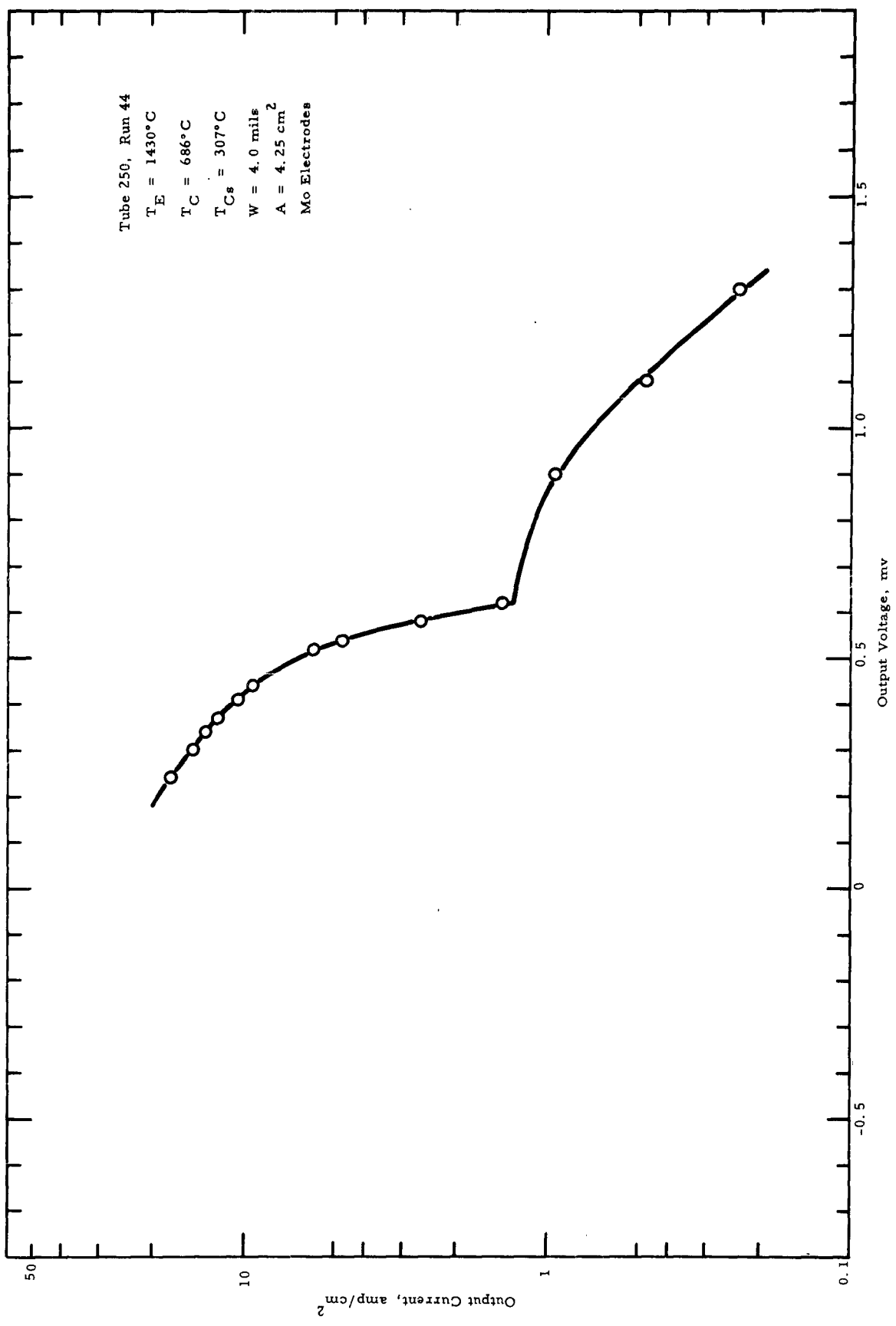


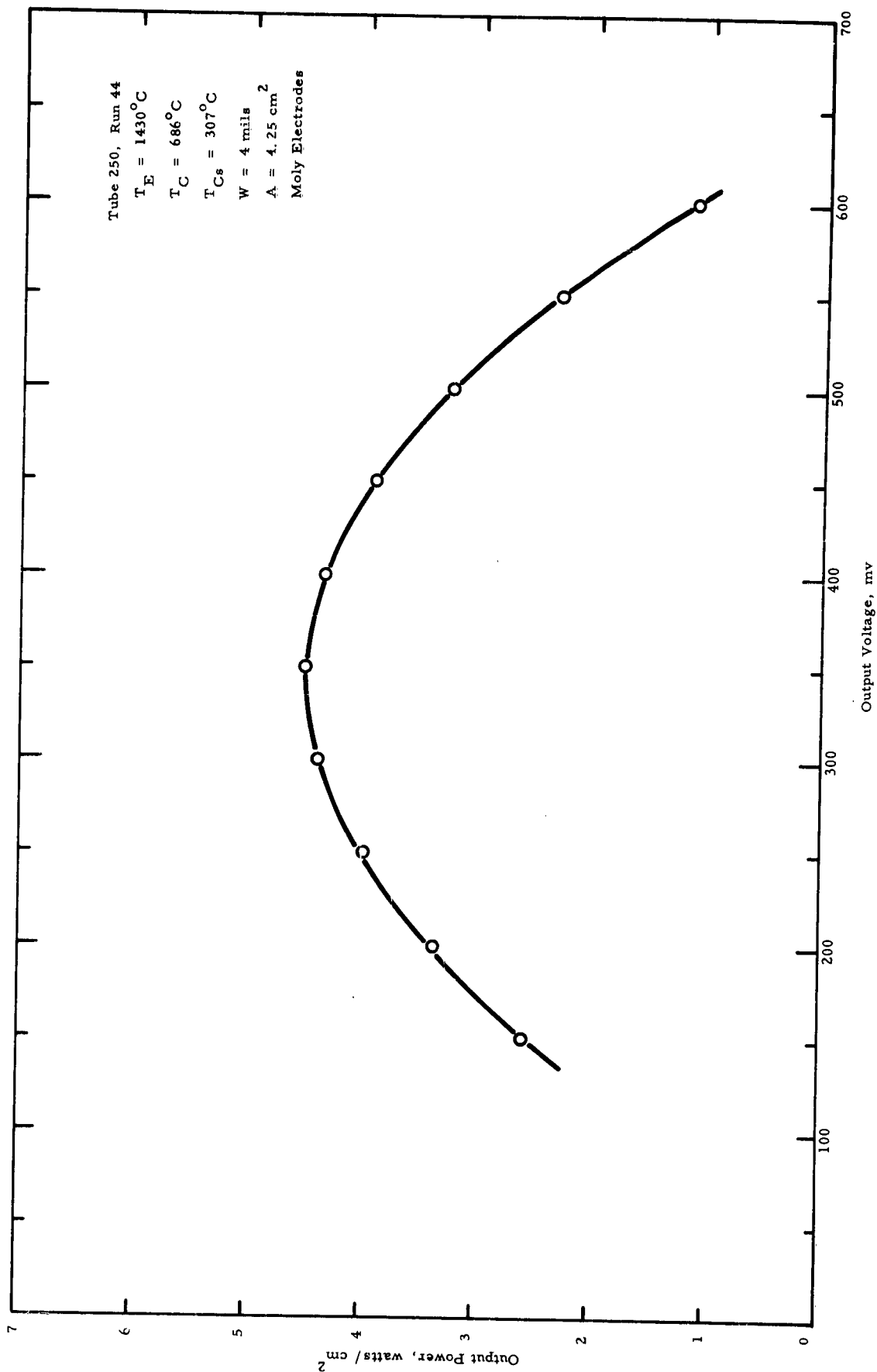


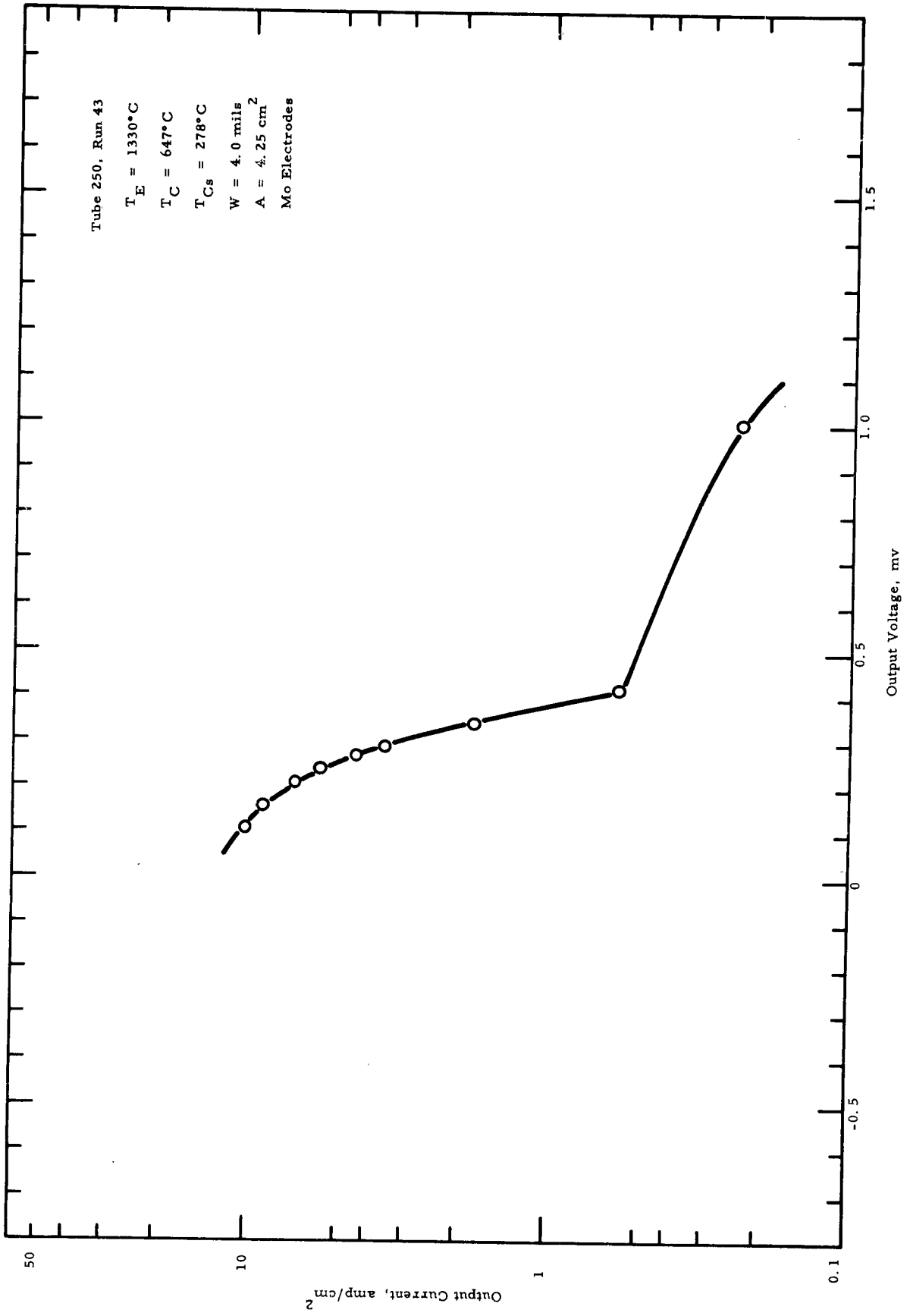


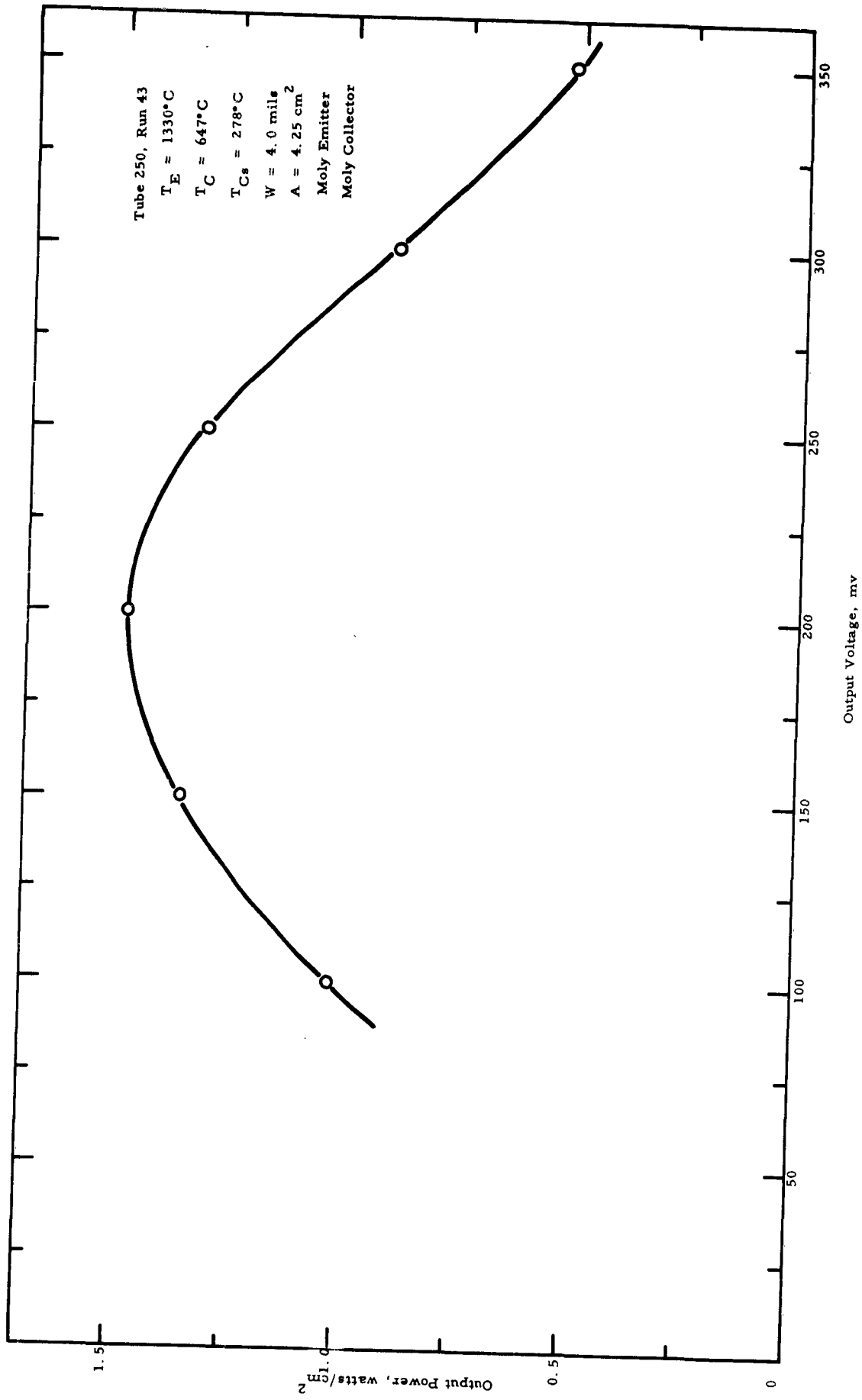


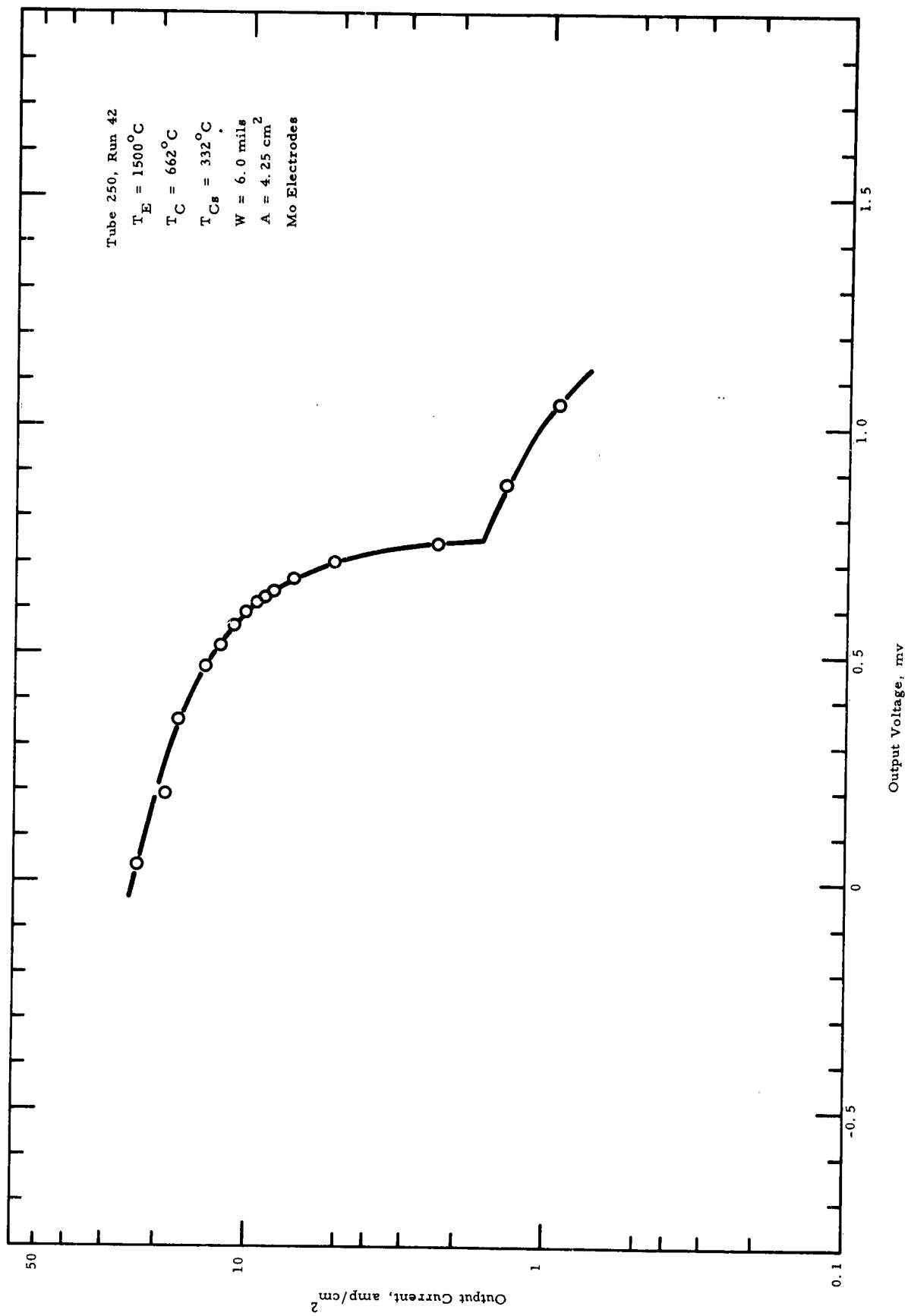


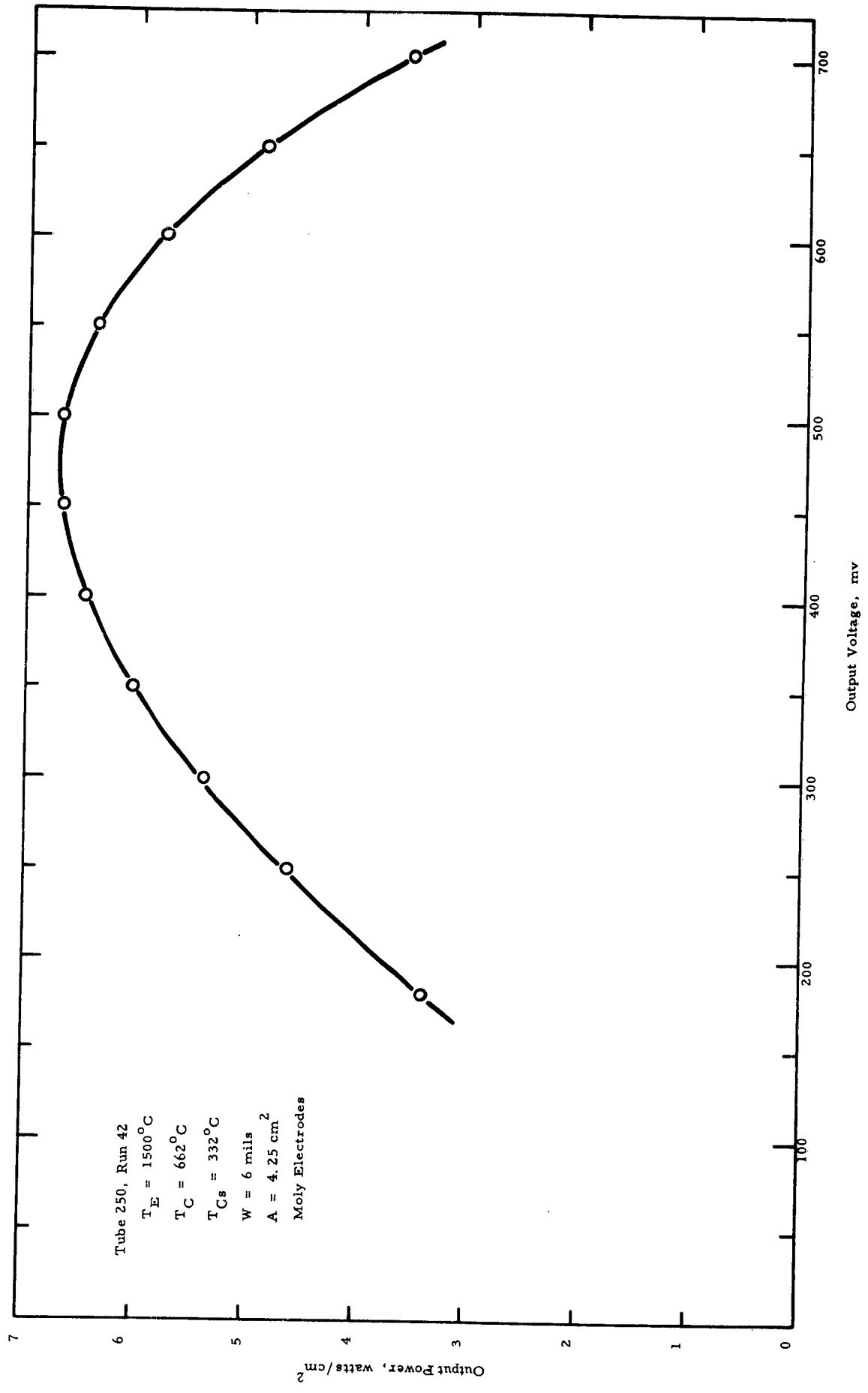


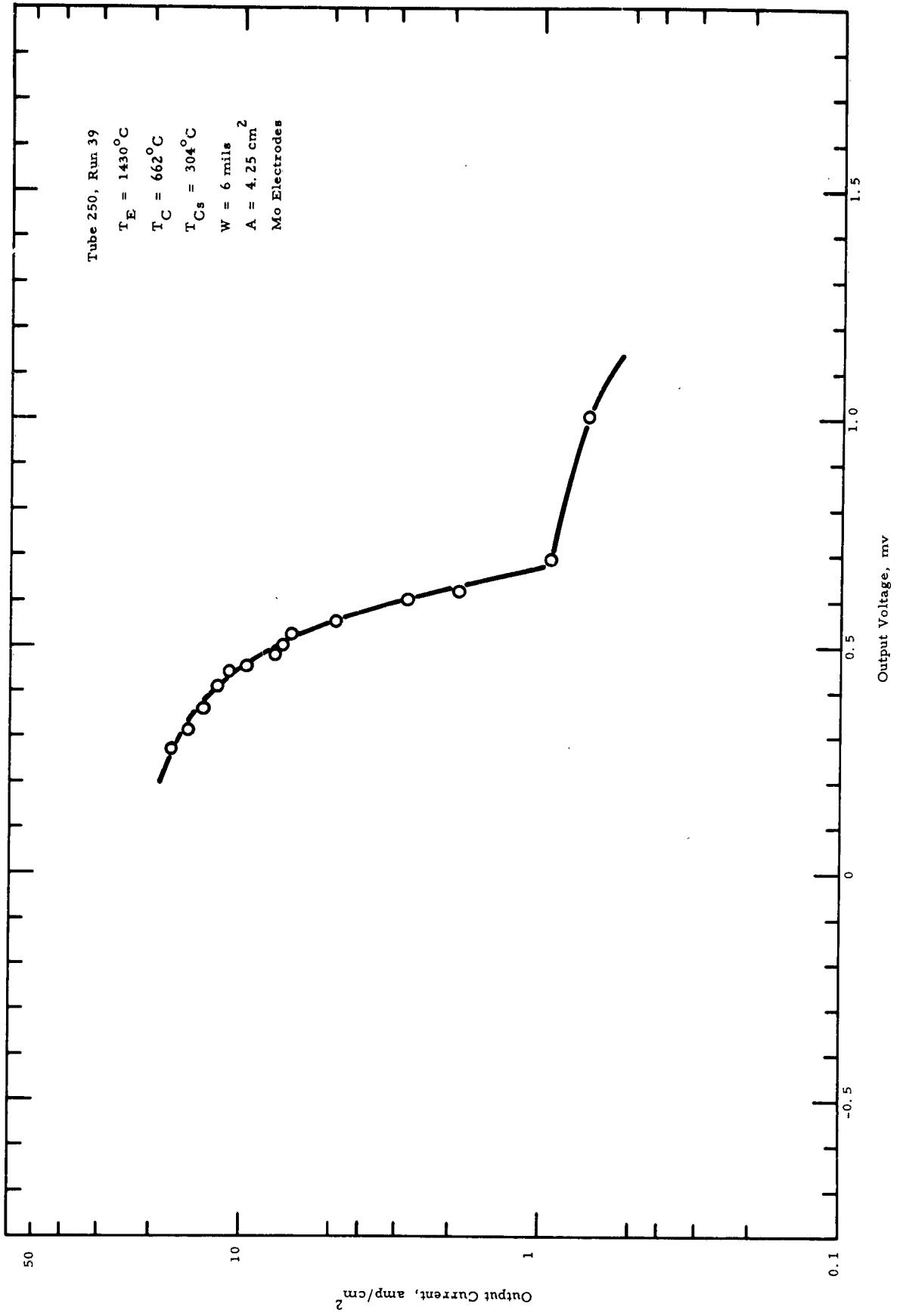


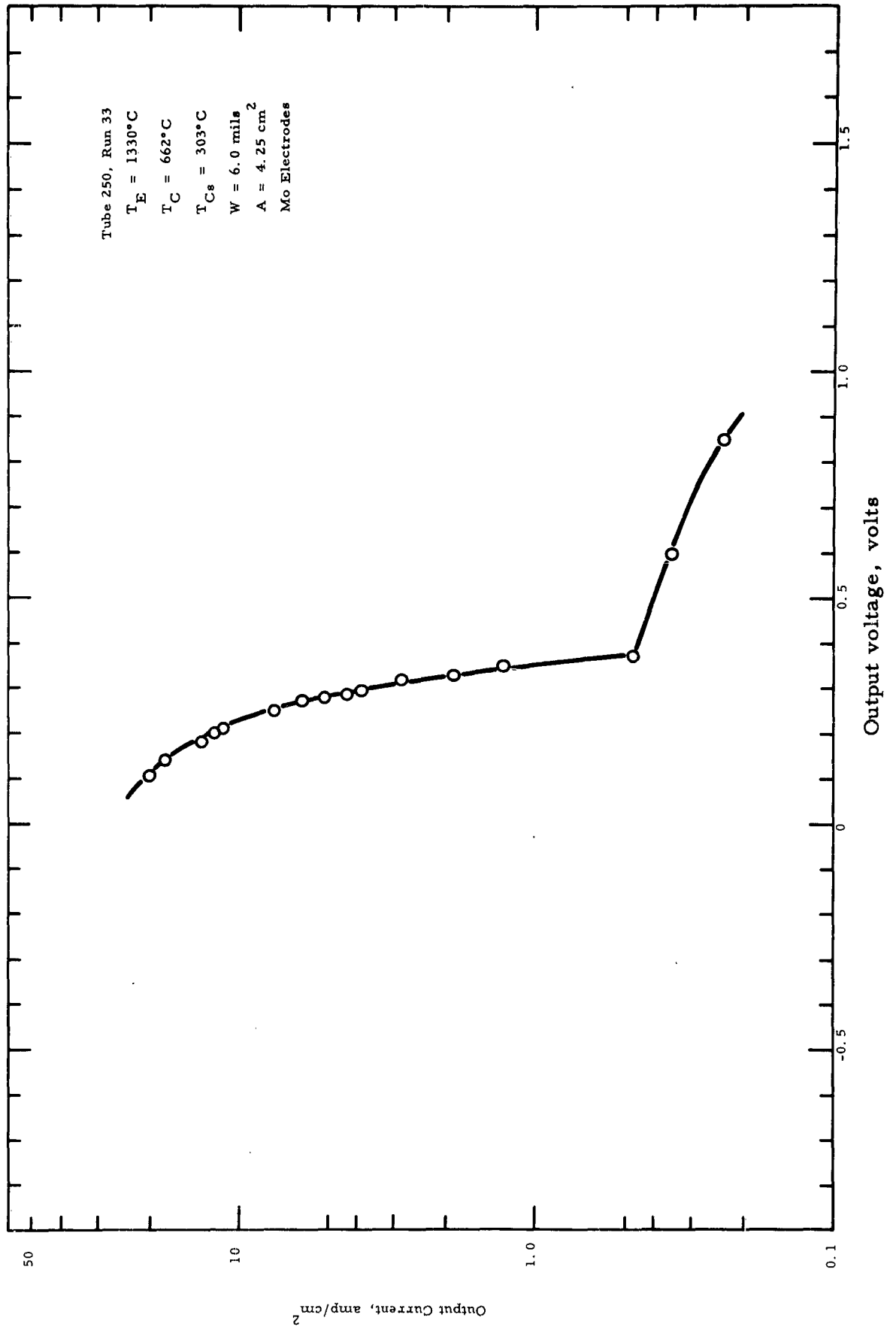


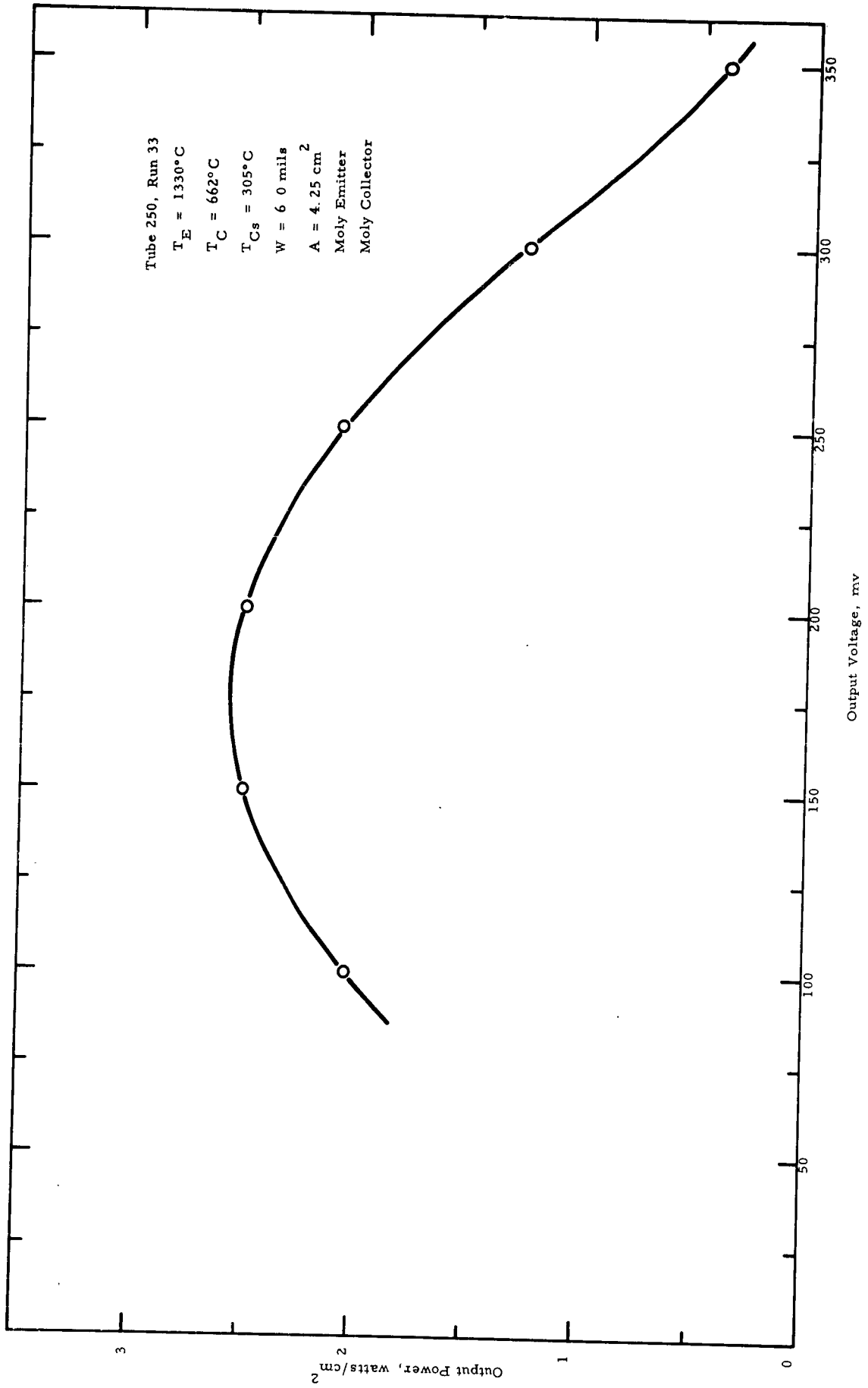


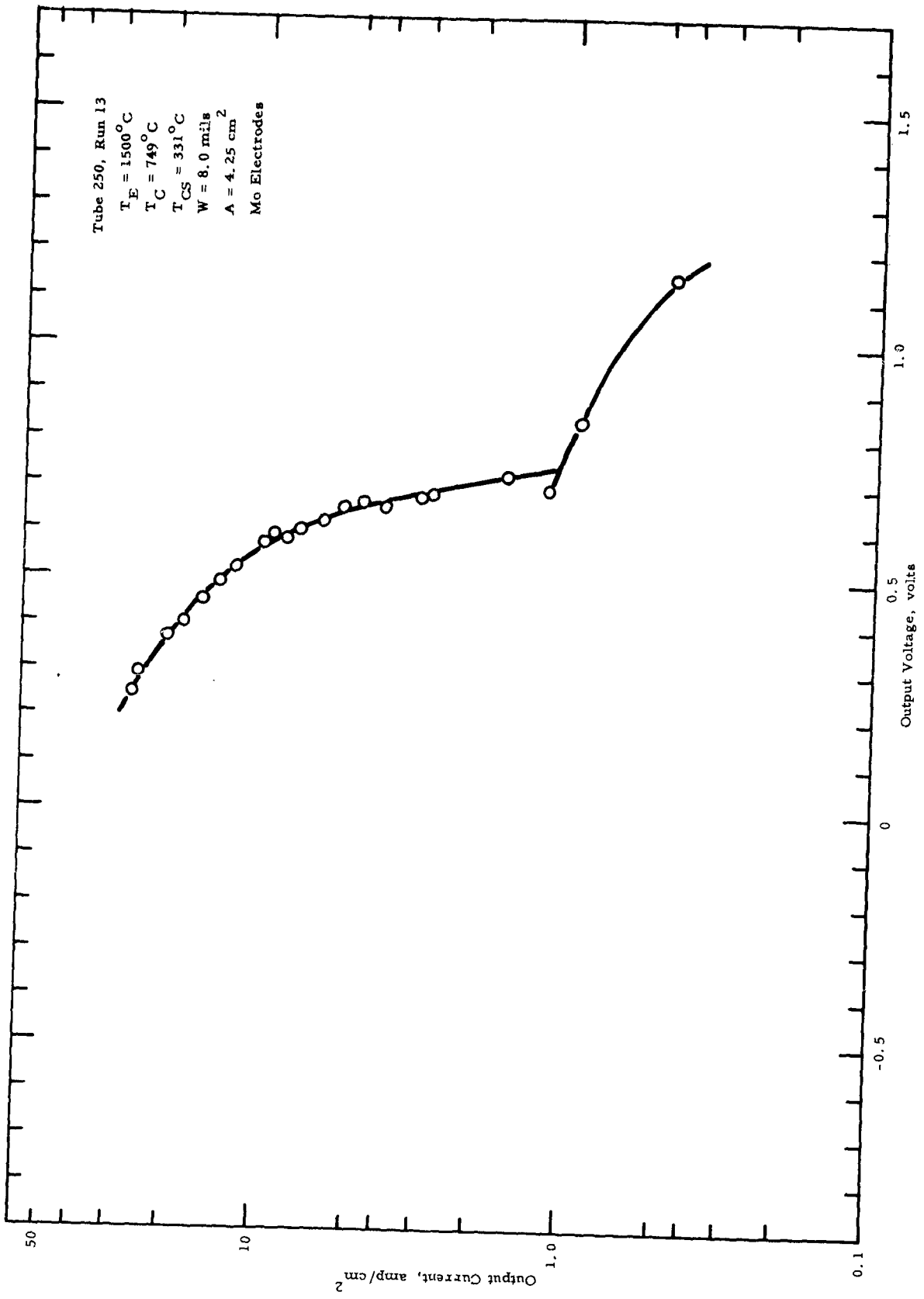


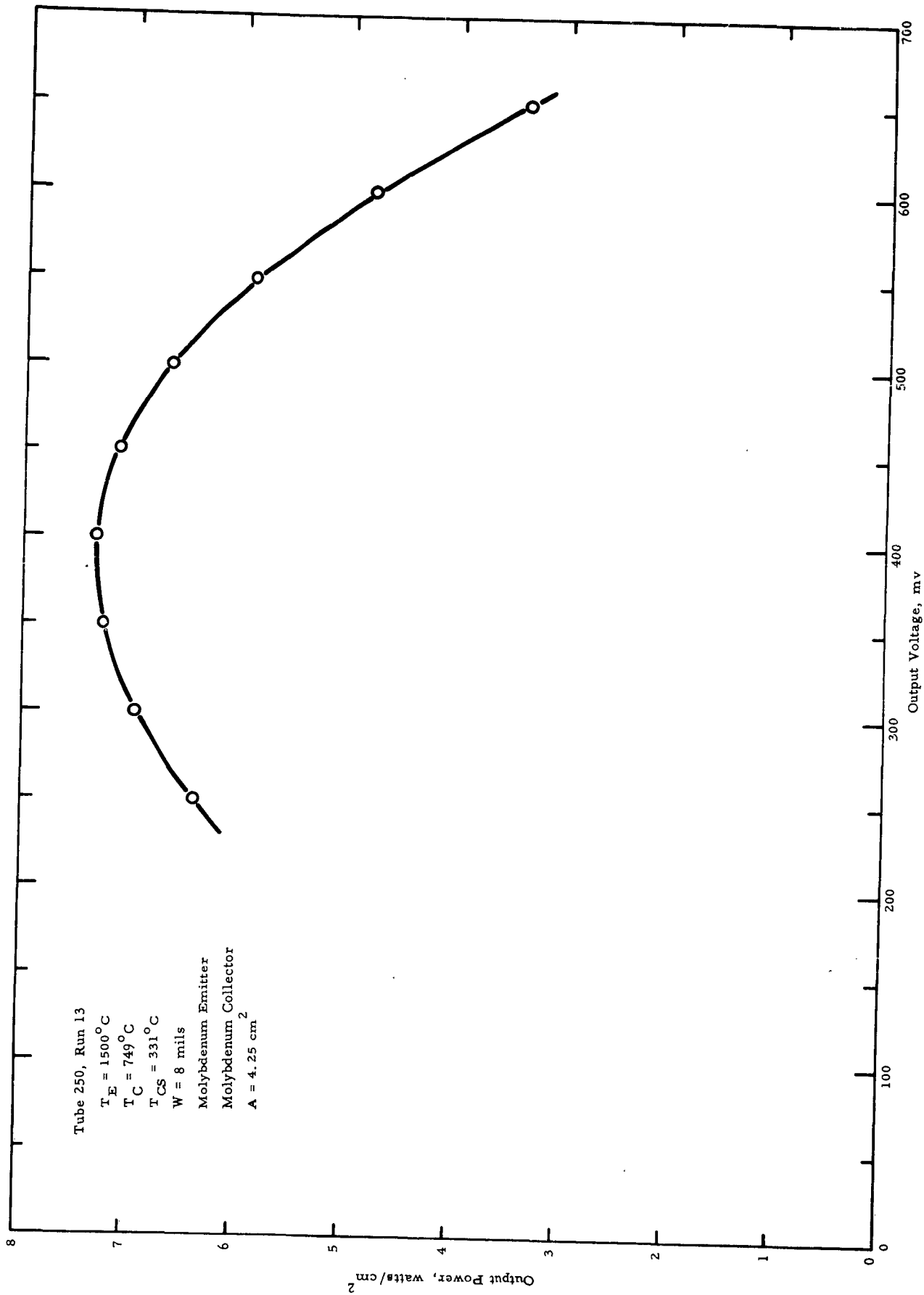


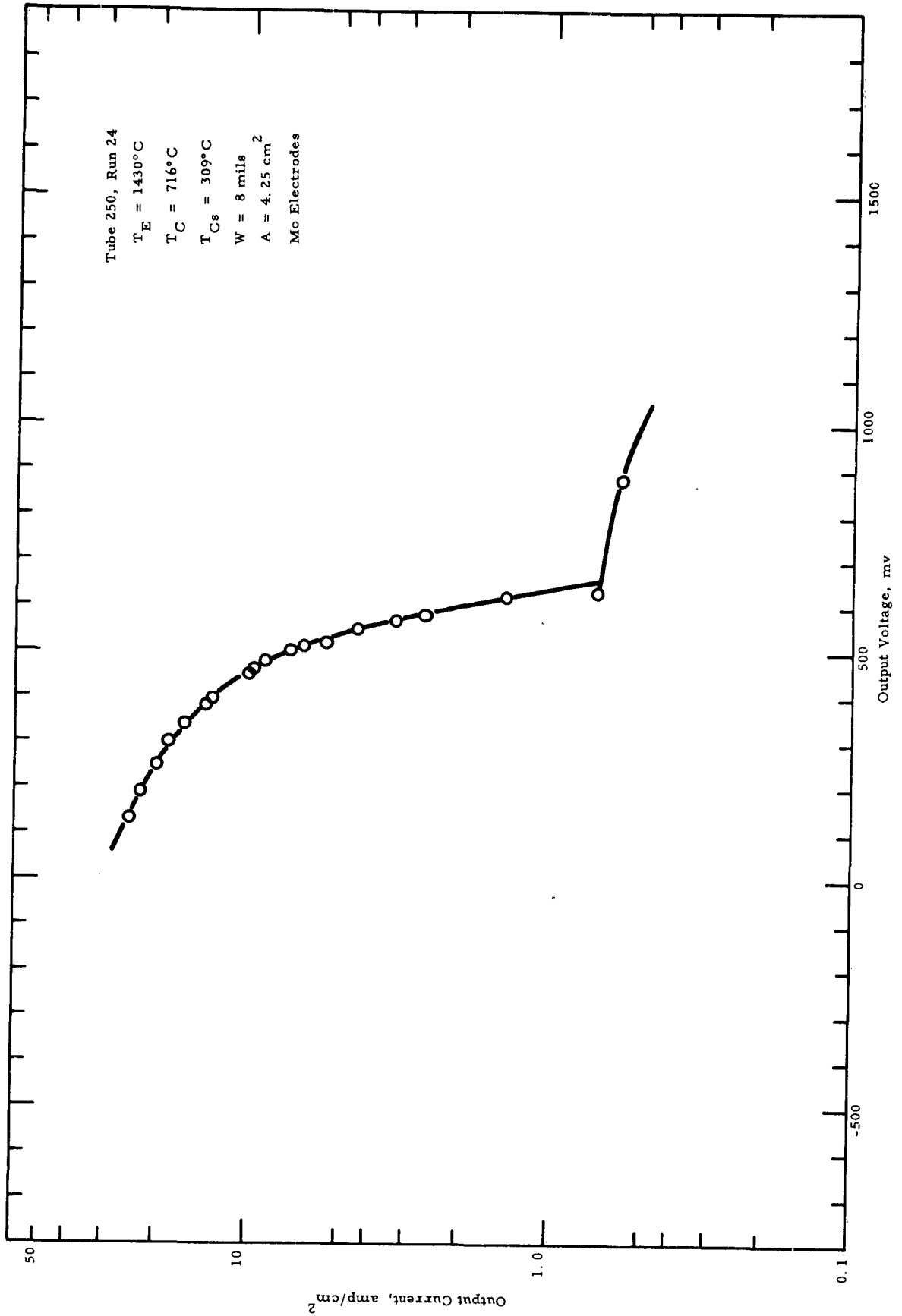


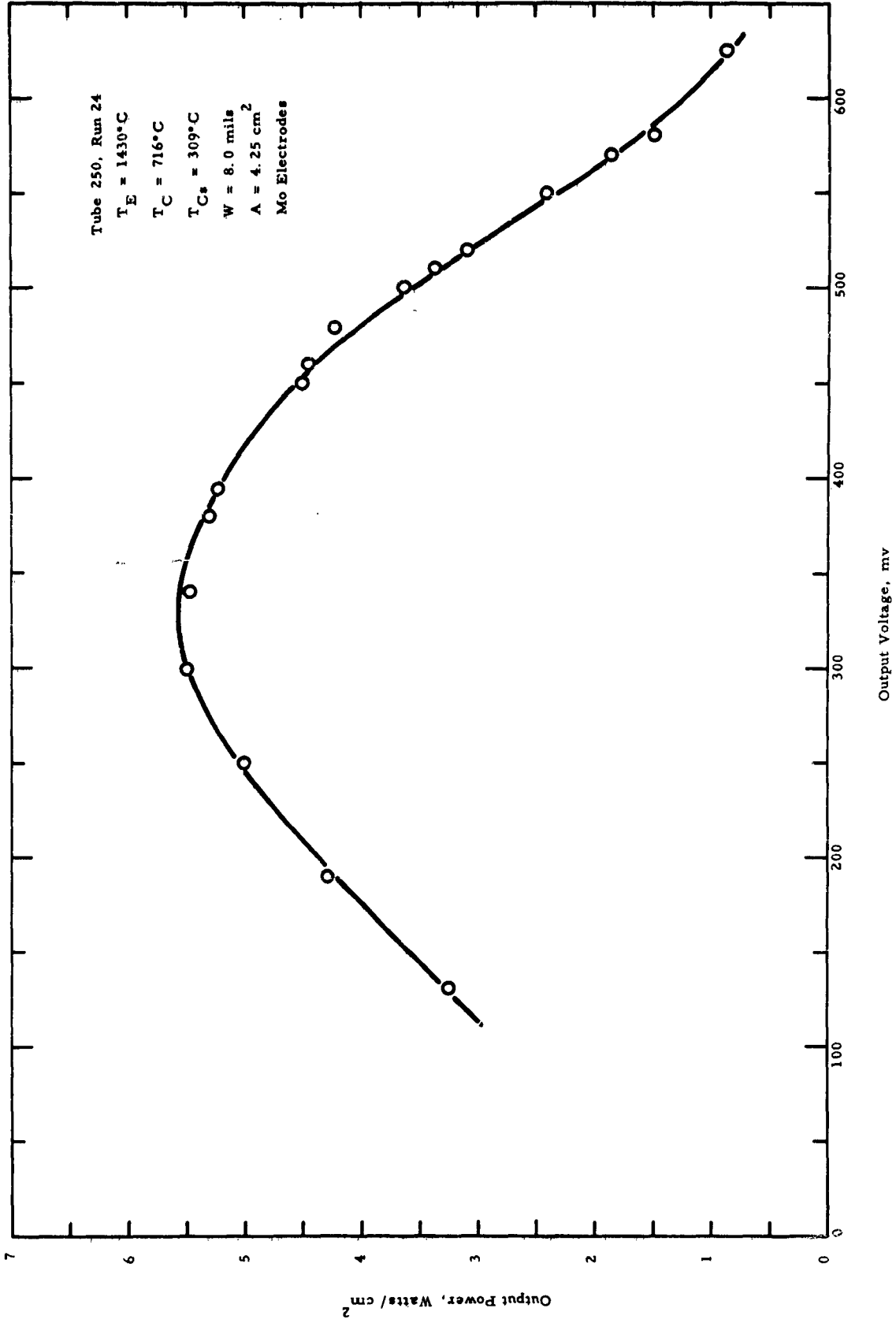


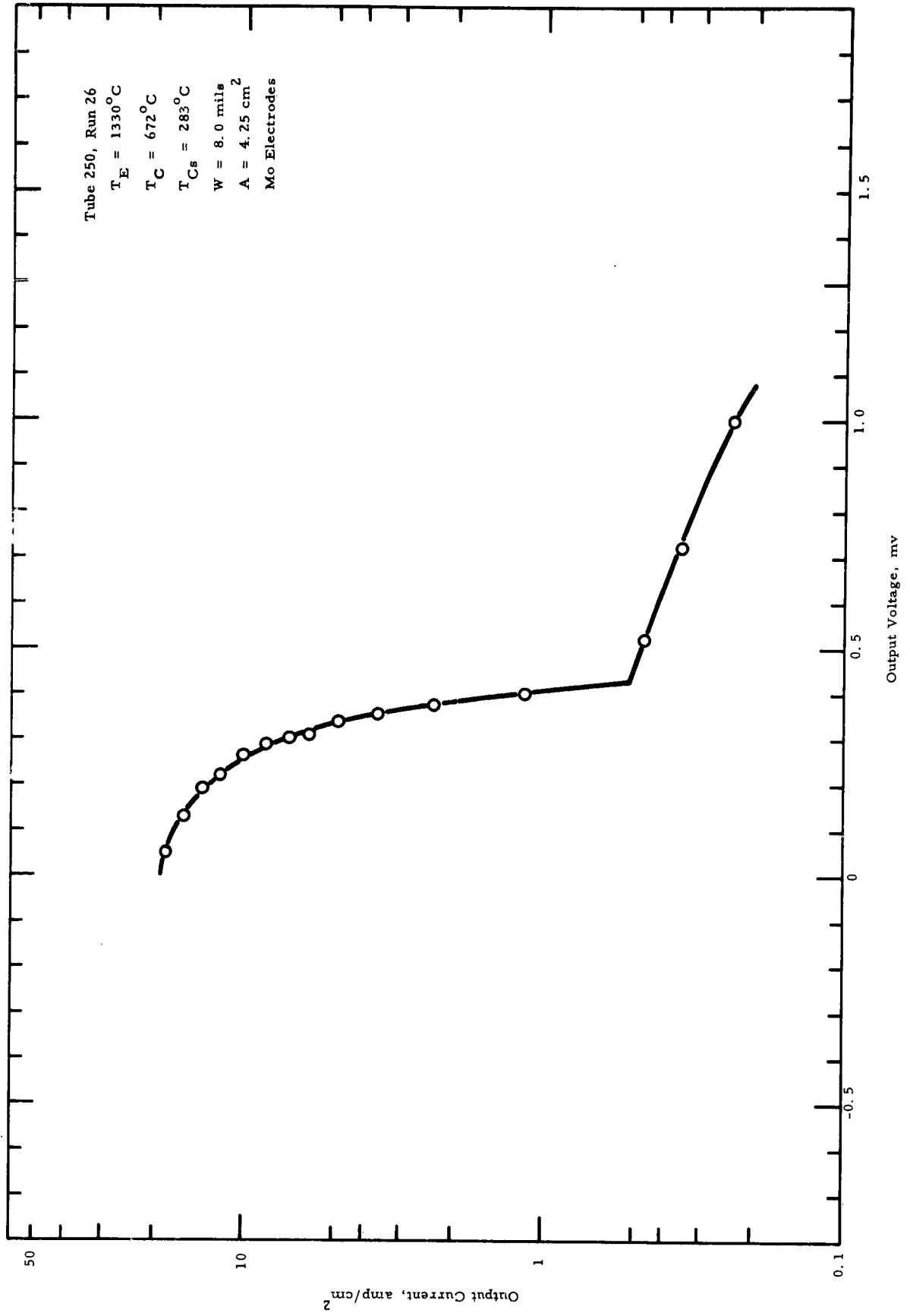


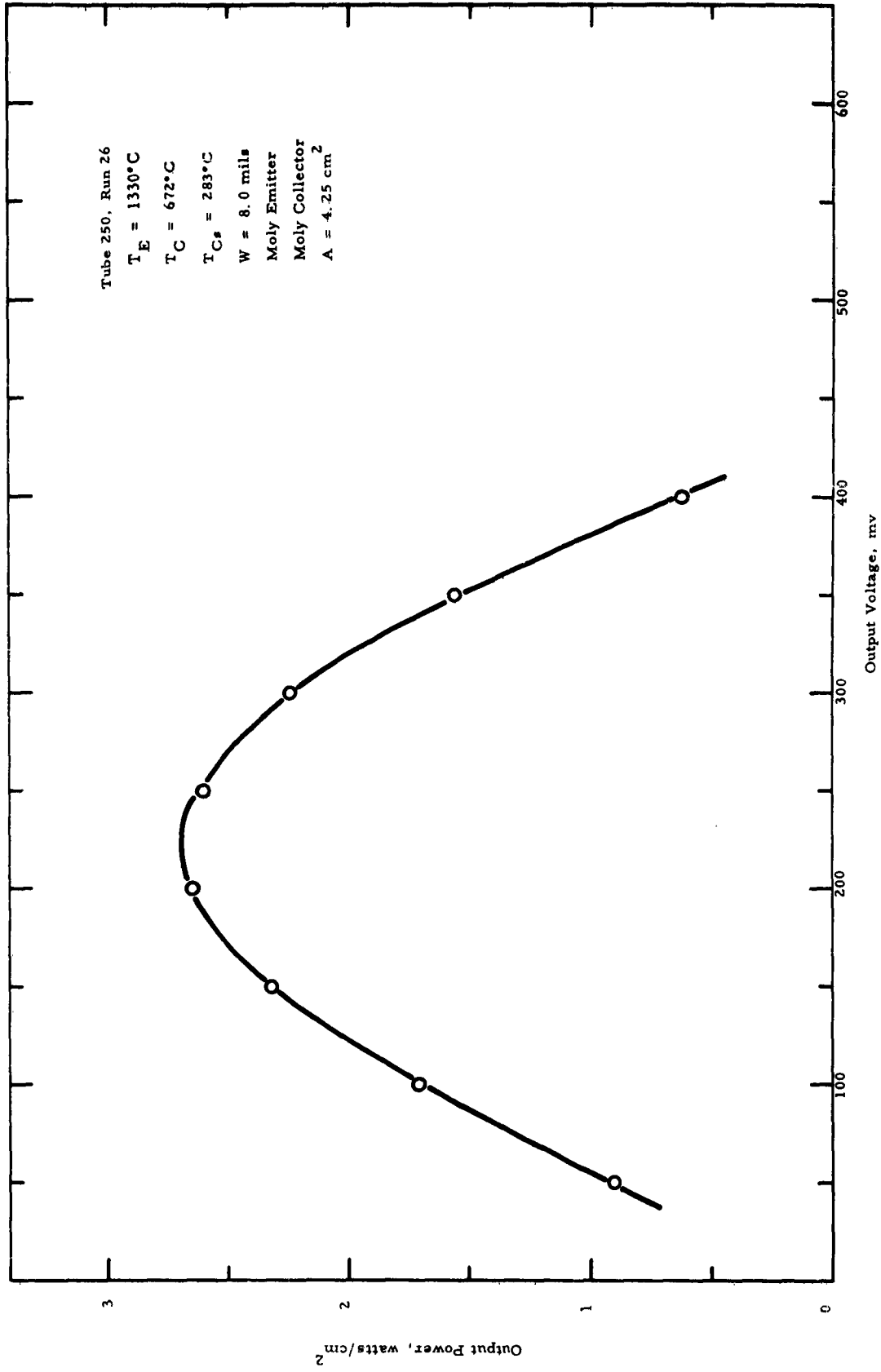












Tube 250, Run 76

$T_E = 1500^\circ\text{C}$

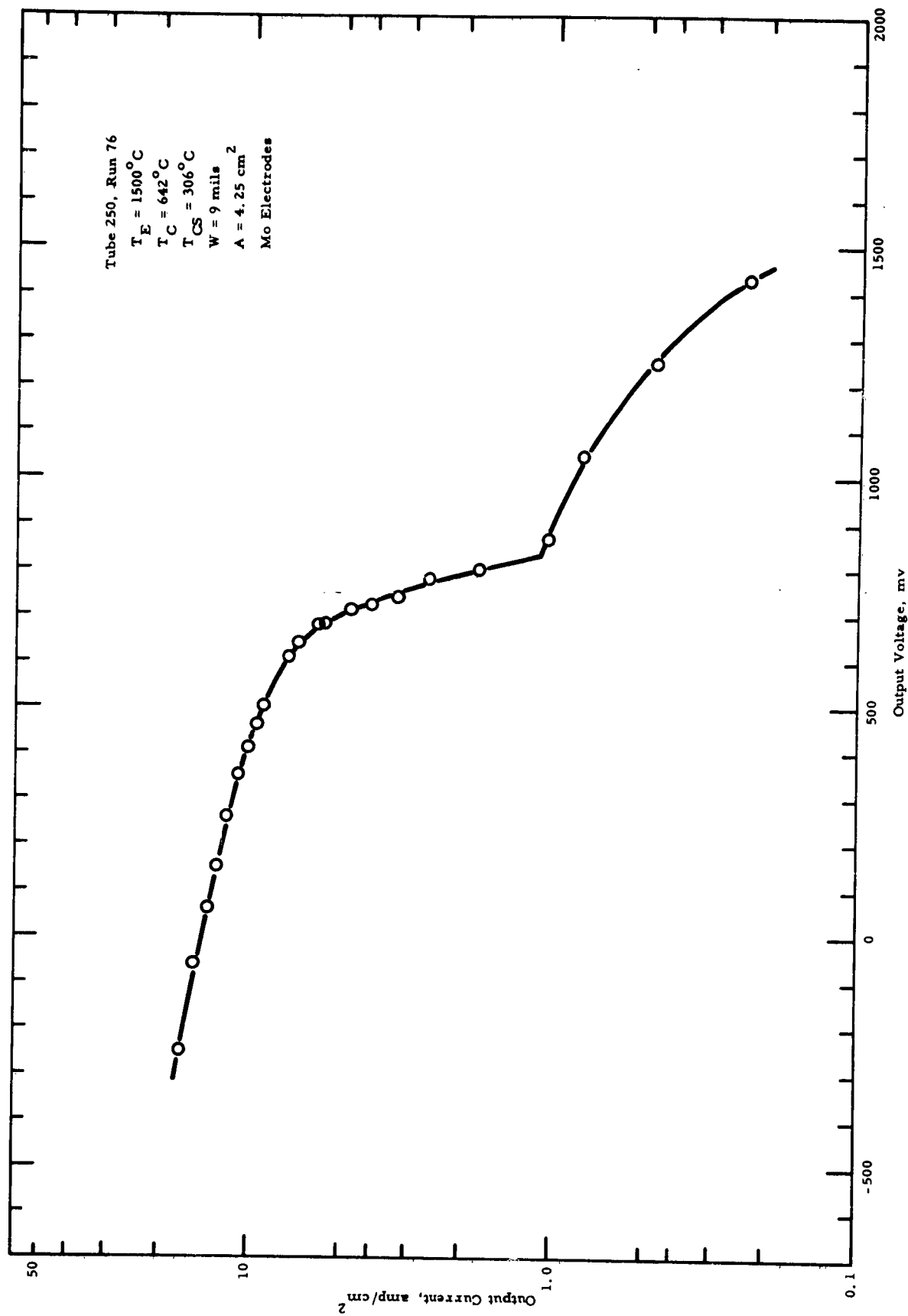
$T_C = 642^\circ\text{C}$

$T_{CS} = 306^\circ\text{C}$

$W = 9 \text{ mils}$

$A = 4.25 \text{ cm}^2$

Mo Electrodes



Tube 250, Run 76

$T_E = 1500^\circ\text{C}$

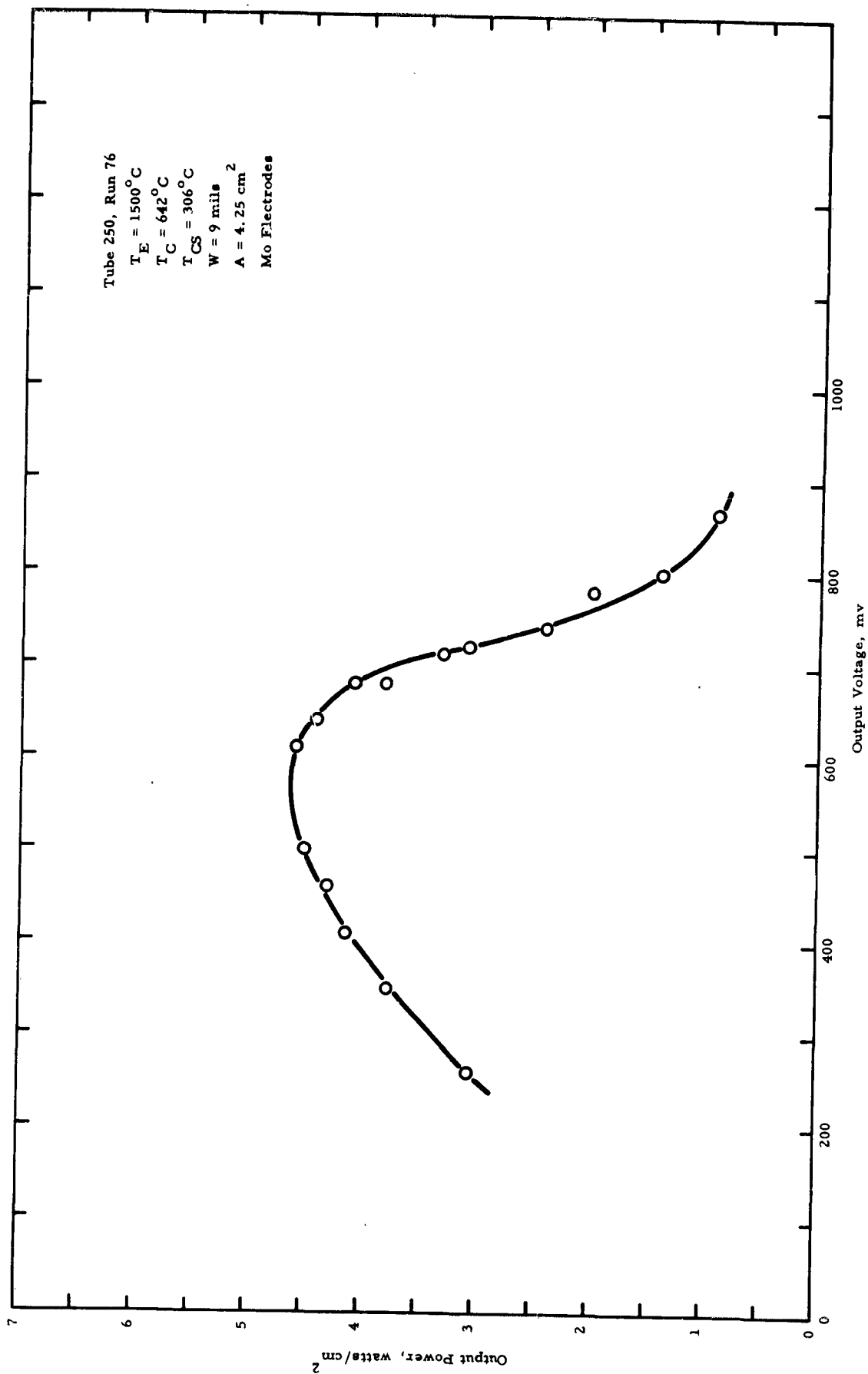
$T_C = 642^\circ\text{C}$

$T_{CS} = 306^\circ\text{C}$

$W = 9 \text{ mills}$

$A = 4.25 \text{ cm}^2$

Mo Electrodes



Tube 250, Run 75

$T_E = 1430^\circ\text{C}$

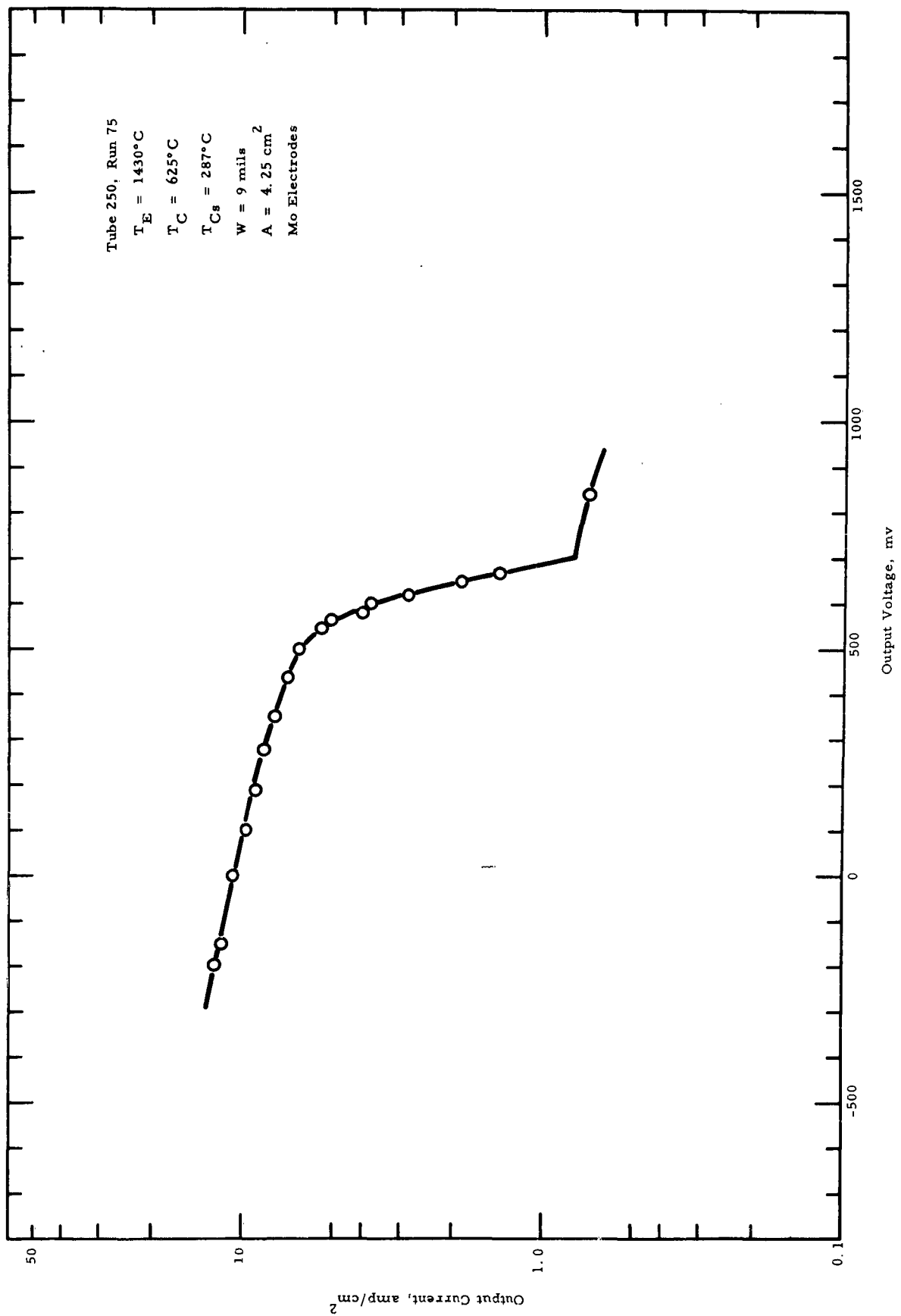
$T_C = 625^\circ\text{C}$

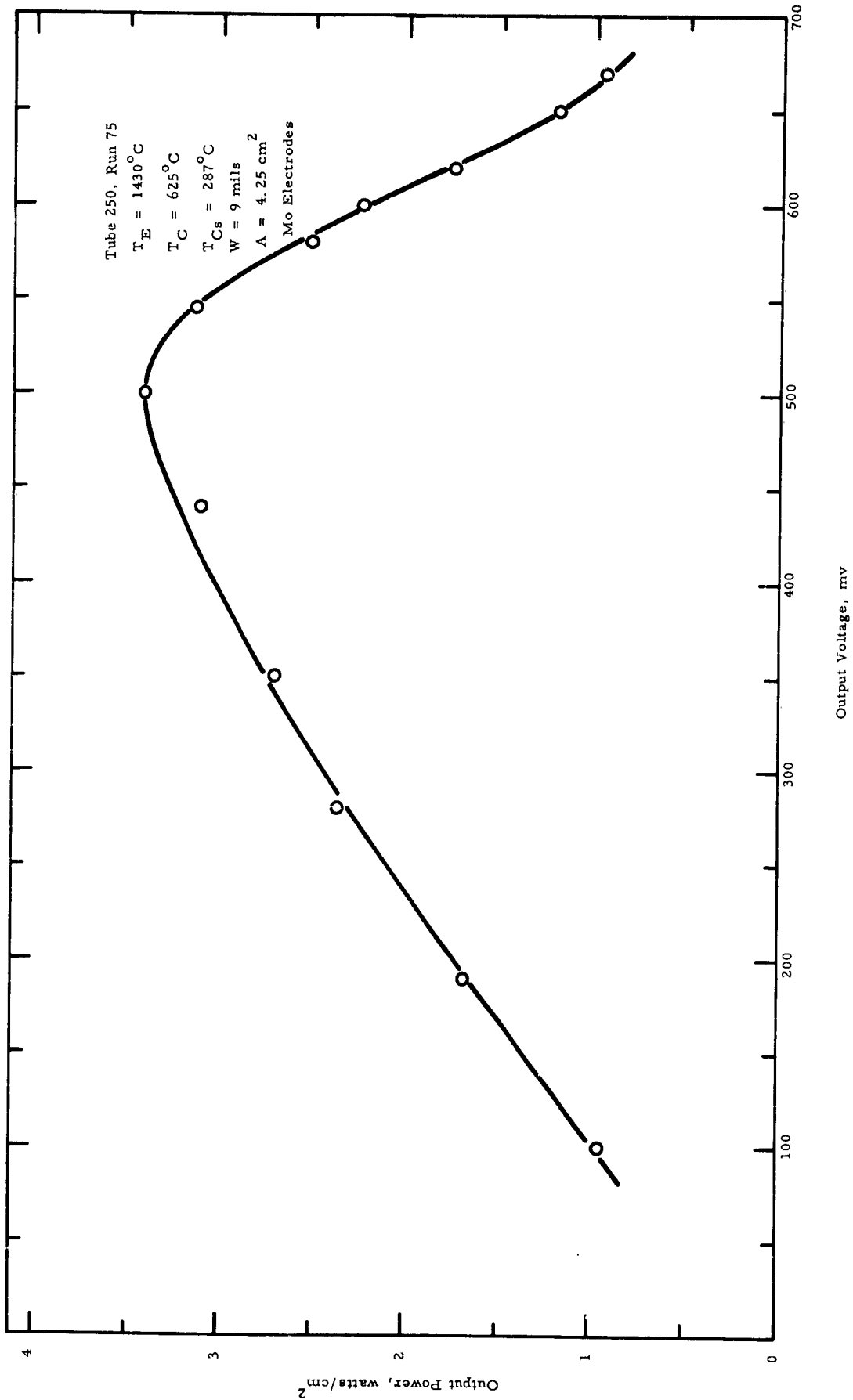
$T_{Cs} = 287^\circ\text{C}$

$W = 9 \text{ mils}$

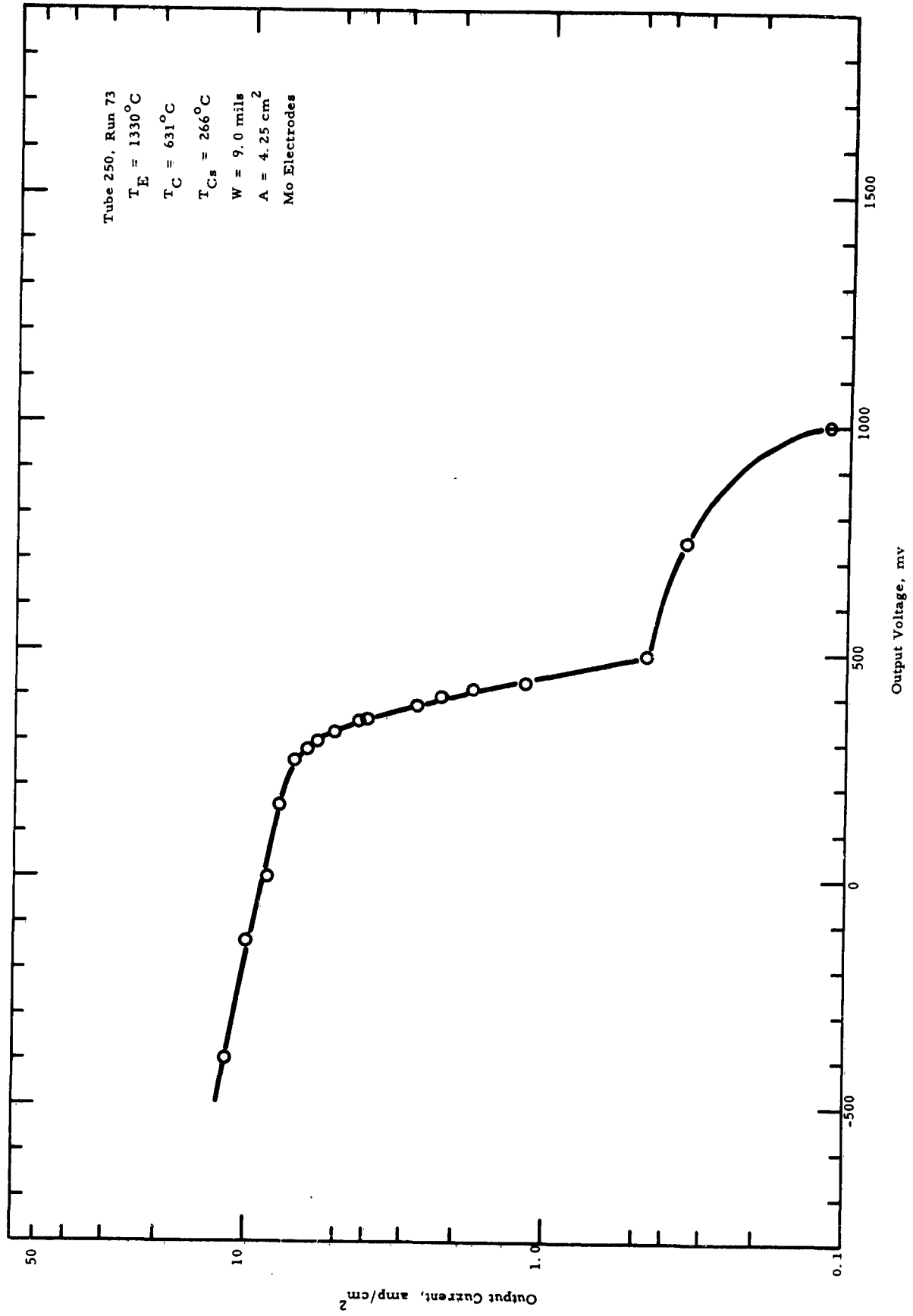
$A = 4.25 \text{ cm}^2$

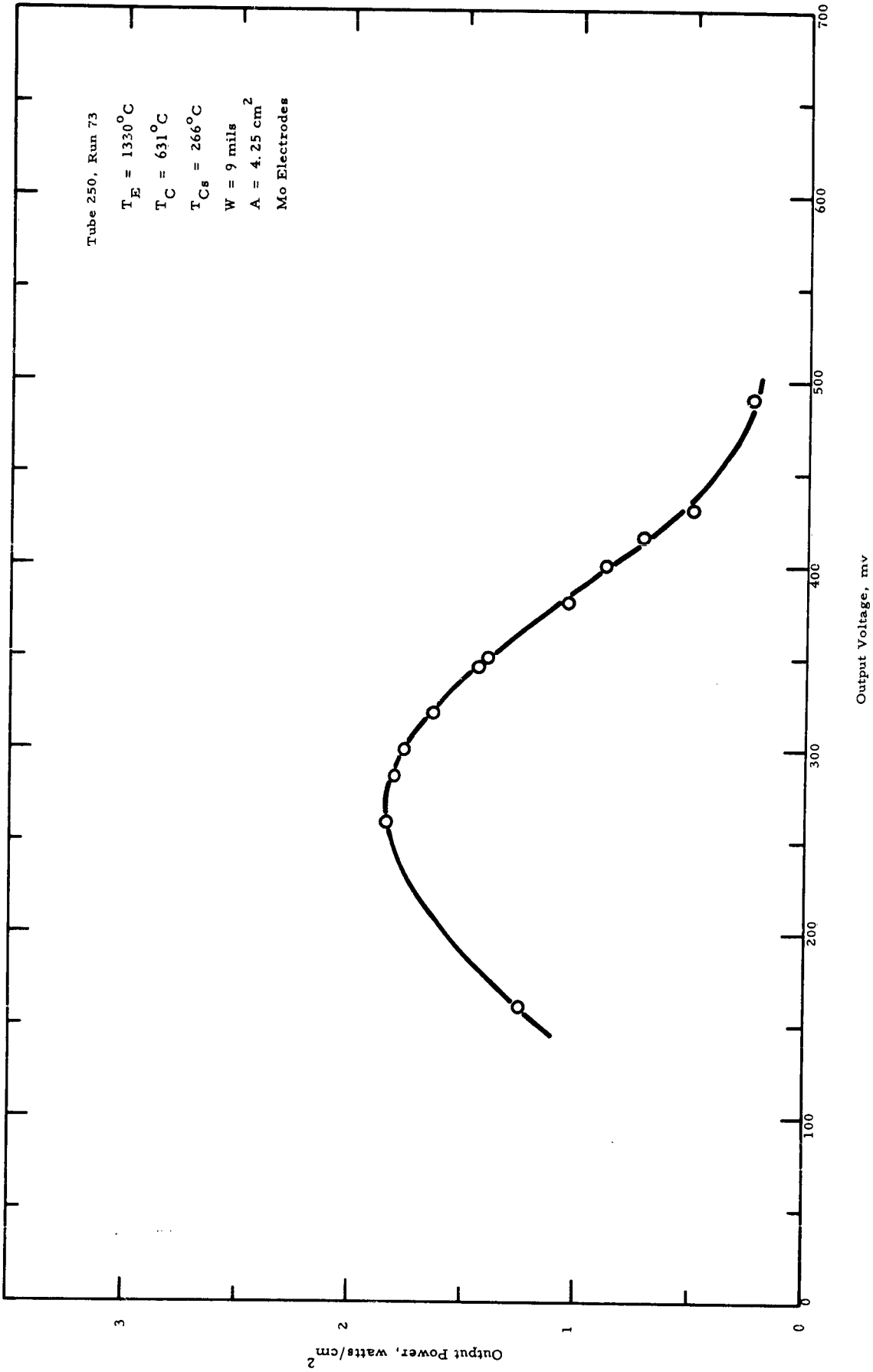
Mo Electrodes

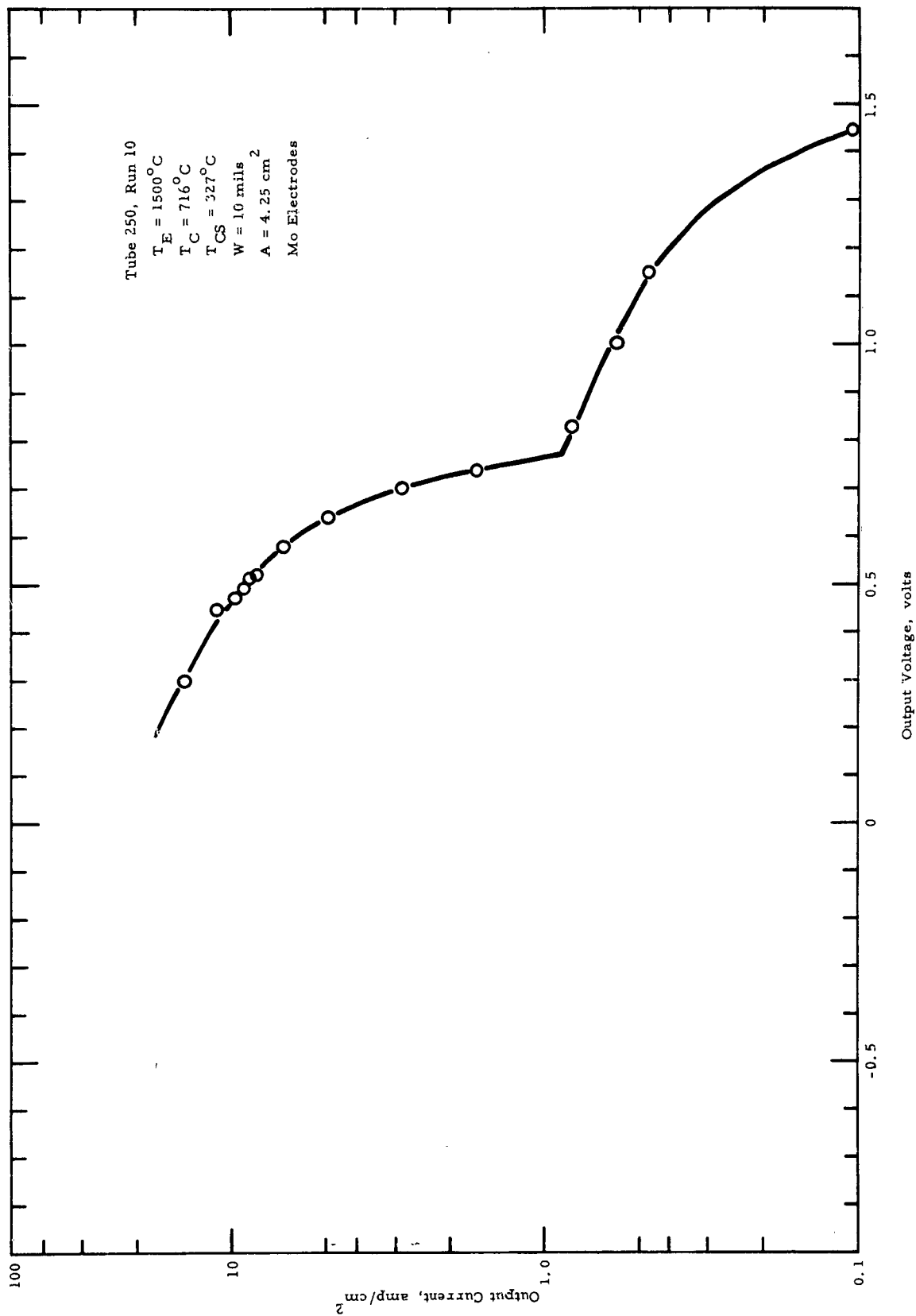


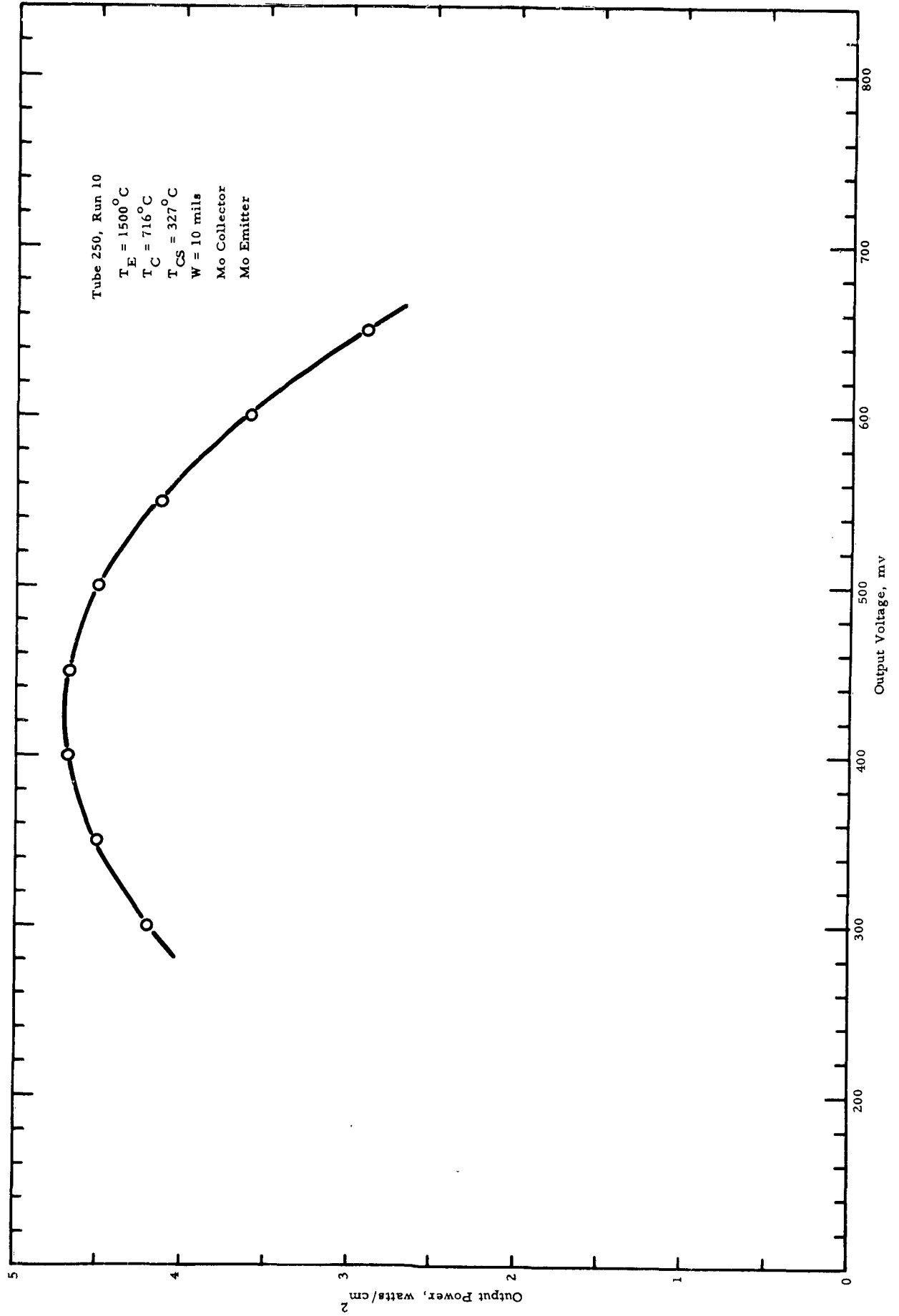


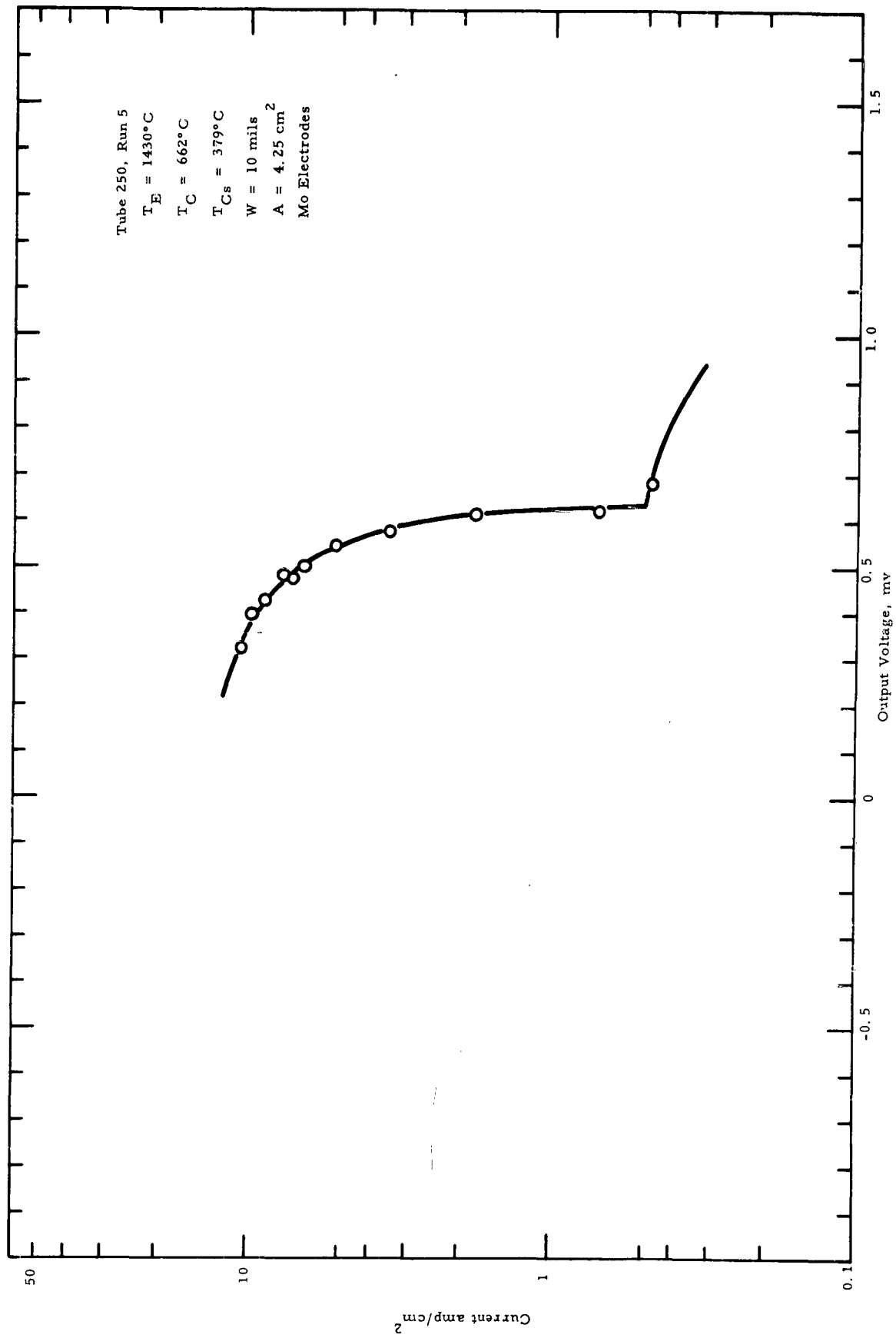
Tube 250, Run 73  
 $T_E = 1330^\circ\text{C}$   
 $T_C = 631^\circ\text{C}$   
 $T_{Cs} = 266^\circ\text{C}$   
 $W = 9.0 \text{ mils}$   
 $A = 4.25 \text{ cm}^2$   
Mo Electrodes

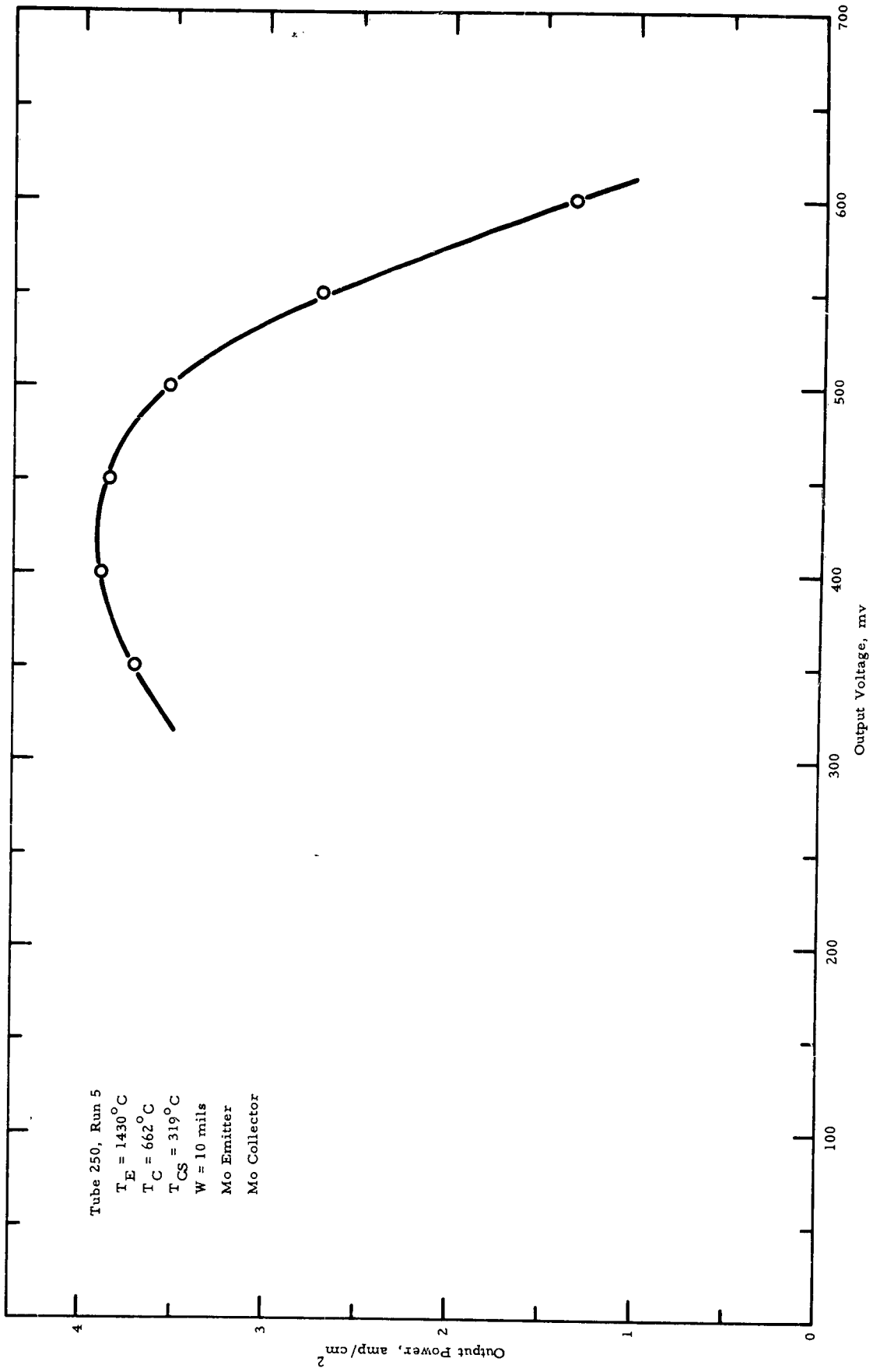


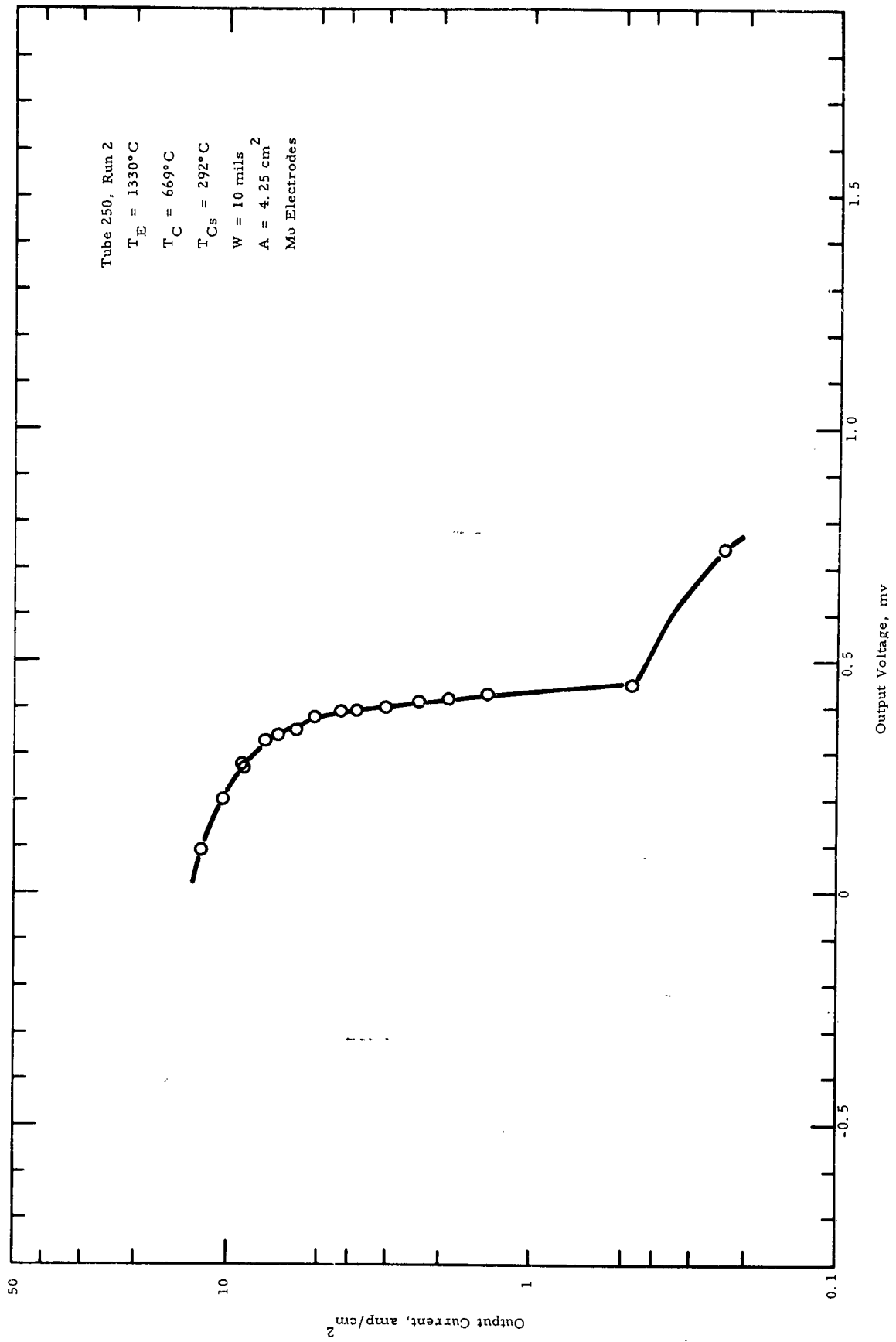


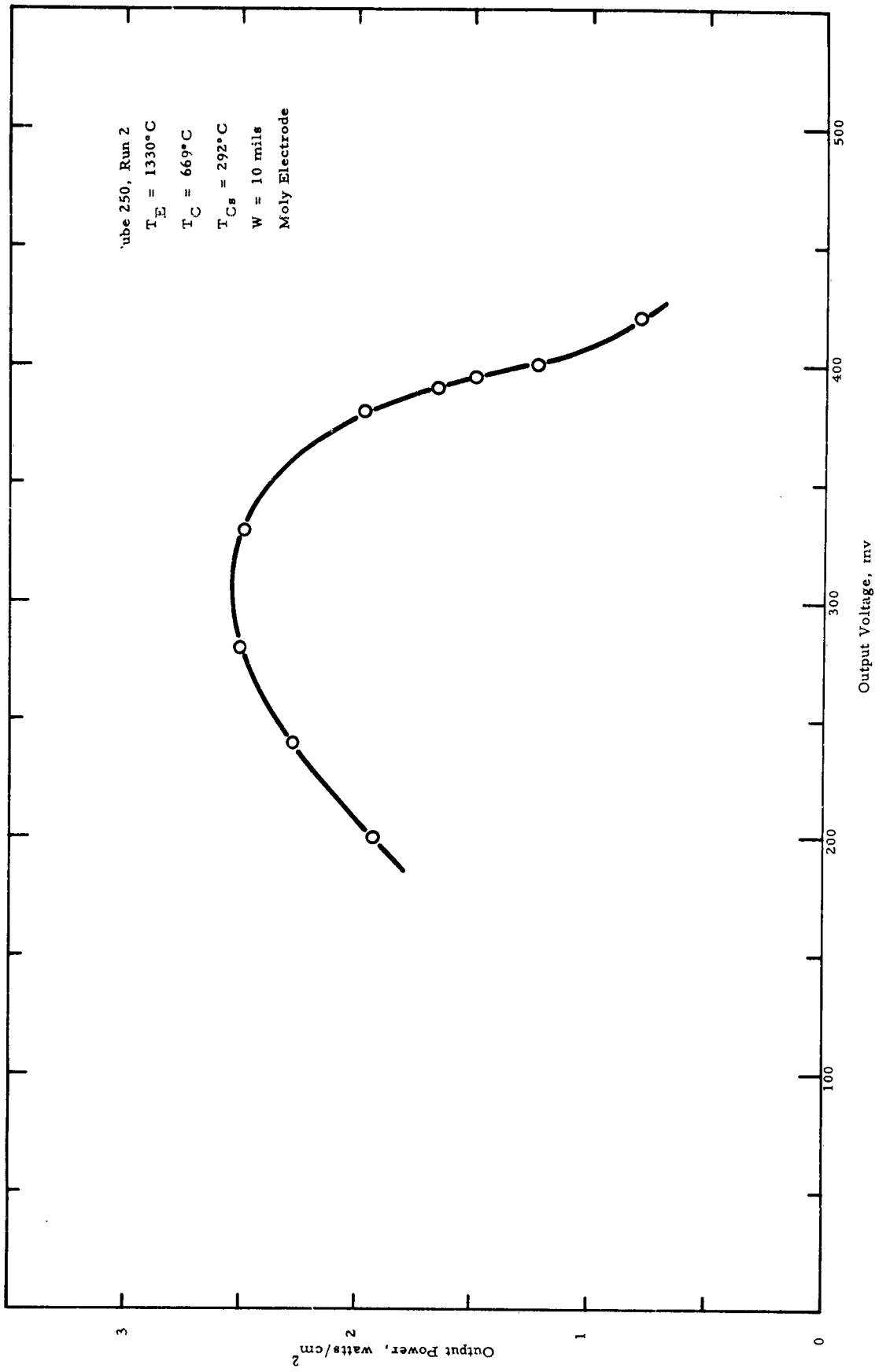


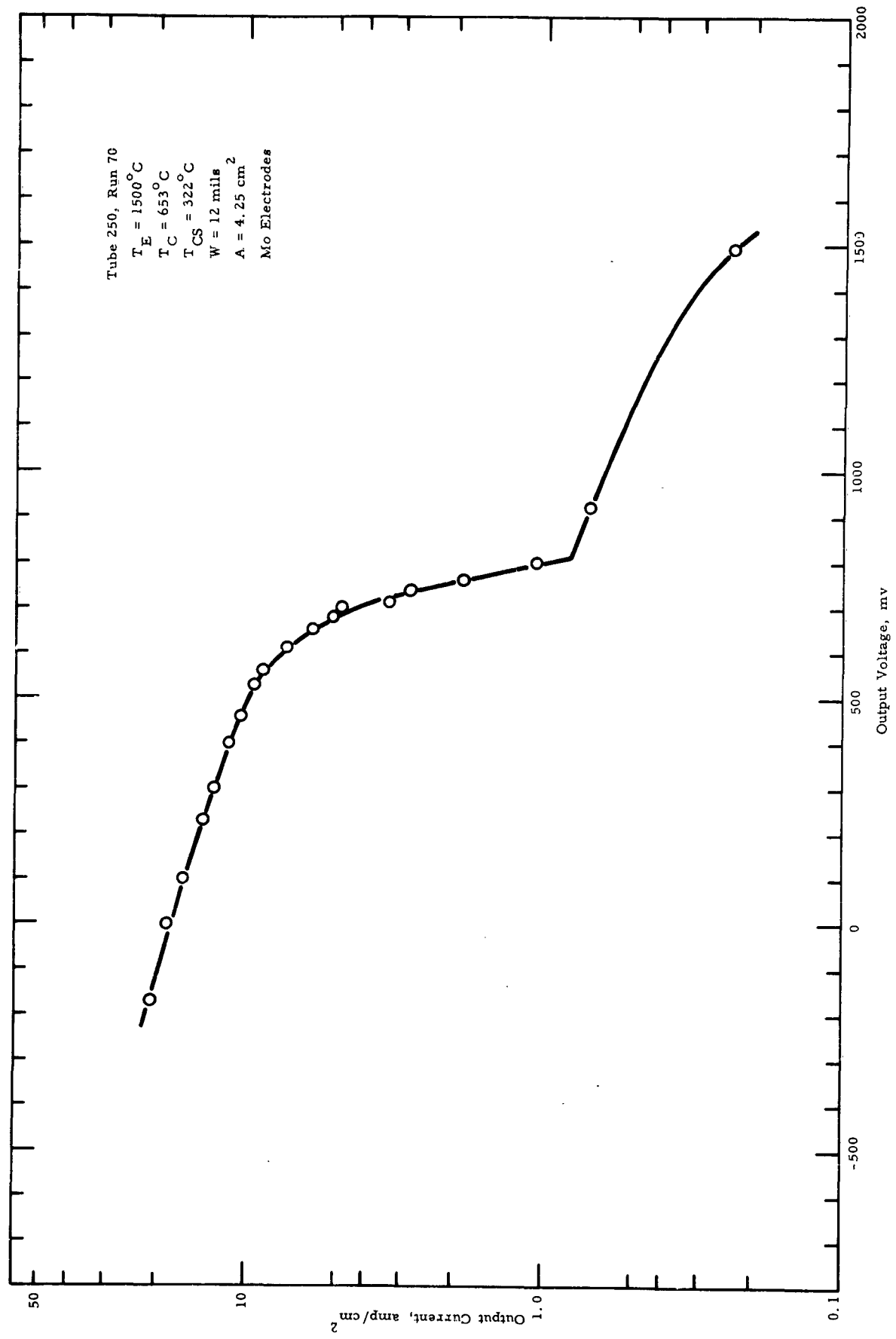












Tube 250, Run 70

$T_E = 1500^\circ\text{C}$

$T_C = 653^\circ\text{C}$

$T_{CS} = 322^\circ\text{C}$

$W = 12 \text{ mils}$

$A = 4.25 \text{ cm}^2$

Mo Electrodes

